EXPERIMENTAL INVESTIGATION OF THE AGITATION OF COMPLEX FLUIDS

A THESIS SUBMITTED TO
THE GRADUATE SCHOOL OF NATURAL AND APPLIED SCIENCES
OF
MIDDLE EAST TECHNICAL UNIVERSITY

BY

ÖZGE YAZICIOĞLU

IN PARTIAL FULFILLMENT OF THE REQUIREMENTS
FOR
THE DEGREE OF MASTER OF SCIENCE
IN
CHEMICAL ENGINEERING

JULY 2006

Approval of the Graduate School of Natural and Applied Sciences

Prof. Dr. Canan Özgen
Director

I certify that this thesis satisfies all the requirements as a thesis for the degree of Master of Science.

Prof. Dr. Nurcan Baç
Head of Department

This is to certify that we have read this thesis and that in our opinion it is fully adequate, in scope and quality, as a thesis and for the degree of Master of Science.

Asst. Prof. Dr. Yusuf Uludağ
Supervisor

Examining Committee Members

Prof. Dr. Ufuk Bakır	(METU, CHE)	
Asst. Prof. Dr. Yusuf Uludağ	(METU, CHE)	
Prof. Dr. Pınar Çalık	(METU, CHE)	
Asst. Prof. Dr. Halil Kalıpçılar	(METU, CHE)	
Dr. Ömür Uğur	(METU, IAM)	

I hereby declare that all information in this document has been obtained and presented in accordance with academic rules and ethical conduct. I also declare that, as required by these rules and conduct, I have fully cited and referenced all material and results that are not original to this work.

Name, Last Name : Özge YAZICIOĞLU

Signature :

ABSTRACT

EXPERIMENTAL INVESTIGATION OF THE AGITATION OF COMPLEX FLUIDS

YAZICIOĞLU, Özge

M.Sc. Department of Chemical Engineering

Supervisor: Asst. Dr. Yusuf Uludağ

July 2006, 159 pages

In this study, agitation of solutions using different impeller and tank geometry were investigated experimentally in terms of hydrodynamics, macromixing time and aeration characteristics. In the first set of experiments a cylindrical vessel equipped with two types of hydrofoil and a hyperboloid impeller or their combinations were used. Vessel and impeller diameters and water level were 300, 100 and 300 mm, respectively. At the same specific power consumption, 163 W/m^3, the so called "hydrofoil 1" impeller provided the shortest mixing time at 7.8 s. At the top hydrofoil 1 impeller submergence of 100 mm, the hyperboloid impeller combination of it was the most efficient by a mixing time of 10.0 s at 163 W/m^3. Ultrasound Doppler velocimetry and the lightsheet experiments showed that the hydrofoil 1, hydrofoil 2 impellers and the stated impeller combination provided a complete circulation all over the tank.

Macromixing measurements were performed in square vessel for Generation 5 low and high rib and Generation 6 hyperboloid impellers. Vessel length, impeller diameters and water level were 900, 300 and 450 mm, respectively. At the same

specific power consumption, 88.4 W/m^3, Generation 6 mixer provided the lowest mixing time at 80.5 s.

Aeration experiments were performed in square tank for Generation 5 low rib and Generation 6 hyperboloid impellers equipped with additional blades. With increasing flow number, the differences between the performances at different rotational speeds became smaller for each type of mixer. At similar conditions the transferred oxygen amount of Generation 6 impeller was about 20% better.

Keywords: Macromixing time, ultrasound Doppler velocimetry, light sheet, hydrofoil impeller, hyperboloid impeller, aeration, oxygen transfer

ÖZ

KOMPLEKS SIVILARIN KARIŞTIRILMASININ DENEYSEL OLARAK İNCELENMESİ

Yazıcıoğlu, Özge

Yüksek Lisans, Kimya Mühendisliği Bölümü

Tez Yöneticisi: Asst. Dr. Yusuf ULUDAĞ

Temmuz 2006, 159 sayfa

Bu çalışmada, solüsyonların karıştırılması değişik karıştırıcı ve tank geometrileri kullanılarak hidrodinamik, makrokarıştırma zamanı ve havalandırma karakteristiği açısından incelenmiştir. Deneylerin ilk bölümünde iki hidrofoil ve bir hiperboloid karıştırıcı ve bunların kombinasyonları kullanılmıştır. Tank ve karıştırıcı çapları ve su seviyesi sırasıyla 300, 100 ve 300 mm'dir. Aynı spesifik güç harcamasında (163 W/m^3) hidrofoil 1 karıştırıcısının 7.8 s ile en az karıştırma zamanını sağladığı belirlenmiştir. Üst hidrofoil 1 karıştıcının su yüzeyinden 100 mm alçakta olduğu durumda, hiperboloid kombinasyonunun 163 W/m^3'lik spesifik güç tüketiminde 10.0 s'lik karıştırma zamanı ile en verimli konfigürasyon olarak belirlenmiştir. Ultrasonik Doppler hızölçüm ve ışık kesiti deneyleri hidrofoil 1, hidrofoil 2 karıştırıcılar ve belirtilen karıştırıcı kombinasyonunun tüm tankta tam bir sirkulasyon sağladığını göstermişlerdir.

Makro karıştırma ölçümleri kare tankta, 5.nesil alçak ve yüksek damarlı ve 6. nesil hiperboloid karıştırıcılar için gerçekleştirildi. Tank ve karıştırıcı çapları ve su seviyesi sırasıyla 900, 300 ve 450 mm'dir. Aynı spesifik güç harcamasında (88,4

W/m^3) 6. nesil hiperboloid karıştırıcısının 80,5 s ile en az karıştırma zamanını sağladığı belirlenmiştir.

Havalandırma deneyleri kare tankta ilave bıçaklı 5. jenerasyon (alçak damarlı) ve 6. jenerasyon hiperboloid karıştırıcılar için gerçekleştirildi. Akış numarası yükseldikçe her bir karıştırıcı için değişik dönme hızlarında performanslar arasındaki fark azalmaktadır. Benzer şartlarda 6. jenerasyon karıştırıcının aktarılan oksijen miktarı açısından 5. jenerasyon (alçak damarlı) karıştırıcıya göre % 20 civarında daha yüksek olduğu belirlenmiştir.

Anahtar Kelimeler: Karıştırma zamanı, ultrasonik Doppler hız ölçümü, ışık kesiti, hidrofoil karıştırıcı, hiperboloid karıştırıcı, havalandırma, oksijen transferi

To my parents,

ACKNOWLEDGEMENTS

I wish to express my deepest gratitude to my thesis supervisors Assoc. Prof. Yusuf Uludağ for all his understanding, patience, support and sound advice in all aspects of my research work. I am very much obliged for his objective attitude, creating very pleasant working conditions.

I should mention, Korhan Erol, Çiğdem Çuhadar, Walter Steidl, Ute Pirner, Ursula Fink, my laboratory mate Ahmed Nassar, my dear parents Suzan and Yılmaz Yazıcıoğlu and my dear sisters Eylem and Ezgi Yazıcıoğlu, and many others that I could not mention here, who gave me helpful suggestions for the improvement of the document and moral support.

I would like to thank Dr. Marcus Höfken for providing me the opportunity to work at Invent Umwelt-und Verfahrenstechnik AG's laboratories.

Thanks are due to all the staff of Invent Umwelt und Verfahrenstechnik AG and Chemical Engineering Department.

TABLE OF CONTENTS

LIST OF TABLES

TABLES

LIST OF FIGURES

FIGURES

LIST OF SYMBOLS

a : Specific interface area, 1/m

a, b : Constants, [-]

A : Gas liquid interface area, m^2

Ar : Archimed number, [-]

b_{blade} : Length of impeller blade (Hydrofoil Impellers), m

b_{hub} : Length of impeller hub (Hydrofoil 2 Impeller), m

B : Baffle length, m

c : Sound velocity, m/s

c_L : Concentration in the liquid phase, kg/m^3

c_s : Saturation concentration, kg/m^3

$c_{s,20}$: Saturation concentration at 20°C, kg/m^3

C : Distance of the baffle to the tank wall, m

C : Time dependent tracer concentration, mol/l

$\overline{C}$: Final tracer concentration, mol/l

C_{speed} : Speed coefficient, m/(s *Hz)

d : Impeller diameter, m

D : Tank diameter, m

D : Diffusion coefficient, cm^2/s

D_M : Molecular diffusivity, m^2/s

D_T : Turbulent diffusivity, m^2/s

e : Specific power consumption, W/kg

f_D : Doppler shift, Hz

f_0 : Transmitting frequency, Hz

F_{prf} : Pulse repetition frequency, [kHz]

Fl : Primary flow number, [-]

Fl_c : Secondary flow number, [-]

Fr : Froude number, [-]

g : Accelaration of gravity, m/s^2

h_w : Water height in the aeration tank, m

H : Henry's constant, bar

H_i : Water height in the tank, m

J : Diffusion flux, mol/m^2s

k : Turbulent kinetic energy, m^2/s^2

k_L : Global mass transfer coefficient obtained from the liquid side, m/s

k_La : Overall mass transfer coefficient, 1/s

K_i : Constant, [-]

l_{blade} : Width of the impeller blade (Hydrofoil Impellers), m

l_{hub} : Width of the hub (Hydrofoil 2 Impeller), m

l_k : Width of the impeller blade (Hydrofoil Impellers), m

l_t : Width of the impeller blade (Hydrofoil Impellers), m

l : Length of square tank, m

l_κ : Kolmogoroff length scale, m

l_T : Turbulent length scale, m

L : Characteristic length scale, m

M : Mixing grade, [-]

$\dot{M}$: Mass flow rate, kg/h

n : Rotational speed, 1/s

Ne : Newton number, [-]

Ne_{turb} : Turbulent Newton number, [-]

OA : Oxygen utilization efficiency, %

OC : Oxygen supply, [kg/h]

p : Pressure, [bar, Pa]

p : Depth of the particle, m

p_i : Partial pressure of component i, bar, Pa

P : Power, W

P_{max} : Maximum measurable depth, m

R : Universal gas constant (=8.31451), J/mol K

Q : Volumetric flow rate discharged from impeller tip, m^3/h

Q_c : Volumetric flow rate of the bulk of in the mixing tank, m^3/h

Q_A : Air flow rate, m^3/h

S : Baffle thickness, m

t : Time, s

t_d : Time delay between transmitted and received signal, s

t_I : Integral length scale, s

t_M : Characteristic time for mixing due to molecular diffusion, s

t_T : Characteristic time for mixing due to turbulent diffusion, s

T : Temperature, °C

T : Torque, Nm

T_{meas} : The measurement time for a single averaged profile, ms

T_{samp} : Time between stored profiles, ms

T_{si} : The time delay, ms

Tu : Turbulence intensity, [-]

u_{eff} : Effective value of the fluctuation velocity (RMS-Value), m/s

u_i : Fluctuation velocity, m/s

u_τ : Wall shear stress velocity, m/s

U_i : Flow velocity, m/s

U_{tip} : Impeller tip velocity, m/s

V : Tank volume, m^3

V : Velocity (in ultrasound), m/s

V_{max} : Maximum measurable velocity component, m/s

w_{blade} : Blade thickness, m

W : Diameter of the shaft, m

We : Weber number

x : Distance of scattering particle from transducer, m

Z : Impeller clearance, m

Greek Letters

α : Boundary layer factor, m/s

β : Mass transfer coefficient, m/s

δ : Phase shift (in ultrasound), [-]

ΔT : Averaged profile measuring time, s

ε : Energy dissipation rate, m^2/s^3

η_E : Pumping rate

θ : Surface renewal time in aeration, s

θ : Ultrasound wave incidence angle, °

θ : Mixing time, s

λ : Taylor microscale, [-]

λ : Ultrasonic wavelength, m

Λ : Macroscale in mixing, m

μ : Dynamic viscosity, Pa.s

μ_c : Continuous gas phase viscosity, Pa.S

υ : Kinematic viscosity, m^2/s

ρ : Liquid density, g/cm^3

ρ_c : Continious gas phase viscosity,kg/m^3

σ : Surface tension, Pa

τ : Kolmogoroff microscale, [-]

τ : Shear stress acting on bubble, Pa

τ_{turb} : Turbulent shear stress, Pa

CHAPTER I

INTRODUCTION

Agitation is one of the most important unit operations in chemical process and allied industries. The overall energy requirement of these processes forms a significant part of the total energy and contributes toward major expenses. Fluid mechanics prevailing in the mixers is complex, and hence the design procedures have been empirical. Empirical correlations normally lead to significant overdesign and result in inflated fixed and operating costs as well as in extra start-up times. Further, the empiricism does not give rational answers to the debottlenecking problems. Therefore, reliable procedures are needed for the design of mixing equipment. In view of this, several attempts have been made in the past, particularly during the last 35 years, to understand the mixing phenomena both experimentally and theoretically (Nere, Patwarhan, and Joshi, 2003).

Major mixing applications of agitation are listed in Table 1.1. They are blending (miscible liquids), liquid-solid, liquid-gas, liquid-liquid (immiscible liquids), and fluid motion. There are also four other categories that occur, involving three or four phases. One concept that differentiates between mixing requirements originates from physical criteria listed in the second column of Table 1.1, in various definitions of mixing requirements can be based on these physical descriptions. The other category in Table 1.1 involves chemical and mass-transfer criteria in which rates of mass transfer or chemical reaction are of interest and have many more complexities in expressing the mixing requirements (Perry and Green, 1999).

Table 1.1 Classification System for Mixing Processes (Perry and Green, 1999)

Physical	**Components**	**Chemical, mass transfer**
Blending	Blending	Chemical Reactions
Suspension	Solid-liquid	Dissolving, precipitation
Dispersion	Gas-liquid Solid-liquid-gas	Gas absorption
Emulsions	Liquid-liquid Liquid-liquid-solid Gas-liquid-liquid Gas-liquid-liquid-solid	Extraction
Pumping	Fluid Motion	Heat transfer

Mixing processes used for suspending and dispersing operations are mainly employed by waste water treatment plants. When a 24 hour working water treatment plant is considered, the energy spent for a single agitator becomes significant. It can be said that more than two third of the energy is consumed for the mixing and aeration part of a waste water treatment plant. Therefore, it is crucial to lower the mixing time and power consumption with innovative agitation technology.

Mixers are employed in waste water treatment plants for suspending the sewage sludge flocks. To lower the consumption of energy and also the operational costs, hyperboloid mixers have been developed. This mixer is distinguished from other mixers by its form and close clearance installation. It is therefore efficient in suspending the precipitated sludge particles with the strong bottom flow they produce. This mixer is also particularly suitable for the small treatment plants, because when required even the smallest treatment plant can be stirred and aerated at the same time. The application of it to small plants is recommended,

especially for isolated places or for coastal regions, because the building long pipelines turns out to be unprofitable for such places (Steidl, 1995).

New design hydrofoil type impellers are also used in waste water treatment plants because of the strong axial flow they produce. These types of impellers are also used for suspending purposes. Especially, the hyperboloid and hydrofoil combinations produce a strong top to bottom flow, and are usually used in water treatment plants.

A good example of the gas absorption process (Table 1.1) which is accomplished by the mixing process is the aeration systems in waste water treatment plants. The dirtiness degree of the waste water discharged to the communal clarification plants is characterized through BOD_5 (**B**iological **O**xygen **D**emand for 5 days) value. This value forms the basis for the design and dimensioning of the required oxygen entry for the biological degradation process of the organic part of the waste water. Lowering the biological oxygen demand (BOD) and increasing the dissolved oxygen (DO) level is achieved through the aeration systems in waste water treatment plants.

The type of flow in an agitated vessel depends on the type of the impeller; the characteristics of the fluid; and the size and proportions of the tank, baffles and agitator. For a processing vessel to be effective, regardless of the nature of the agitation problem, the volume of fluid circulated by the impeller must be sufficient to sweep out the entire vessel in a reasonable time. Also, the velocity of the stream leaving the impeller must be sufficient to carry the currents to the remotest parts of the tank. In mixing and dispersion operations the circulation rate is not the only factor, or even the most important one; turbulence in the moving stream often governs the effectiveness of the operation. Turbulence results from properly directed currents and large velocity gradients in the liquid. Circulation and turbulence generation both consume energy. Although both flow rate and power dissipation increase with stirrer speed, selection of the type and size of the impeller influences the relative values of flow rate and power dissipation (McCabe, Smith and Harriot, 1993).

A rotating impeller, which requires direct energy input, is the most important part of the typical mixing equipment. The efficiency of the mixing process depends on the design of the impeller (blade number, shape, and size). Also, the location of the impeller (off-bottom clearance, distance from the vessel center, i.e., eccentricity) and its size relative to the vessel have a profound impact on the flow pattern and the mixing efficiency thereof (Nere, Patwarhan, and Joshi, 2003).

One of the objectives of this study is to investigate the efficiency of the hydrofoil and hyperboloid impellers, as well as combinations of these, in the cylindrical tank by power consumption and macromixing measurements. The conductivity technique was used to determine the macromixing characteristics of the impellers. This technique employs a probe which measures the conductance of the salt solution as a function of time that can be converted to a concentration versus time scale using calibration of the conductivity device.

Nere et al. (2003) emphasizes that extensive studies should be carried out in the case of hydrofoil impellers. In this respect, this study will make a contribution to the literature for the case of hydrofoil impellers. The investigations of the combination of hydrofoil impellers with hyperboloid impellers will also be an interesting contribution to the multiple impeller studies, e.g. to the work of Gao et al. (2003) who investigated the macromixing characteristics of multiple hydrofoil impellers.

The flow fields produced by the impellers in the cylindrical tank were determined by the modern ultrasonic measuring technique, the so-called Ultrasonic Doppler Velocimetry (UDV). Apart from determining the flow fields, locally produced turbulence by the impellers could also be determined, so that conclusions for the locally dissipated energy could be made. Lightsheet experiments, by which the flow in the agitated tank can be visualized, were also performed for the cylindrical tank. This combination of flow measuring technique and the visualization of the flow itself permits a plastic illustration of the flow conditions in the agitated tank and thus lead to a deeper understanding of the flow field produced by the impellers. UDV and lightsheet techniques, which are non-

invasive and non-destructive, enabled direct visualization of complex flow field in the agitated tanks. Therefore assessment of the agitation quality was possible using the flow pattern in terms of circulation structure and dead volumes.

Another objective of this study is to investigate the efficiency of different types of hyperboloid impellers, by macromixing measurements in a square tank, whose geometry has been extensively employed in waste water treatment.

Two different hyperboloid mixers designed for aeration purposes were also examined for their aeration characteristics in a stirred tank. The mixers were provided with an aeration ring and the DO (**D**issolved **O**xygen) measurements were performed in the stirred tank.

CHAPTER II

THEORETICAL BASICS OF MIXING AND AERATION

In this chapter theoretical basics of mixing and aeration in an agitated tank are given. In the following parts, first the general properties of turbulent flow are explained briefly, since typical agitation processes involve turbulent flow field. Further the power consumption characteristics of an agitated tank as well as the dimensionless numbers that are necessary and important in agitation are given. Information about mixing will be followed with the part where the macromixing and impeller characteristics are explained. Finally, theoretical basics of mass transfer in aeration will be explained.

2.1. Turbulence and Flow Field in Agitated Tanks

2.1.1. General Properties of Turbulent Flow

Most of the flows that are common in industrial applications including agitation are of turbulent type. Therefore it is beneficial to review general characteristics of turbulence to understand the agitation process. In this section basics of the turbulent flow in agitated tanks are described briefly based on various researchers' works.

Turbulence can result either from contact of a flowing stream with solid boundaries or from contact between two layers of fluid moving at different

velocities (McCabe, Smith and Harriot, 1993). Turbulent flows have the following properties:

- A flow is called turbulent when it passes the limit Re_{crit}. If the Reynolds number is smaller, the turbulence motions will be damped by frictional forces.
- Turbulent flows dissipate energy as heat, that is, the energy must be given from the outside for the fluctuating turbulent motions to prevail.
- The smallest element of a turbulent flow itself is large compared to the length of the free path of the molecule. The equations of continuum mechanics also apply for turbulent flows.
- Turbulent flows are three dimensional, friction containing eddy flows, in which the inner friction play an important role for the formation of the boundary layer contained in the eddies (Strauss, 1991).
- Altough the smallest eddies contain about 10^{12} molecules, all eddies are of macroscopic size, and turbulent flow is not a molecular phenomenon.
- Turbulent flow consist of a mass of eddies of various sizes coexisting in the flowing stream. Large eddies are continually formed. They break down into smaller eddies, which in turn evolve still smaller ones. Finally, the smallest eddies disappear (McCabe, Smith and Harriot, 1993).
- Mechanisms of turbulent flows are accidental, that is for the investigation of such flows one should be leaded by statistical methods (Strauss, 1991).

Nagata (1975) explained the basic skeleton of the theory of turbulence primarily from the book of Hinze (1959): The turbulence in a mixing vessel may not be homogeneous, but the theory of local isotropy proposed by Kolmogoroff (1941) may be applicable in general. Though the velocity and pressure at a certain point in a turbulent field fluctuate irregularly, turbulence may be expressed as a statistically continuous function with respect to time and space. Taylor (1935) has shown that the Fourier transform of velocity correlation between two adjacent points corresponds to an energy spectrum function which covers the various scales of turbulence (Nagata, 1975).

The fluid in a turbulent flow can be considered as consisting of lumps and eddies. The largest eddies have sizes of the same order of magnitude as the largest length scale of the process equipment (vessel or impeller size, L), whereas the smallest eddies are such that viscous dissipation takes over and these smallest eddies are dissipated into heat. Kolmogoroff length scale is characterized by $\mathrm{Re}_\kappa = l_\kappa u_\kappa / \upsilon \sim 1$. The size of the smallest eddy is denoted by l_κ. The value of l_κ depends on the turbulent energy dissipation rate per unit mass and the kinematic viscosity of the fluid and is given by $l_\kappa = \left(\upsilon^3 / \varepsilon\right)^{1/4}$. There exists a whole range of eddy sizes between L and l_κ, and this is usually represented by an energy spectrum. Tennekes and Lumley (1972) have given an excellent review of the structure of turbulence, the eddy sizes, their interrelations, the energy spectra, etc. Brodkey (1966) has reviewed various aspects of turbulent motion and its influence on mixing. Molecular diffusion takes place at the Kolmogoroff scale and causes homogeneity at the scale of the smallest eddy, while eddy diffusion is responsible for the transport of material at all of the scales. The different size of eddies have different lifetimes. Depending on the velocity, size, and lifetime, different eddies cause eddy dispersion to different extents. All of these factors have to be taken into account while quantifying eddy diffusion, and such a detailed analysis of the eddy dispersion process is extremely complicated. To overcome these difficulties, eddy diffusion is usually characterized in terms of eddy diffusivity. Eddy diffusion or molecular diffusion, which is described in terms of diffusivity, is characterized by the corresponding diffusion time. For molecular diffusion, the characteristic time is given as $t_M = l_\kappa^2 / D_M$. Similarly the characteristic time for eddy diffusion is $t_T = l_T^2 / D_T$. If the diffusivities are known, then the mixing time θ_M or θ_T can be estimated (Nere, Patwarhan, and Joshi, 2003).

In the turbulent flow range, macro scale eddies, which contain a larger part of the turbulence energy, and micro scale eddies which contribute to the viscous dissipation overlap with each other and give complicated effects upon various phenomena in the mixing vessel. The larger eddies contain much less energy than the smaller ones and reach only 20% of total kinetic energy at most. Eddies

which make contribution to the total kinetic energy of turbulence, are called the energy containing eddies. The smallest eddies fluctuate and dissipate much more rapidly than the large energy containing eddies (Nagata, 1975).

In a typical turbulent flow, large eddies continuously break into the smaller ones and eventually become small enough to be dissipated by viscous effects. Energy must then be continuously provided to the flow to maintain the turbulence. In agitation energy is delivered to the tank content by means of impellers.

Brodkey (1966) states that any motion which might have a regular periodicity is not considered to be turbulent. The instantaneous velocity at a point can be represented by its average value and superimposed fluctuation:

$$U_i(t) = \overline{U_i} + u_i'(t) \tag{2.1}$$

Instead of the velocity fluctuation usually the effective value, root-mean-square (r.m.s.) value, of it is used:

$$u_{eff} = \sqrt{\left(\overline{u'^2}\right)} \tag{2.2}$$

The relation between the effective value of the velocity fluctuation u_{eff} and the time averaged velocity $\overline{U_i}$ can be called turbulence intensity Tu:

$$Tu = \frac{\sqrt{\overline{u_i'^2}}}{\overline{U_i}} \tag{2.3}$$

Turbulence intensity refers to the speed of the rotation of eddies and the energy contained in an eddy of a specific size (McCabe, Smith and Harriot, 1993).

2.1.2. Important Dimensionless Numbers in Mixing

Throughout the application of dimensional analyses to the problems in the agitation technology, it is observed that the dimensionless numbers enable the information obtained in the laboratory scale to be transferred to the industrial large scales. When the geometrical similarity is provided and the all the dimensionless numbers are constant, the behavior of the operation at different sizes is also similar. A further advantage of working with dimensionless numbers is the independency of represented relations from the measure (Steidl, 1995). In the following the most important dimensionless numbers concerning typical agitation and mixing processes are given:"

Reynolds Number

The Reynolds number is determined from the ratio of inertial forces to viscous force of the fluid. In fluid mechanics Reynolds number plays an important role in the characterization of the flows. In the agitation technology, Reynolds number is formed mainly with the mixer diameter d, tip speed U_{tip} and kinematic viscosity υ:

$$Re = \frac{U_{tip} \cdot d}{\upsilon} = \frac{n \cdot \pi \cdot d^2}{\upsilon} \qquad (2.4)$$

If the Reynolds number is > 10^4, a fully turbulent agitator flow occurs. With the Reynolds number < 100, flow becomes laminar. Within the region 100 < Re < 10^4, the flow field in the tank exhibits transition characteristics.

Froude Number

Another important dimensionless number for characterization of the flow in a stirred tank is the Froude number. It is the ratio of the inertial forces to gravity.

$$Fr = \frac{n^2 \cdot d}{g} \tag{2.5}$$

Archimed number

It is given by the following:

$$Ar = \frac{Re^2}{Fr} \tag{2.6}$$

Newton Number

The Newton number Ne is the ratio of the agitator power P and the actual power spent in the fluid:

$$Ne = \frac{P}{\rho \cdot n^3 \cdot d^5} \tag{2.7}$$

It is depended on the stirred tank configuration and the Reynolds number. In the turbulent region it remains nearly constant for a given tank configuration.

2.1.3. Power Consumption in Turbulent Mixing

Power draw is the energy per time which is transferred from the impeller to the fluid. It is an integral quantity fundamental to mixing and dispersion processes since energy is needed to cause the fluid motion necessary for mixing. For single phase turbulent flow, power calculation has been mainly approached through dimensional analysis and experimental measurement of torque.

Power basically has the same fundamental units as the product of $\rho, n^3,$ and d^5. The dimensionless group for turbulent flow is typically $P/\rho n^3 d^5$ and is called the power number. For an agitated tank, a traditional relationship for power in the form of a series of assumed power laws can be written as:

$$\frac{Pg_c}{\rho n^3 d^5} = K\left(\frac{\rho n d^2}{\mu}\right)^a \left(\frac{n^2 d}{g}\right)^b \left(\frac{D}{d}\right)^c \left(\frac{Z}{d}\right)^d \ldots\ldots \qquad (2.8)$$

where a, b, c, d and K are constants.

The first dimensionless group is the impeller Reynolds number, the second is the Froude number, and the rest accounts for the effects of geometry (i.e., impeller clearance and baffle width) which includes number of effects (i.e., number of blades, baffles and impellers) (Tatterson, 1991).

Turbulent flow is required, in order to obtain a high mixing grade of solutions, except the high viscosity ones like pastes, in stirred tanks. In order to achieve a high mixing grade standard baffled vessels are widely used.

Ciofalo et al. (1996) have explained the necessity for baffles as follows: If the baffles which characterize the standard geometry are not supplied, the liquid tends to move mainly along circular trajectories, resulting in small relative velocities between impeller and fluid and weak radial flows directed towards the

tank walls. Installation of the baffles effectively destroys the circular liquid patterns, inhibiting the vortex formation so that the liquid surface becomes almost flat. Moreover, axial flows become much stronger, leading to an improved mixing rate.

Working with turbulent flow in baffled tanks requires a high power input. In this respect, determination of the two important values; power consumption and mixing time is important. Experimental and predictive studies most of which are focused on baffled tanks have been carried out in order to determine the stirred tank characteristics.

In most of the experimental studies flow field in a stirred tank is measured in details by the laser Doppler velocimetry (LDV) technique. Some of the researchers who employed this technique for the investigation of stirred tanks are Costes and Couderc (1988), Wu and Patterson (1989), Ranade and Joshi (1990), Schäfer et al. (1997). Ultrasound Doppler velocimetry (UDV) has also been employed by various researchers for the investigation of stirred tank hydrodynamics, for example, Bouillard et al. (2001), Brito et al. (2001) and Steidl (1995).

Computational Fluid Dynamics (CFD) technique is a cost effective design tool which is also employed to study the turbulent flow in stirred vessels. However turbulence and agitation are so complex in nature that this technique needs to be much more developed possibly with high performance computing techniques, but still, it remains as a challenging task.

Armenante et al. (1997) have stated that validation of CFD as a predictive tool requires comparison of the numerical results with experimental velocity data. He has added that most of the CFD work carried out to date, as far as flow in mixing vessels is concerned, has been centered on applications dealing with baffled vessels. Some of the predictions which have been presented are the studies of Schäfer et al. (2004), Armenante et al. (1997), Ciofalo et al. (1996) and Kresta and Wood (1993).

2.1.4. Macromixing and Mixing Time

The process of mixing occurs as a result of the motion at three levels: molecular eddy and bulk motion. The molecular motion of individual species reduces the concentration differences, and the process is known as molecular diffusion. Mixing on this level is called micromixing. Improper micromixing leads to segregation (Levenspiel, 1991). If the stirred reactor is operated under turbulent conditions, then there is a motion of a chunk of molecules or eddies. The eddy motion also gives rise to material transport and is called eddy diffusion or dispersion. The bulk motion or the convective motion also has a property of providing spread of materials needed for mixing. Usually, the bulk motion is superimposed on either molecular or eddy diffusion or both. Mixing on this scale is called macromixing (Nere et al., 2003). In this study, it is mainly dealt with the large scale liquid-phase turbulent mixing, that is, macromixing.

The macromixing or blending time is the time required to mix the freshly entering material with the contents of the whole vessel (www.scientificupdate.co.uk/pdfs/generic_pdfs/mixing.pdf, 2006). It corresponds to a macroscopically determined mixing time if the macromixing time is much longer than the micromixing time. In the turbulent regime this condition is satisfied (Schäfer, 1999).

As stated above macromixing time (θ) is the time required for the response at a defined point to reach the required percent (mixing grade) of the total change following a pulse injection. The mixing grade (M) is defined by the following equations:

$$M = 1 - \frac{\Delta C}{\overline{C}} \tag{2.9}$$

$$\Delta C = 2\left|C - \overline{C}\right| \tag{2.10}$$

where C is the time dependent tracer concentration and $\overline{C}$ is the final tracer concentration. The macro mixing, referring to the value M=95 %, is terminated as soon as $\Delta C \leq 0.1$ is observed.

For the determination of the macromixing time, there are different methods that have already been applied. With physical measuring processes mixing grade up to 95% can be reached in rule. On the other hand chemical measuring methods provides the measurement of a whole mixing grade in the mixing tank. The measured mixing time is dependent on the conditions of the experiment. Especially, the dimension of the measuring probe, according to which the dimensions of the volume element is determined, has an effect on the determination of the concentration fluctuations. A detailed discussion on the mixing grade and mixing time determination can be found in Hiby (1979) and Nere et al. (2003). Different measuring processes have been analysed in Mann et al. (1997) and Nere et al. (2003). In this study macromixing times were determined by conductivity measurements, in which a conductivity probe is employed to measure the conductivity change in the stirred tank. A typical conductivity change set up is depicted in Figure 2.1 along with typical concentration versus time response. Here the mixing time, θ denotes the point at which $\Delta C \leq 0.1$ condition is met.

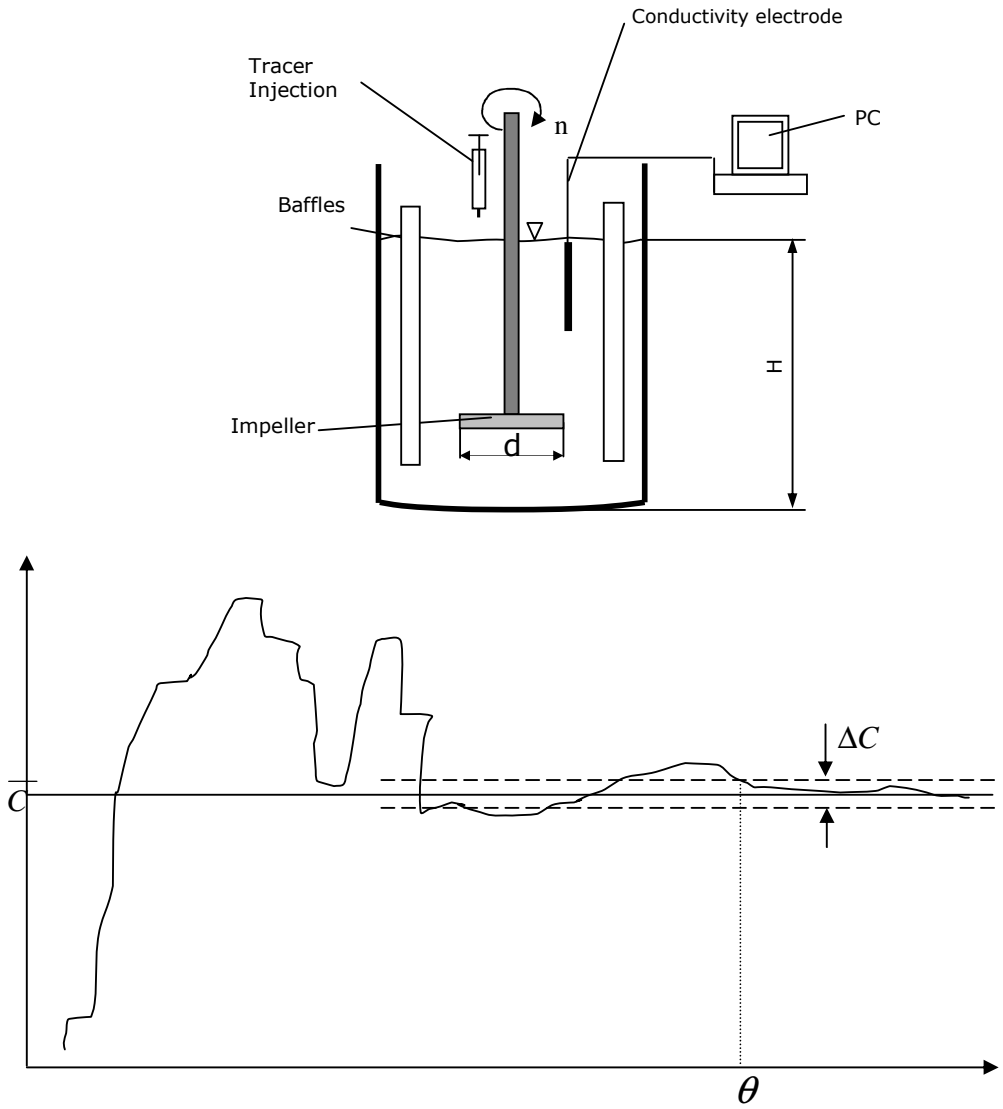

Figure 2.1 Macromixing time set-up and macromixing curve

2.1.5. Homogenization and Discharge Characteristics of the Impellers

When the Reynolds number is not small, discharge flow from the impeller generates vertical circulation flow and gives a mixing action. The impellers can be compared according to their discharge efficiency. The volumetric flow rate is proportional to nd^3 in the completely turbulent range (Nagata, 1975).

The mixing time which can be achieved by one mixer depends on the properties of the fluid, diameter of the impeller and the rotational speed for a given geometry. A dimesionanalytic investigation of this dependency provides the homogenization characteristic, which is the process relationship between the dimensionless mixing time –or homogenization- number $n\theta$ and the mixing Reynolds number Re.

Zlokarnik (1967) investigated the typical homogenization characteristic for different inversely reversely proportional to the Reynolds number (i.e., $n\theta \propto 1/\mathrm{Re}$) in laminar flow region for all types of impellers except the helical impeller.

In turbulent region, the dimensionless mixing time numbers have constant values for the Reynolds numbers larger than 10^3-10^4. The value of this constant depends on the form of the impeller and on the diameter relationship d/D.

The homogenization characteristic is closely related to the pumping and circulation efficiency of the mixers. The pumping power of the mixer is determined from the standardized pumping rate which is called the primary flow number. It is obtained from the mixer generated volumetric flow rate, Q, which is the total flow leaving the impeller, measured at the tip of the blades:

$$Fl = \frac{Q}{nd^3}. \qquad (2.11)$$

Fl gives the discharge flow from the tips of the impeller and not the total flow produced. The high-velocity stream of liquid leaving the tip of the impeller entrains some of the slowly moving bulk liquid, which slows down the jet but increases the total flow rate. The amount of the bulk fluid is greater than the amount discharged from the impeller tips ($Q_C > Q$). The entrainment is considered in the secondary flow number, which is obtained from the circulation flow:

$$Fl_C = \frac{Q_C}{nd^3}. \qquad (2.12)$$

A general overview of the pumping rates can be found in Tatterson (1991) and Fentiman et al's (1998) works.

The circulation characteristics are often used to forecast the mixing time. The detailed information for the formulation of circulation models can be found in Khang et al. (1976) and Nienow (1997).

2.1.6. Mixing and Pumping Efficiency of the Impellers

Evaluation of the mixing and pumping efficiency of the impellers requires information about the power input as well as the dimensionless pumping, discharge and mixing time number data. Power characteristics of the impellers describe a process relation between the power input and Reynolds number. The Newton number remains constant in turbulent conditions, where the effect of resistance can be neglected. A summary of the Newton number of different types of impellers can be found in Tatterson's (1991) work.

A relation between the pumping rates with the Newton number yields the pumping efficiency of the impellers. The better the pumping efficiency, the less power is required for pumping the same volumetric flow. The pumping efficiency for impellers can be defined as follows:

$$\eta_{E1} = \frac{Fl_1^{\,3}}{Ne}\left(\frac{d}{D}\right)^4 \tag{2.13}$$

A second dimensionless number for the secondary pumping rate is:

$$\eta_{E2} = \frac{Fl_2^{\,3}}{Ne}\left(\frac{d}{D}\right)^4 \tag{2.14}$$

It is more reasonable to compare the impellers on the basis of η_{E2}, because total convective fluid transport and the energy input are considered in this case (Schäfer, 1990).

2.2. Aeration

The agitation of gas-liquid systems has much application in physical and chemical gas absorptions, for example, aerobic fermentation, waste water treatment, catalytic hydrogenation of vegetable oils and oxidation of hydrocarbons. In gas-liquid agitation, the following items must be considered:

- The state of dispersion, i.e., the size distribution of bubbles
- Gas hold-up and retention time in vessel
- Dispersion and coalescence of gas bubbles

- Convection currents and degree of backmixing
- Mass transfer across the interface of gas and liquid (Nagata, 1975).

2.2.1. Theoretical Considerations

Let us denote the diameter of gas bubbles by d_p, shear stress acting on the bubbles by τ , and the viscosity, density and interfacial tension by μ, ρ and σ, respectively. Suffixes show the dispersed phase and the continuous phase respectively. Forces acting on gas bubbles are: Shear stress, τ and surface tension, σ / d_p. When these two forces are equal, bubbles are in equilibrium size. Therefore the maximum diameter of bubbles is determined by the ratio of these forces, the Weber number:

$$We = \frac{\tau d_p}{\sigma}. \tag{2.15}$$

For bubbles ascending an descending in liquids, the ratio of lifting or settling force ($(1/6)\, d_p \Delta\rho g$) and surface tension is involved, and the We-number has the form:

$$We = \frac{{d_p}^2 \Delta\rho g}{6\sigma}. \tag{2.16}$$

Concerning the dispersion of gases in mixing vessels, the shear stress due to turbulence must be considered. The primary eddies produced by impellers have scale (L) of similar magnitude to the dimension of the main flow. The large primary eddies until finally their energy is dissipated into heat by viscous flow. According to Kolmogoroff's theory on the local isotropy, the scale (l_κ) of the smallest eddies where the energy dissipation may occur is expressed by:

$$l_\kappa = \frac{\mu_c^{3/4}}{\rho_c^{1/2}} (P/V)^{-1/4} . \qquad (2.17)$$

2.2.2. Mass transfer in aeration

For the evaluation of the efficiency of aeration system in terms of mass transfer the aeration coefficient $k_L a$ is used.

This system dependent constant can be determined with the help of theoretical derivations and empirical experiments where the considerable parameters are reduced. According to the theory of Higbie (1935) the following relation is given for the aeration coefficient:

$$k_L a = 2 \cdot \frac{A}{V} \sqrt{\frac{D}{\pi \cdot \theta}} \qquad (2.18)$$

With this formula the parameters for the mass transfer in aeration can be described as follows:

- A : Surface area

With pressurized air the surface A is the sum of the surface area of bubbles present in the tank and of the water surface. The interface area is dependent on the air flow rate and the retention time of the bubbles in the water. It is inversely proportional to the bubble diameter.

- $1/\theta$: Surface renewal time

The velocity of the surface renewal is determined by mobility of the bubble surface area.

- D : Diffusion coefficient of the oxygen in water (temperature dependent)

- V : Volume of the aerated water (constant).

Equation 2.18 is not for practical use for the calculation of the aeration coefficient, since the value of surface area A and the value of the surface renewal time θ are not possible observed. It can be said that the diffusion coefficient as well as the parameters A and θ can be taken as constants at the same waste water temperature.

2.2.2. Parameters for the oxygen transfer and aeration system

In waste water technology a couple of parameters are used for the design and the evaluation of the aeration facilities. Some of these parameters are shortly explained here.

According to the guidelines of ATV (1996), the oxygen supply is given as α-OC-Value which is obtained from the amount of oxygen which is dumped into the waste water per hour:

$$\alpha OC = \frac{kgO_2}{h} \text{ (in waste water)} \qquad (2.19)$$

Since the mass transfer efficiency of aeration systems are mostly examined with clean water because of easier and safer methods, an additional OC value is obtained for clean water conditions:

$$OC = \frac{kgO_2}{h} \text{ (clean water)} \qquad (2.20)$$

The αOC-Value is obtained with the help of the α-Value:

$$\alpha = \frac{\alpha OC}{OC} = f(wastewater, aerationsystem) \qquad (2.19)$$

The α-Value depends on the properties of the waste water and on the aeration system.

The OC-value is also shown as OC_{20}-Value, since it is always obtained from clean water at 20°C. Additionally, the OC_{20}-Value is often obtained from the volume of the sludge activation tank and given in the [kg O_2/m^3h] units. In this respect, OC_{20}-value does not give the required oxygen transfer, instead, it characterizes the possible oxygen transfer of an aeration system (at 20°C in clean water), which should be experimentally determined (Frey, 2000).

CHAPTER III

ULTRASOUND DOPPLER VELOCIMETRY AND LIGHSHEET FLOW VISUALIZATION TECHNIQUES

3.1. UDV TECHNIQUE

There are different non-intrusive flow measurement techniques; these are briefly laser Doppler velocimetry (LDV), ultrasonic Doppler velocimetry (UDV) and nuclear magnetic resonance (NMR). LDV technique has a very high resolution capability and the velocity component of a single particle which is perpendicular to the axis of the light beam is measured. The maximum measurable velocity is not limited and it does not require calibration. It cannot be used in non transparent liquids and it is quite fragile. NMR technique has a high accuracy and allows 2D and 3D measurements however its applications are quite expansive. UDV technique has a lower resolution capability compared to LDV and the velocity component which is in the direction of the axis of the ultrasonic beam is measured. In this technique velocities of a great number of scatterers are measured simultaneously and therefore the mean value of all the particles present in the sampling volume are obtained. The maximum measurable velocity and depth are limited in UDV. It does not also require calibration and contrary to LDV it can be used in non transparent liquids and it is portable.

In UDV, instead of emitting continuous ultrasonic waves as in LDV, an emitter sends periodically a short ultrasonic burst and a receiver collects continuously echoes issues from targets that may be present in the path of the ultrasonic beam. By sampling the incoming echoes at the same time relative to the emission of the bursts, the shift of positions of scatterers are measured (Signal-

Processing SA, 2006). Schematic picture of UDV measurement is given in Figure 3.1.

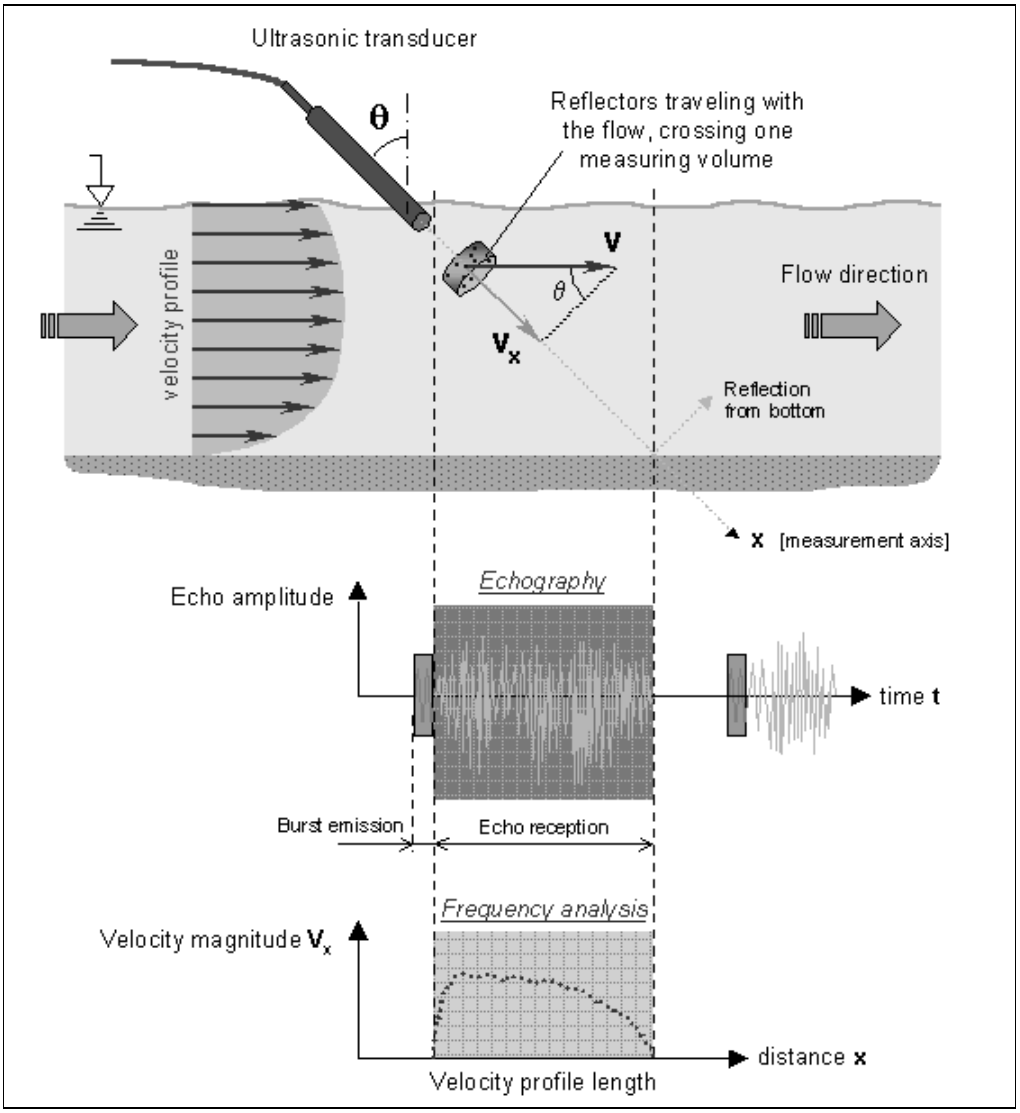

Figure 3.1 UDV measurement on a flow with free surface (Met-Flow SA, 2005).

An ultrasonic transducer transmits a short emission of ultrasound (US), which travels along the measurement axis L_m, and then switches to the receiving mode. When the US pulse hits a small particle in the liquid, part of the US energy scatters on the particle and echoes back. The echo reaches the transducer after a time delay

$$t_d = \frac{2x}{c} \tag{3.1}$$

where t_d is time delay between transmitted and received signal [s], x is the distance of scattering particle from transducer [m] and c is the speed of sound in the liquid [m/s].

If the scattering particle is moving with non-zero velocity component into the acoustic axis L_m of the transducer, Doppler shift of echoed frequency takes place, and received signal frequency becomes 'Doppler-shifted':

$$\frac{v}{c} = \frac{f_d}{2f_0} \tag{3.2}$$

where v is the velocity component into transducer axis [m/s], f_d is the Doppler shift [Hz] and f_0 is the transmitting frequency [Hz].

If UDV succeeds to measure the delay t_d and Doppler shift f_d, it is then possible to calculate both position and velocity of a particle. Since it is presumed that scattering particles are small enough to follow the liquid flow, it can also be presumed that the UDV has established the fluid flow component in the given space point. The basic feature of UDV is the ability to establish the velocity in many separate space points along measurement axis.

Channel width

This is the width of a measurement volume and hence determines the spatial resolution. Channel width is given by formula

$$w = c\frac{n}{2f_0} = \frac{n\lambda_0}{2} \tag{3.3}$$

where w is the channel width [m], n is number of cycles per pulse. In the formula, the 2 in denominator means that once the pulse has reached one end of the measured cylinder it has to cover twice the distance to the other cylinder end to come back at the same point.

Channel distance

This is the distance between two measurement volumes. The channel distance remains constant throughout the measurement window (i.e., channels 0 - 127). It can be varied in integer multiples of the spatial resolution (i.e., channel width) selected.

Overlapping

The "overlapping" phenomenon is literally the overlap of two consecutive measuring volumes due to a channel distance set smaller than the channel width itself, depending on the US burst length.

Measurement window

The measurement window is defined as the distance between channels 0 (starting channel) and 127 (window-end channel). This is given as

$$W = \text{Starting channel} + 127 * \text{channel distance} \quad (3.4)$$

where W is the measurement window length [m]. The window-end position has to be smaller than the maximum depth (that is, maximum depth >= W), so that values are limited automatically when setting the channel distance and starting position.

Maximum depth and Maximum velocity

The maximum measurable depth is determined by the pulse repetition frequency F_{prf}:

$$P_{\max} = \frac{c}{2F_{prf}} \quad (3.5)$$

where $P_{\max}$ is the maximum measurable depth [m] and F_{prf} is the pulse repetition frequency [Hz].

The maximum depth decreases with increasing F_{prf}. Due to the Nyquist sampling theorem related to F_{prf}, the maximum detectable Doppler shift

frequency is limited. This implies that there is a limitation on the maximum velocity that can be measured. This limit is:

$$V_{\max} = \frac{cF_{prf}}{4f_0} \tag{3.6}$$

where $V_{\max}$ is the maximum measurable velocity component [m/s]. From the above two equations, the following constraint can be obtained for this method of measurement:

$$P_{\max} * V_{\max} = \frac{c^2}{8f_0} = const. \tag{3.7}$$

Since for a given measuring situation both c and f_0 are constant, the product $P_{\max} * V_{\max}$ is also constant. This means that, for a given transmitting frequency, we have to compromise between maximum measurable depth, and maximum measurable velocity.

Velocity resolution

We can now determine the velocity resolution. From the equation following equations can be derived:

$$V_{\max} = \frac{c^2}{8f_0 P_{\max}} \tag{3.8}$$

$$\Delta V = \frac{V_{\max}}{127} \tag{3.9}$$

Number "127" originates from 7 data bits used during data processing (plus the 8th bit for sign). When higher resolution is required, $V_{\max}$ must be smaller. This requires that the maximum depth $P_{\max}$ be larger (i.e., F_{prf} be smaller). Table 3.1 summarizes the results for water. It shows theoretical values only; during practical measurement, other limitations apply (e.g. absorption for the maximum measurable distance).

Table 3.1 Maximum Depth and Velocity data for US probes.

f_0 [MHz]	$P_{\max}$ [mm]	$V_{\max}$ [mm/s]	$P_{\max} * V_{\max}$ [mm²/s]	ΔV [mm/s]
0.5	100	5476	547,600	43.1
	750	730.1	547,600	5.7
1	100	2738	273,800	21.6
	750	365.1	273,800	2.9
2	100	1369	136,900	10.8
	750	182.5	136,900	1.4
4	100	684.5	68,450	5.4
	750	91.3	68,450	0.7
8	100	342.3	34,225	2.7
	750	45.6	34,225	0.4
(c = 1480 m/s)				

Doppler Coefficient and the Speed Coefficient

The raw data, which is generated and recorded on the disk, is in units of frequency detected during the measurement time. Thus the Doppler shift frequency f_D can be obtained from the raw data using the formula

$$f_d = rawdata * C_{Doppler} \tag{3.10}$$

where the Doppler coefficient, $C_{Doppler}$, is given by

$$C_{Doppler} = \frac{F_{prf}}{2*128} \tag{3.11}$$

The raw data is the data measured by UDV in internal units. Velocity along beam axis is given by

$$v = C_{speed} \cdot f_d \tag{3.12}$$

and the speed coefficient is given by

$$C_{speed} = \frac{c}{2f_0}. \tag{3.13}$$

where C_{speed} is in the unit [m/(s *Hz) = m]. The data can be converted to a velocity using the formula

$$V = rawdata * C_{Doppler} * C_{speed} * \frac{1}{\sin\theta} \tag{3.14}$$

where θ is the US wave incidence angle normal to the flow [deg].

Flow direction

Since flow direction is detected at all measured positions, the measured data can have both positive and negative values. A positive value means the flow direction is in the beam direction (i.e., moving away from the transducer) and a negative value means the opposite (i.e., moving toward the transducer). It is possible to ignore this function; this being of value when the flow has only a single direction (i.e., no recirculating eddies) and sign detection is not needed. In this case, the 'aliasing' that arises when computing the Doppler shift frequency is corrected, and the maximum detectable velocity is thereby doubled. 'Aliasing' in this case means that two velocities (with the same values but different signs) can exist for a single measured value of 'raw data'. It should be noted that when sign detection is ignored, the constraint condition and the velocity resolution described earlier become:

$$P_{\max} \cdot V_{\max} = \frac{c^2}{4 f_0} \tag{3.15}$$

$$\Delta V = \frac{V_{\max}}{255}. \tag{3.16}$$

This might be very useful in many circumstances. (Again, number "255" originates from 8 data bits used during data processing with no bit necessary for sign).

RF Gain

Since the attenuation of ultrasound in liquid and solid media follows an exponential law, distant particles give weaker echo than particles closer to the transducer. The amplification of the received echo is therefore adjusted so that this attenuation is compensated for. The amplification is time dependent, and is called the gain distribution. The RF gain factor modifies the slope of the gain distribution. The gain distribution can be adjusted by setting its start and end values. Both can be set from factor 1 to factor 9. When both are set at the same value, the distribution is constant (flat). A factor of one is equivalent to 6dB.

US Emission Voltage

Overall amplification gain may also be controlled by changing the strength of ultrasound emission through the change of voltage applied to the transducer (namely US emission voltage). Depending on the kind of liquid, maximum depth, condition of reflectors, etc., these parameters need to be optimized.

Time resolution

The time resolution of the measurement of a single profile is determined by the data acquisition time, which itself depends on the pulse repetition frequency F_{prf} or the maximum depth. It is given by the number of repetitions N_{rep} used in the Doppler shift calculation and:

$$\Delta T = \frac{N_{rep}}{F_{prf}} \tag{3.17}$$

where ΔT is the averaged profile measuring time [s], N_{rep} is the number of profile measurement repetitions (default = 32) and F_{prf} is the pulse repetition frequency [kHz]. Examples are given in the following table which are calculated for c = 1480 m/s (water) and N_{rep} = 32 (default).

Table 3.2 Pmax, Fprf and ΔT values for water

P_{max} [mm]	F_{prf} [kHz]	ΔT [ms]
100	7.4	4.3
200	3.7	8.6
750	0.987	32.4

Measuring time

In principle the time interval between measured profiles is equal to the time resolution ΔT:

$$T_{meas} = \Delta T \,. \tag{3.18}$$

Sampling time

Sometimes it is useful for the user to slow down data acquisition. This can be the case when longer time series are measured and the user wants to limit the data file volume. This is why it is possible to set certain additional delay between measured profiles. Sampling time is then

$$T_{samp} = T_{meas} + T_{si} \tag{3.19}$$

where T_{samp} is the time between stored profiles [ms], T_{meas} is the measurement time for a single averaged profile [ms] and T_{si} is the delay set by user [ms] (Met-Flow SA, 2005).

3.2. LIGHTSHEET FLOW VISUALISATION TECHNIQUE

Applications of light sheet technique are widely used to obtain both quantitative and qualitative information about a flow field in fluid dynamics. This technique provides the visualization of flow along a projected line. In most light sheet applications, different types of lasers, most of which are quite expensive, are used as the light source. The experimental light sheet system is composed of a linear light source, and a camera recorder. The scatterer particles are required to be injected to the flow in order to enable the reflection. The particles become visible along the light sheet so that the image formed can be recorded by a camera. As the particle diameter of scatterers get smaller, they enable the visualization of the smaller flow structures. The sensitivity of this technique depends on the power of the light source, the sensitivity of the camera and the scattering ability of the particles. Wang et al. (1997) have stated that this technique suffered due to non-uniform illumination. Nath et al. (1999) have

stated that low luminious intensity of the lightsource could be compansated by a highly sensitive video camera. This technique forms the basis of the Particle Image Velocimetry through which quantitative information about the velocities in a flow field can be obtained. A lightsheet set up for a Particle Image Velocimetry measurement, where a double pulsed laser is used as a light source, is given in Figure 3.2. In this study this technique was used for qualitative puposes.

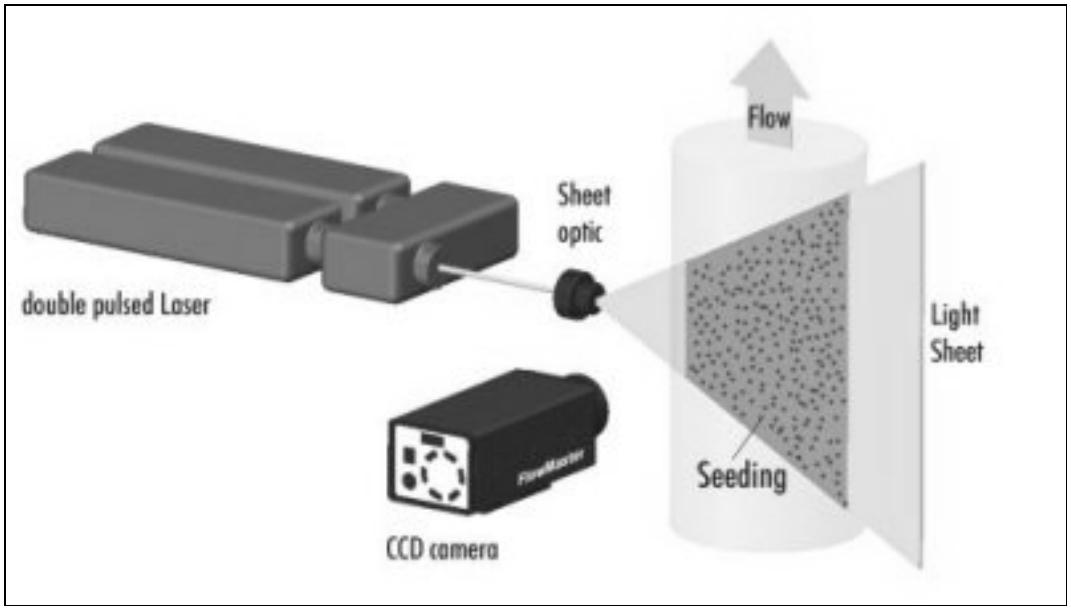

Figure 3.2 System components for Particle Image Velocimetry

CHAPTER IV

LITERATURE REVIEW ON MIXING AND AERATION

Mixing efficiencies of different types of impellers have been investigated experimentally in earlier studies. Experiments were designed to measure power consumption, aeration and macro mixing characteristics and flow field in the tank. Some of the works on thesis subjects are shortly described below as well as those on the ultrasound Doppler velocimetry, lightsheet-flow visualization techniques, which were also employed in this study.

4.1. Power Consumption and Macromixing Time

4.1.1. Impeller Design

Shiue and Wong (1984) have compared the performance of various types of curved blade and pitched blade turbine impellers in a fully baffled, dished bottom tank at $\mathrm{Re} > 10^4$ in terms of the parameter $P\theta^2/\mu T^3$, which essentially is the energy required to achieve a certain degree of mixing. They found that the power and homogenization numbers are independent of the Reynolds number. When compared on an equal power number basis, it can be easily concluded that axial flow impellers show higher energy efficiency as compared to radial flow impellers (Nere, Patwarhan, and Joshi, 2003).

Sano and Ushi (1985) have worked with various types of pitched blade turbine and disk turbine impellers at Re>5x10^5 and have shown that the non dimensional mixing time, the power number, and the discharge flow number in the turbulent regime are independent of the Reynolds number.

Rewatkar and Joshi (1991) have studied three types of impellers, namely, disk turbine, upflow and downflow pitched blade turbines at n=0.4-9.0 rps and $d = 0.167D$ to $0.5D$ in 1.5 m tank. They have shown that when compared on equal power consumption per unit mass basis, the downflow pitched blade turbine shows the smallest mixing time. They have proposed a correlation for the mixing time for the case of downflow pitched blade turbine based on the data on the mixing time reported to date as a function of various variables:

$$n\theta = 5.37 B_A^{-0,87} (W_b / d)^{-0,314} n_b^{-.482} (D/d)^{1.83} (Z/D)^{-0.27} (H/D)^{0.413}. \qquad (4.1)$$

They have investigated the effects of blade angle, blade width, blade number, d/D ratio, etc., at the same power consumption. The mixing time was found to decrease with an increase in the blade angle. The 45 % pitched blade turbine impeller was found to be the most energy efficient. Their study clearly brings out the importance of the impeller design features (diameter, blade width and angle, etc.) on the energy efficiency of mixing. (Nere, Patwarhan, and Joshi, 2003)

Ruszkowski (1994) worked with different types of pitched blade turbine impellers which has different diameters, i.e. $D/2$ and $D/3$, and with varying numbers of blades, i.e. 4 and 6, and blade angles (30°, 45°, 60°), also with the standard six-bladed DT ($D/3$) and a propeller ($D/3$) of impellers and investigated the effect of impeller design on the mixing time. He found that the mixing time is mainly determined by the power input into the tank without being depended on the mixer type. He used the power number to account for the impeller type and obtained the following correlation:

$$\theta = 5.3\left(\frac{1}{n}\right)\left(\frac{1}{Ne^{1/3}}\right)\left(\frac{D}{d}\right)^2 \qquad (4.2)$$

However he further stated if the mixing time depended only on power input then the exponent of D should not have been 2, because exponent 2 indicated that there was a further effect of impeller diameter on mixing time. He rearranged the equation to show the dependence of mixing time on impeller diameter, given constant scale and constant power input:

$$\theta = 5.91D^{2/3}\left(\frac{\rho V_L}{P}\right)^{1/3}\left(\frac{D}{d}\right)^{1/3} \qquad (4.3)$$

Relying on Ruszkowski's results, Nere et al. (2003) stated that the extent of an increase in discharge at a given power consumption and subsequent lowering of mixing the time may depend on the impeller design and added that this was true in view of the significant effect of the impeller design on the flow number.

Distelhoff et al. (1997) have extensively investigated the mixing time characteristics along with the flow and power characteristics for a variety of impellers, namely PBTD (pitched blade turbine), DT (disk turbine), curved-blade DT, and a hyperboloid agitator. The mixing times for axial flow impellers were found to be shorter by about 1-2 s (17-34%) as compared to the radial flow agitators at equal power consumption. This study demonstrated the significant effect of the impeller design on the mixing time. It can further be noticed that, for the same flow numbers, the mixing times are different under otherwise similar conditions.

Fentiman et al. (1998) have developed a new profiled hydrofoil impeller. They have studied the power and mixing time characteristics of this impeller along

with the flat balde turbine and the curved blade turbine impeller. They found on the basis of the pumping/circulation efficiency that the new impeller promised to be more energy efficient when compared with those currently used in the industry. They have carried out complete characterization of the flow field generated by the profiled blade impeller using extensive LDV measurements and power and mixing time measurements. It was observed that the dimensionless mixing time ($n\theta = 48$) was comparable to previously reported values for designs such as propellers, curved-blade turbines, etc. The mixing time was also correlated well by the correlations of Prochazka (1961) and Landau and Shiue and Wong (1984). The power number for this impeller was observed to be 0.22, which is substantially smaller than that of propellers (0.4-0.6), PBTs (1.6-2.1), and Rushton turbines (5-5.5). Hence the mixing efficiency of this novel impeller was expected to be higher. Thus, their study indicated the dependence of the mixing time and energy efficiency on the impeller design so as to have higher discharge flow at lower power consumption. Their results also showed that improvement is possible as a result of a change in the impeller design (Nere, Patwarhan, and Joshi, 2003).

Schäfer (2001) worked with a profile form 417 A hydrofoil impeller in a 400 mm diameter tank. The Reynolds number region he worked was between 100000-250000. He found the Newton number of the hydrofoil impeller as 0.145; it is close to that of the Fentiman's (1998) 0.22. Schafer (2001) has stated that this value was lower by a factor of 10-30 compared to other standard impellers' Newton numbers. The dimensionless mixing time found by Fentiman (1998) and Schäfer (2001) were 48 and 48.25, respectively; which were nearly the same.

To compare the macromixing efficiency of different impellers, Schäfer (2001) graphically showed the mixing time versus specific energy consumption data. He compared the macromixing efficiency of the hydrofoil impeller with other standard impellers, i.e. 6-Blade Rushton turbine, pitched blade turbine, and with the Ruszkowski correlation (Equation 4.3) for d/D 0.375. He found that the hydrofoil impeller had a better macromixing efficiency compared to the standard

impellers in the entire measured region. He stated that while the results of the standard impellers were in the region of the Ruszkowski's empirical correlation, an estimation of macromixing efficiency through the proposed correlation wasn't possible anymore for hydrofoil impeller. The hydrofoil impeller reached the estimated macromixing time at considerably lower specific energy consumption, corresponding to 25% of the value which the Ruszkowski correlation estimated.

Gao et al. (2003) have reported the mixing times in a stirred tank of 0.476 m diameter with single and multiple impellers. They have worked with a 4 baffled dished bottom tank and standard Rushton disc turbine (6 blade), 3-narrow blade hydrofoil impeller, 3-wide-blade hydrofoil impeller and 5-wide-blade hydrofoil impeller agitators. For single impeller cases the d/D ratios were 0.393, 0.399, 0.525 and 0.546 for standard Rushton disc turbine (6 blade), 3-narrow blade hydrofoil impeller and 3-wide-blade hydrofoil impeller, respectively. They stated that for single impeller agitators the mixing times were almost the same for the different types radial and axial flow impellers.

The d/D ratio was 0.393 and 0.399 for Rushton disc turbines and 3-narrow blade hydrofoil impellers, respectively, for both both dual and trible cases. The clearances between the bottom impeller and the vessel base were all set to one third of the tank diameter for different agitator configurations. The submergences of top impeller were set to two thirds of the vessel diameter for all agitator configurations. For the multiple hydrofoil impeller agitators, the mixing times of triple 3-narrow blade hydrofoil impellers were found to be almost the same as the dual and single 3-narrow blade hydrofoil impellers. For Rushton turbines, the mixing times was found to increase as the number of impellers or the aspect ratio increases, also the multiple 3-narrow blade hydrofoil impeller configuration resulted in shorter mixing time than that of multiple Rushton turbines considerably (Gao et al., 2003).

In summary, various studies have been conducted to investigate the efficiency of a variety of impeller designs. The major emphasis has been on the most common type of impellers, namely, pitched blade turbines, flat blade turbines, and marine-blade propellers. Impellers, which are capable of producing top to bottom circulation at relatively low power, are the most efficient impellers. Hence, in general axial flow impellers are the most energy-efficient when compared to radial flow impellers. In particular, the propeller has been found to be relatively more energy-efficient, while DTs are the least energy-efficient as far as turbulent liquid-phase mixing is concerned. There are different designs of hydrofoil impellers reported in the literature. Hence, extensive studies should be carried out in the case of hydrofoil impellers. Minor dimensions such as blade and disc thicknesses have also been found to have an influence on the flow, power, and mixing characteristics, and in some cases modification of these dimensions may prove relatively more beneficial as compared to major dimensions such as the blade length and blade width. Studies on wide variety of impeller types with a specific emphasis on the hydrofoil impellers could have been beneficial (Nere, Patwarhan, and Joshi, 2003).

4.1.2. Impeller Clearance

Shiue and Wong (1984) investigated the effect of Z/D (0.5 and 0.325) for flat blade turbines and found that the homogenization number gets reduced to 34 (for Z/D=0.325, Ne=4.3) from 76 (for Z/D=0.5, Ne=4.8). It can be stated that, as the clearance of the disk turbine decreases, the power number increases.

Rao et al. (1988) have investigated the effect of impeller clearance for downflow pitched blade turbine and disk turbine. They have reported that the mixing time decreases as the impeller cleareance decreases in the range $Z = D/3$ to $D/6$ for disk turbine. This result can be seen as in the line with the results of Shiue and Wong. For downflow pitched blade turbine, the value of the mixing time was

found to increase with a decrease in the impeller clearance (Nere, Patwarhan, and Joshi, 2003).

Nere et al. (2003) has stated that the impeller off-bottom clearance plays an important role in the overall flow pattern generated by an impeller and also affects the power consumption. The mixing time decreases as Z/D increases up to 0.5 for an axial flow impeller. The dependence of the mixing time on Z/D can be justified in view of the uniformity of the flow pattern, presence of dead zones, effective turbulent energy dissipation rate distribution, and values of minimum and maximum energy dissipation rates as a function of Z/D and the impeller design. From the past investigations, it can be recommended that Z/D should be kept equal to 0.33 for downflow pitched blade turbine (45^0) and disk turbine, while it should be kept at 0.5 in the case for flat blade turbines. Further, power characteristics along with the mixing performance as a function of impeller off-bottom clearance for a variety of impeller types are lacking in the literature. Therefore it is worthwhile to work on them with a specific emphasis on high efficiency axial flow impellers (hydrofoils).

In this study, Z/D ratio was 0.33 and two different hydrofoil type impellers (the so-called hydrofoil 1 and 2) were examined regarding their mixing time performance on the basis of equal power consumption. The hydrofoil 1 impeller and hyperboloid combinations were also examined with the upper hydrofoil mixer clearance changed also for their mixing time performance on the basis of equal power consumption. It can be said that the experiments performed in the scope of this study partly corresponds to the recommendations of Nere et al. (2003).

4.1.3. Mixing Time Measuring Technique

Being one of the main mixing time measurement techniques the conductivity technique employs a probe which measures the conductance of the solution as a

function of time that can be converted to concentration versus time scale using proper calibration. In this case, the tracer has to be an electrolytic solution leading to substantial change in the conductivity of the tank contents. One of the characteristics of this technique is that the probe only measures local conductivity, so that it may result in an inaccurate mixing time if the mixing time indicated by the probe is a function of the probe position. This drawback could be eliminated by making measurements of the mixing time at multiple locations. The effects of a number of factors, namely, the location of probe, size of the probe and number of probes, need to be taken into consideration in order to have a proper estimation of the mixing time. These effects have been studied and published with the following main outcomes:

Thyn et al. (1976) investigated the effect of measured volume size on the homogenization time for a baffled vessel agitated by a standard DT. Conductivity measurements were carried out at 14 different locations. They found that the mixing time is a function of the ratio of probe to vessel volumes and independent of the location of the detection probe and point of tracer addition. They showed that the measured value of the mixing time decreases as the logarithm of the ratio of volume of the detection probe to the volume of liquid increases. Sasakura et al. (1980) carried out extensive investigations regarding the effect of the measurement location on the mixing time in a vessel stirred FBTs. They found that the mixing time is independent of the measuring position.

Rielly and Britter (1985) investigated the effect of the tracer addition location, trace volume, and probe size on mixing time measurements. The mixing time was defined as the time required reaching the conductivity within ± 10% of the corresponding to the final concentration difference. As the probe size was increased, the mixing time was found to decrease. Further, no effect of a tracer source volume was observed on the mixing time.

Fentiman et al. (1998) have also observed that the tracer injection location has no effect on the mixing time measurements.

In their review article Nere et al. (2003) state that contradictory results have been reported in regards to the effect of the location of tracer addition on the mixing time. They further state that the time of injection has been found to have an impact on the mixing time measurement. They propose that as little tracer volume as possible should be injected in the smallest amount of time possible without disturbing the local flow significantly.

4.2. Ultrasound Doppler Measurements

In the literature of fluid mechanics various studies can be found which employs the ultrasonic Doppler velocimetry (UDV) technique. It is either used to investigate a pipe flow or the flow field in a stirred tank especially for liquid metals or other opaque liquids. The number of studies in which the UDV is employed to investigate the stirred tank with water as the working flud is however limited. Mostly the laser Doppler velocimetry (LDV) has been utilized in stirred tanks for such purposes. Below some studies in literature in terms of the used fluid, scatterer and wall material type are examined.

Bouillard et al. (2001) has investigated the laminar and turbulent regimes of Newtonian and Non-Newtonian (complex mixture) fluids in a stirred tank by UDV. They worked with two types of impellers; a Rushton Disc Turbine and a propeller. The d/D ratios for the Rushton turbine and the propeller were 0.417 and 0.5, respectively. They compared the measured velocity profiles in the stirred tank with those obtained by microimpeller (intrusive) method and by LDV (non-intrusive). They stated that the presence of bubbles in the liquid phase greatly hampered the reliability of the UDV technique, but when this constraint was removed or minimized, the technique remained adequate for rapid spatial mapping of flow velocity in pure liquid and emulsion (opaque) systems in a non-intrusive way.

Brito et al. (2001) measured the flow velocity in a vortex of liquid gallium, using the UDV. They spanned a disk at the top of a copper cylinder filled with liquid gallium, and created a turbulent vortex with a dominant nearly axisymmetric velocity field with little variation in the axial direction a disk and created a turbulent vortex with a dominant nearly axisymmetric velocity field with little variation in the axial direction. The d/D ratio was 0.8. They stated that the velocity profiles were shown to be well resolved and in quantitative agreement with earlier observations. In their experiments with liquid gallium, they used $ZrBr_2$ particles of 50 μm diameter as scatterers since the density of these were close to that of the liquid galliums. The wall material they used was copper (C=5010m/s) because of its heat resistancy. The sound speed of liquid gallium was 1860 m/s. They also performed experiments with water and the used wall material was polycarbonate to allow visual observations. The used tracer particles for water were polyamide powder.

Nowak (2002) determined the velocity profiles in a boundary layer of a turbulent water flow by means of UDV. According to him, the advantage of this method is the acquisition of the complete velocity profiles along the sound propagation line within very short time intervals. He obtained the time-averaged velocity profiles from 1024 profiles acquired within a measuring time of 13.3 s. He stated that this time was long compared with the characteristic time scales of a turbulent flow, as a consequence the time averaged results gave no access to a statistical analysis of the flow. He used TiO_2 particles as scatterers since he found that the quality of the signals were much better than that of co-polymers. He used PEHD (c=2430 m/s) as wall material for water (c=1483 m/s) since he found the quality of the signals better compared to PVC (c=2380 m/s), Mylar (2540 m/s) and PMMA (2610m/s).

Ozaki et al. (2001) tried to develop a novel signal processing technique of echo signals to improve the time resolution of the UDV. They applied their system to water pipe flow. The tracer particles they used were made of polyethylene and density of them was 960 kg/m^3. The size of tracer particles changed between 3

to 30 μm. They used a 4 MHz probe and the thickness of the acrylic polymer pipe wall region that they located the probe was 2 mm for the for the ultrasound pulses to get inside and for the echo to come through the pipe wall out.

Taishi et al. (2002) investigated the effects of the measurement volume on the mean velocity profile. They also studied the Reynolds stress measurement for fully developed turbulent flows in a vertical pipe. They compared their results with the data obtained by direct numerical simulation. They have found that the application of the UVP method is satisfactory in measuring the mean velocity profile accurately. They have also noted that as it gets closer to the wall, the measured local velocity profile becomes higher than the true value. However, this deviation can easily be compansated.

Yamanaka et al. (2000) emphasized the two major advantages of the UDV technique compared with LDV. First, UDV has the capability to measure the velocity profile measurement along the ultrasound path, effectively instantaneously, additionally it is applicable to the measurement of opaque fluids. They studied the relationship between the test fluids and the microparticles suspended in the fluid as reflectors of ultrasonic pulses, and sound speeds of the test fluids and the wall materials. They used SB-100 and MB-100 polystyrene microparticles and adjusted the density of the test fluid to that of the particles. 18 vol. % (c=1590 m/s) and 68% (c=1860 m/s) glycerol water solutions were used for SB-100 and MB-100 polystyrene microparticles, respectively. The used wall material was plexiglass with a sound speed of 2320 m/s.

In the UDV technique, it is necessary to add a certain amount of tracer particles into the liquid so that the amplitude of the received echo increases enhancing signal to noise ratio (S/N). When no particles are added into the water, only the impurities contained in the water can also backscatter the ultrasonic beam. However, in this case S/N may not be sufficiently high, since the measuring probe receives signals through a wall. Höfken et al. (1995) worked with a 10 mm

plexiglass wall and they couldn't obtain strong signals only from the impurities in water.

Steidl (1995) has performed probe measurements with five different particles to obtain the best signal through the tank wall. He investigated the effects of particles whose size ranged from 45 μm to 1.5 mm.Particle material and size effects were observed on the UDV signals. As particles get larger scattering of the echo and settling in the tank can pose problems for the measurements. The tracer particle types, wall materials and working fluids used by above given researcher's works are summarized in Table 4.1.

Table 4.1 Working fluids and tracer particles used in some UDV researches

Researchers	Working Fluid	Tracer Particles	Wall Material	Result
Yamanaka et al. (1997)	18 vol% glycerol water solution, ρ =1045 kg/m3	SB-100 polystyrene, ρ =1045 kg/m3 diameter=83 μ m	Plexiglas	Improved S/N
Yamanaka et al. (1997)	68 vol% glycerol water solution, ρ =1117 kg/m3	MB-100 polystyrene, ρ =1117 kg/m3 diameter=83 μ m	Plexiglas	Improved S/N
Brito et al. (2001)	Water	Polyamide powder	Polycarbonate	Improved S/N
Brito et al. (2001)	Liquid gallium	$ZrBr_2$ (zirconium boride)	copper	Improved S/N
Nowak et al. (2002)	Water	TiO_2 particles	PEHD	Improved S/N
Nowak et al. (2002)	Water	TiO_2 particles	PVC, Mylar, PMMA	Bad results
Ozaki et al. (2001)	Water	Polyethylene particles, 3 to 30 μ m	Acrylic Polymer	Improved S/N
Taishi et al. (2002)	Water	Nylon powder diameter=80 μ m	Plexiglas	Improved S/N
Bouillard et al. (2001)	Water	Hollow silver coated bead particles	Plexiglas	Improved S/N
Steidl (1995)	Water	Polyester spangle gold 25/60[1]	Plexiglas	Improved S/N
Steidl (1995)	Water	STANDART Aluminium powder Lack OT[1], Roundspangle black, plastic[2] and Polyester spangle gold 25/60[1]	Plexiglas	Bad results

[1] Producer : Eckart-Werke, 90763 Fürth/Bay, Germany.

[2] Producer: Dragon-Werk Georg Wild GmbH & Co KG, Rose-Str. 20, 95412 Bayreuth, Germany.

4.3. Lightsheet Experiments

Steidl (1995) performed laser light sheet experiments in order to investigate the flow in a 400 mm length square tank qualitatively. He made trials with different types of aluminium particles to determine the best particle for the visualization of the flow field in the stirred tank. The following particle types were investigated:

Table 4.2 Particle types for the laser-lightsheet (Steidl, 1995)

Particle type	**average corn size in [µm]**
STANDART Aluminium powder 1111	45
STANDART Aluminium powder Lack OT	80
STANDART Aluminium spangle fine	250

He found that the particles with a corn diameter of 80 µm were optimal for the visualization of the flow in the tank. He stated that principally both other particles can also be used in the experiments and finer particles are generally more suitable for the visualization of fine structures of flow.

4.4. Aeration

Many models have been presented to predict gas–liquid mass transfer to/from clean bubbles, i.e. bubbles with a mobile surface. Most of these models assume that mass transfer is controlled by the rate of surface renewal, as described by

Higbie's penetration theory (Higbie, 1935). According to this theory, the liquid-phase mass transfer coefficient for a bubble with a mobile surface is given by

$$k_L = \frac{2}{\sqrt{\pi}}\sqrt{\frac{D}{\theta}} \tag{3.4}$$

The problem with the application of Equation 3.4 lies in the calculation of the surface renewal time θ. Two major approaches have been suggested, which depend on the scale of flow that is assumed to influence mass transfer.

The first one, proposed by Higbie (1935), himself relates the contact time to the bulk liquid flow around the bubble assuming that

$$\theta = \frac{d_B}{u} \tag{3.5}$$

where d is the bubble diameter and u is the bubble slip velocity, leading to the following equation:

$$k_L = 1.13\sqrt{\frac{u}{d_B}}D^{1/2}. \tag{3.6}$$

An alternative approach starts from a refinement of Higbie's theory by Danckwerts (1951), who proposed that the average surface renewal rate results from exposure to eddies with variable contact time, leading to Equation 3.7:

$$k_L = \sqrt{Ds} \quad . \tag{3.7}$$

Lamont and Scott (1970) calculated the fractional rate of surface-element replacement, *s*, through an eddy cell model, postulating that mass transfer is mainly dependent on the motion of small-scale eddies in the dissipation range of the spectrum. They deduced that

$$k_L = cD^{1/2}\left(\frac{\varepsilon}{\upsilon}\right)^{1/4} \tag{3.8}$$

where ε is the turbulent energy dissipation, υ is the kinematic viscosity and c = 0.4 is a constant. Kawase et al. (1987) presented an alternative approach, resorting to Kolmogoroff's theory of isotropic turbulence, valid for power-law liquids. This leads to Equation 3.8 above for the particular case of Newtonian liquids, with constant c = 1.13. Prasher and Wills (1973) obtained c = 0.592 from experimental data in a stirred tank. The major differences between Equations 3.6 and 3.8 are that equation 3.6 predicts an important variation in k_L with diameter, excluding turbulence as an independent variable, whereas equation 3.8 predicts a decisive influence of turbulent energy dissipation on k_L, making it independent of bubble diameter (Alves et al, 2005).

Calderbank et al. (1960) had developed techniques for measuring the interfacial area in gas-liquid dispersions and consequently made it possible to measure the liquid phase mass transfer coefficients in gas-liquid dispersions such as are produced in aerated mixing vessels, and sieve and sintered plate columns. Nagata (1975) states that Calderbank has observed the interfacial area of air in agitated water by a light transmission technique. In a mixing vessel agitated in 100-400 rpm under aeration Q_A = 1 ft^3/min, there are two maxima of interfacial are in the vicinity of an impeller and in the middle height between the impeller and the free surface.

Chisti et al. (2001) has investigated the gas holdup, mixing, liquid circulation and gas–liquid oxygen transfer characterized in a large (~1.5m3) draft-tube airlift bioreactoragitated with Prochem® hydrofoil impellers placed in the draft-tube. They made measurements both in water and in cellulose fiber slurries. They found that the use of mechanical agitation generally enhanced mixing performance and the oxygen transfer capability relative to when mechanical agitation was not used; however, the oxygen transfer efficiency was reduced by mechanical agitation.

Kawase et al. (1986) developed a theoretical model for volumetric mass transfer coefficients in bubble columns which was based on Higbie's penetration theory and Kolmogoroff's theory of isotropic turbulence.

As explained in Chapter 2, according to the theory of Higbie (Higbie, 1935) there is a relationship between the residence time of the fluid particles at the interface and the oxygen transfer coefficient. The residence time of the fluid bubbles is depended on the bubble surface consequently on the size of the bubble. Experimental researches of this dependency have been done by Motarjemi (1978), Pasveer (1955) and Bishof (1994).

CHAPTER V

EXPERIMENTAL WORK

5.1. Set-up of Cylindrical Tank Experiments

The experimental set-up is shown in Figure 5.1. It is mainly composed of a mixing tank, a rotating impeller, a conductivity electrode, torquemeter and a PC whose details are given below.

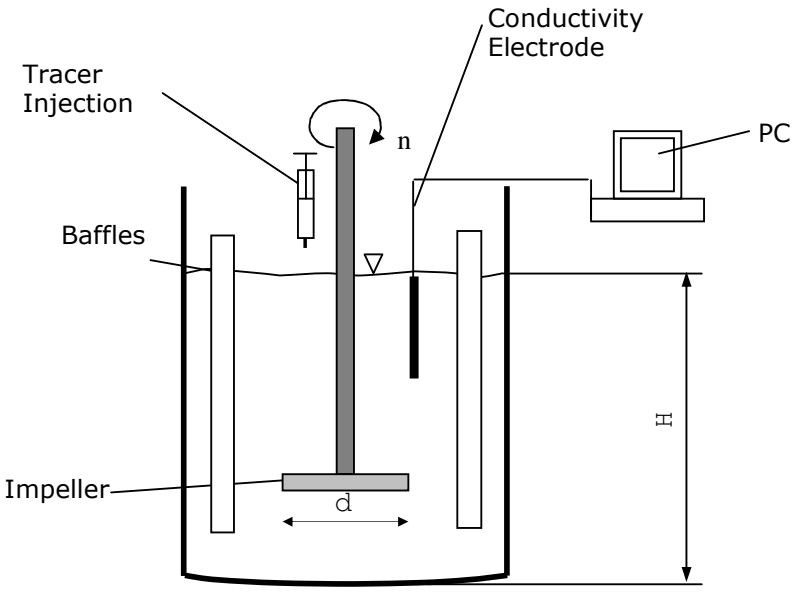

Figure 5.1 Experimental Set-up for Mixing Time Experiments

5.1.1. Drive motor

As the mixer drive, the three phase ac motor of the firm SEW Eurodrive with a motor power of 0.55 KW was used. The gear box was connected with a flange to the motor. The rotational speed of the motor is adjusted via a frequency converter, which was also produced by the firm SEW Eurodrive. The connections between the mixer shaft and the drive motor were done using flexible couplings.

5.1.2. Mixing tank

For the experiments a cylindrical mixing tank with flat bottom was used. In Table 5.1 the details of the tank geometry are given.

Table 5.1 Dimensions of the cylindrical stirred tank configuration

D	Diameter of the mixing tank	300 mm
H	Water height	300 mm
B	Length of the baffles	24 mm
S	Thickness of the baffles	2 mm
C	Distance of the baffles to the tank wall	6 mm
d	Mixer diameter	100 mm
Z	Mixer clearance (Hydrofoil 1 & Hydrofoil 2)	100 mm
Z	Mixer clearance (Hyperboloid)	10 mm
W	Diameter of the mixer shaft	8 mm

Hyperboloid impeller which had been designed as a close clearance impeller was placed at a clearance of 10 mm ($Z = d/10$) from the tank bottom. In the hydrofoil 1 and hyperboloid impeller combination, the hyperboloid mixer was placed at a clearance of 10 mm ($Z = d/10$) from the tank bottom and the hydrofoil1 impeller which is on the same shaft was placed 100 mm (d) lower than the water surface. The baffles were located in the stirred tank with 90° angle (see Figure 5.2).

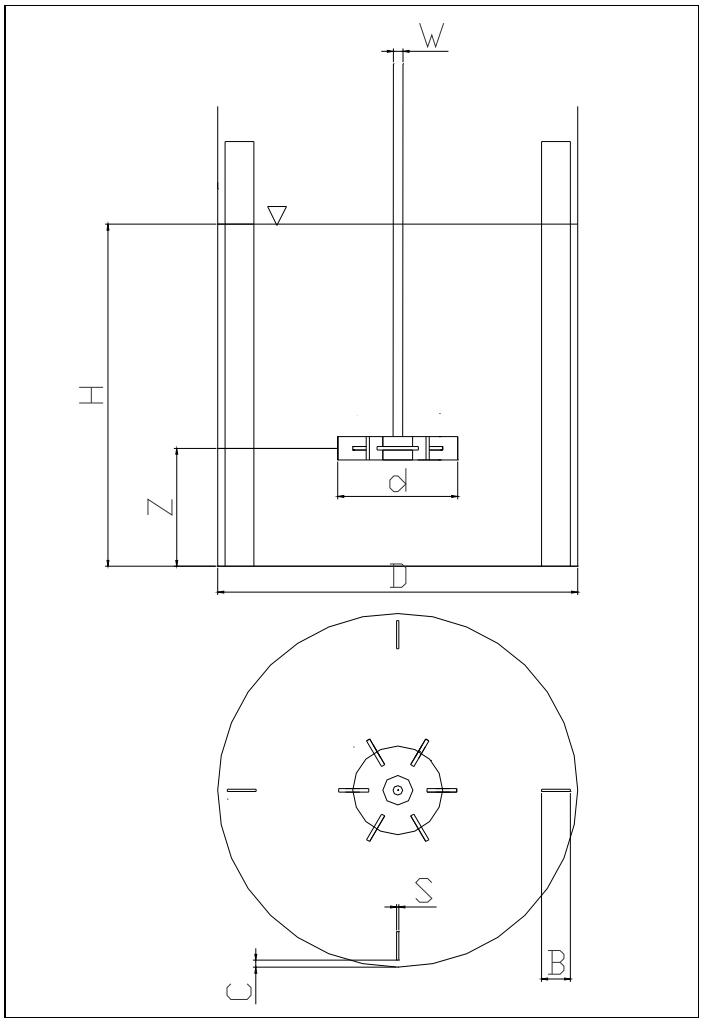

Figure 5.2 Stirred tank configuration

5.1.3. Mixers

In the experiments the hydrofoil 1, hydrofoil 2, hyperboloid and 6 Blade Rushton turbine impellers were used. Properties of the investigated mixers are given in Table 5.2. Photos of hydrofoil 1, hydrofoil 2 and hyperboloid impellers can be seen in Figures 5.3, 5.4 and 5.5. Dimensional drawing of 6 Blade Rushton turbine is given in Figure 5.2.

Table 5.2 Dimensions of the investigated impellers

Nr.	Mixer type	d (mm)	Number of blades
1	Hydrofoil 1 mixer	100	2
2	Hydrofoil 2 mixer	100	2
3	Hyperboloid mixer (Gen.5, low rib)	100	8 transport ribs
4	6 Blade Rushton turbine	100	6

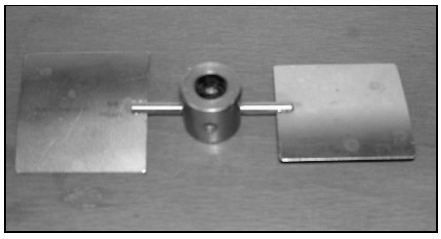

Figure 5.3 Hydrofoil 1 Impeller

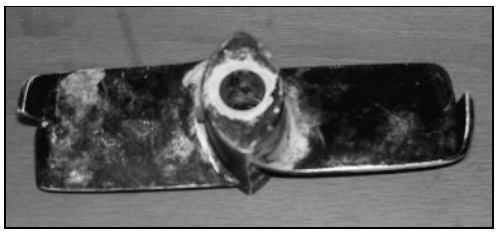

Figure 5.4 Hydrofoil 2 Impeller

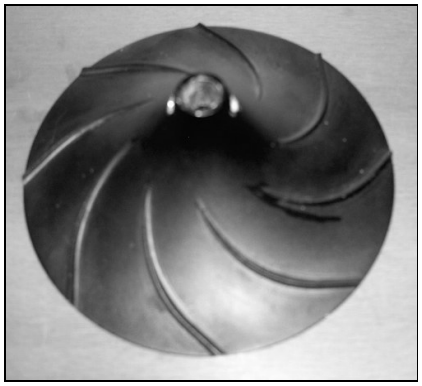

Figure 5.5 Hyperboloid Impeller

Specifications of hydrofoil1 impeller is given in Table 5.3.

Table 5.3 Specifications of hydrofoil 1 impeller

	D = 300 mm	
Profile form	*417 A*	
Diameter	100 mm	$0.333D$
Number of blades	2	-
Blade angle	15°	-
l_{blade}	33 mm	$0.33d$
b_{blade}	33 mm	$0.33d$
w_{blade}	0.7 mm	$0.007d$
d_{hub}	15 mm	$0.05D$
h_{hub}	15 mm	$0.05D$
W	8 mm	$0.027D$

The available specifications of Hydrofoil 2 impeller is given in Table 5.4.

Table 5.4 Specifications of hydrofoil 2 impeller

	D = 300 mm	
Diameter	100 mm	$0.333D$
Number of blades	2	-
l_{blade}	42 mm	$0.42d$
b_{blade}	30 mm	$0.3d$
w_{blade}	2 mm	$0.02d$
b_{hub}	17 mm	$0.057D$
l_{hub}	30 mm	$0.1D$
h_{hub}	25 mm	$0.083D$
W	8 mm	$0.027D$

5.1.4. Conductivity meter & Amplifier

The conductivity cell WTW – TetraCon 325, WTW GmbH, Weilheim, Germany, has a relatively small measuring volume ensuring reliable measurements. The WTW-LF 340A conductivity meter was used to transfer the conductivity signals.
An amplifier was used to amplify the analogue signals coming from the conductivity meter before they are transmitted to the analogue-digital converter in the mixing time experiments.

5.1.5. Torquemeter

For the torque measurements TYP 34 ST, HBM-Hottinger Baldwin Messtechnik GmbH, Germany, torquemeter which was placed between the drive motor and the impeller, was used. Flexible couplings were used for the connections.

5.1.6. Ultrasound Doppler Velocimeter

The measurements were performed with the UDV system (Met-Flow SA, Switzerland), which allows the measurement of the fluid velocity at 128 points along the beam direction. By using the Ultrasound Doppler Velocimeter one can measure a complete velocity profile along the direction of the probe in a few seconds.

At each measurement cycle of the device 1024 profiles are taken, the data of which can be further saved to a floppy. The device works with a main frequency of 4 MHz and the diameter of the focused ultrasound beams were 5 mm. The thickness of the measurement volumes depends on the sound velocity of the investigated fluid and the value for water is 0.75 mm. Four different ultrasonic beam lengths can be set by the device itself where certain limitations exist regarding the maximum measurable velocities or the resolution of the velocity values. These are given in Table 5.3 for water (c =1480 m/s).

Table 5.5 Depths and the maximum measurable velocities in UDV system.

Maximum Depth	Maximum Velocity	Resolution
91 [mm]	722 [mm/s]	5.6 [mm/s]
189 [mm]	361 [mm/s]	2.8 [mm/s]
378 [mm]	181 [mm/s]	1.4 [mm/s]
758 [mm]	90 [mm/s]	0.7 [mm/s]

5.2. Experimental Procedures for Cylindrical Tank Experiments

5.2.1. Power Consumption Measurements

Torque versus impeller rotational speed measurements were done for the impellers hydrofoil 1, hydrofoil 2, hyperboloid and a combination of the hyperboloid and the hydrofoil 1 impeller using water as the working fluid.

In order to obtain the torque data at a certain rotational speed, the mixers were first rotated in air, and the torque on the mixer shaft was measured for each rotational speed. Then, the system was operated with water and the torque data were recorded again at the same rotational speeds. The torque data obtained for air were further subtracted from the torque data obtained for water to get the final torque data.

A simple calculation was carried out to obtain the Newton Number from the torque data.

First the Power in Watts was obtained from the torque data;

$$P = T\omega \tag{5.1}$$

$$\omega = 2\pi n \tag{5.2}$$

$$P = Ne * \rho * n^3 * d^5 \tag{5.3}$$

where P is power in Watts, T is torque in N.m and n is the rotational speed in RPS and Ne is the dimensionless Newton Number.

A sample calculation is carried out with raw data of the hydrofoil 1 impeller according to the above given formulas. (See Appendix E) Torque was

measured as $T = 0.04$ Nm for hydrofoil 1 impeller at a rotational speed of 783 RPM. Under this conditions Re, Ne and P were calculated as 130505, 0.15 and 3.28 Watt, respectively. Using this procedure the $\mathrm{Re} - Ne$ curves for the three mixers were constructed.

5.2.2. Macromixing Time Measurements

5.2.2.1. Measurement Procedure

The procedure used in the experiments was based on monitoring concentration change of a tracer with respect to time at a fixed point. An electrolyte substance was added as the tracer to the vessel. The concentration of this substance was measured by a conductivity meter. The 95 % mixing time was determined from the changes in conductivity after introducing 21 ml (0.1 % of the tank volume) of aqueous sodium chloride solution (10 w/w %) to the free surface of the liquid near the mixer shaft.

The conductivity recording was always started at the same time with the addition of the salt solution and until one or two minutes after the injection depending on the stirrer studied, so that steady concentration versus time behavior is obtained. The conductivity electrode was located inside the vessel, so that the conductivity cell was approximately at the midpoint of the liquid height and in the middle between the shaft and the vessel wall.

Before starting the measurements, it was necessary to calibrate the conductivity cell against the possibility that the relative concentration fluctuations less than 5 % of the middle value could be resolved and the maximum limit value of the electrolyte concentration was kept until the time when a proportional relationship between the concentration and the conductivity was achieved.

The conductivity signal coming from the conductivity cell was transferred through the conductivity meter, the amplifier and an analogue-digital converter to the PC, where the data was recorded.

To ensure a sufficient statistical safety in the results, the average of a number of measurements must be taken. For the same operating conditions the mixing time was calculated six times and they were averaged after eliminating the maximum and minimum values.

At each measurement the beginning and the end concentrations were recorded for 16 seconds and the mixing period was recorded for 65 seconds. The recording was done for every 10 milliseconds.

A calibration curve is required to convert the conductivity data in Volts to the concentration data. NaCl solutions at different concentrations (mmol/l) were prepared with deionized water. The conductivities of these solutions were measured. The care was taken for the water temperature in the foregoing experiments to be the same with that of the calibration experiments. Average of two measurements was considered for each concentration

There exists a lag time for the conductivity meter to display the conductivity value when the probe is inserted into the solution. The lag time for the conductivity probe was determined by measuring the time lost from the moment where the probe is inserted into the solution until the conductivity value appears on the conductivity meter. For the measurement the stop watch is started simultaneously with the insertion of the probe into the solution. The lag time is usually about 2-3 seconds. The lag time of the conductivity meter was measured as 2.1 s.

5.2.2.2. Macro Mixing Time Calculation Procedure

The conductivity versus time data were stored in computer and were further evaluated to get the mixing time via the prepared Excel sheet. First the

conductivity data in Volts were converted to the concentration data (mmol/l) with the help of the calibration curve. Then the concentration versus time curve was drawn as shown in Figure 5.6.

The dashed lines in Figure 5.6 show the upper (105 %) and lower (95 %) limit values. In order to calculate these values the average start and the average end values are calculated. The average start value is the average of the data of the first 8 seconds recording before the tracer solution is added. The average end value is the average of the last 8 seconds data of the 65 seconds recording. Here it is assumed that at the end of 65 second agitation, complete mixing is achieved and concentration becomes uniform in the tank. The concentration increase was obtained by subtracting the average end value from the average start value.

The lower limit was then calculated by multiplying the average concentration increase with -(100-95)/2/100, where 95 is the mixing grade, and further adding it to the concentration increase and taking the absolute value of it.

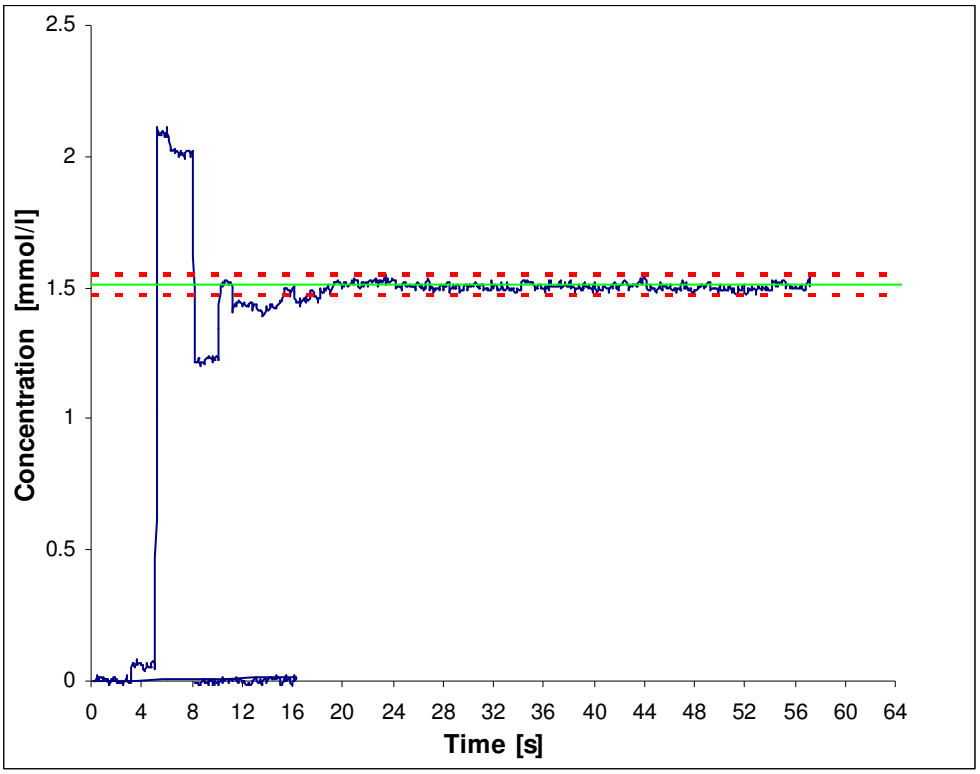

Figure 5.6 Typical experimental concentration versus time response

The upper limit is determined in the same way as the lower limit, i.e. by multiplying the average concentration increase with (100-95)/2/100 and further adding it to the concentration increase and taking the absolute value of the result. The line in between the upper and lower limit is the average concentration increase value.

Henzler's (1994) method was used to evaluate the data; at least 6 experiments were performed for each rotational speed. The mixing time values of each experiment were averaged after eliminating the maximum and minimum values. The lag time of the conductivity meter was then subtracted from the average value and the final mixing time value was obtained.

5.2.3. Ultrasound Doppler Velocimeter Measurements

Polyesterspangle 25/60 gold (Regular hexagon, Edge length 0.60 mm, Height 0.25 mm) particles were used as scatterers in the experiments. The tank wall was made of glass. The thickness of the wall was 4 mm. The sound speed of water was taken as 1480 m/s which was also the set value of the device. In the experiments axial and radial measurements were performed. 5 measurements were done for each measuring point. The rotational speeds of the impellers were adjusted to 382 RPM (Re=63666), which corresponds to 2 m/s tip speed.

Axial Measurements

The measurements in the axial plane were done as shown in Figure 5.7. The UDV probe head was located downwards at a certain height from the liquid surface. By installing the probe at different radii a whole plane of the axial velocity can be measured. (Steidl, 1995) In the experiments the measurements were taken with 1 cm spacing in between the mixer shaft and the tank wall at the set axial heights.

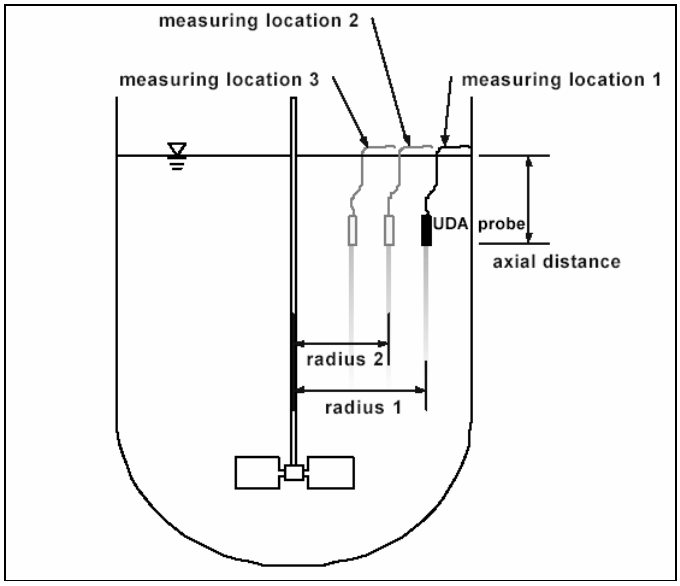

Figure 5.7 Axial UDA measurements

Radial Measurements

The measurement of radial velocity profiles is similar to the measurement of the axial planes. In this case the sensor can be placed horizontally either outside or inside the vessel. (Steidl, 1995) In the experiments the probe was fixed on the outside of the mixing tank via a plexiglas wall having holes on it and attached to the one side of the mixing tank. The probe was placed on the holes depending on the location at which measurement was required. Ultrasonic gel was used as the coupling medium. A representative picture can be seen in Figure 5.8.

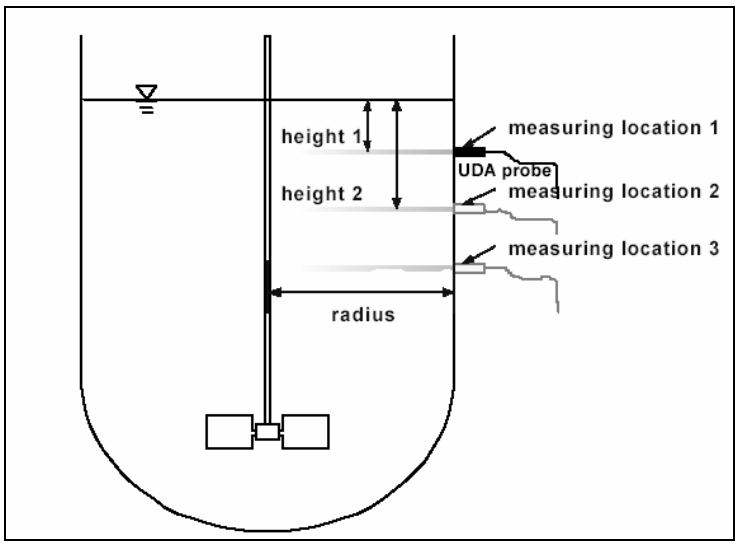

Figure 5.8 Radial UDV measurements

5.2.3.1. Calculation Procedure for the UDV Measurements

For the evaluation of the binary data recorded by the UDV Monitor, the UVP Graph program developed by Steidl (1995) was used. The outputs of the UVP Graph program were further sent to the supplementary programs DrawStr (Steidl, 1995) and Dat2Tec (Steidl, 1995), which prepared data for the TecPlot to display the stirred tank and the velocities in x and y direction.

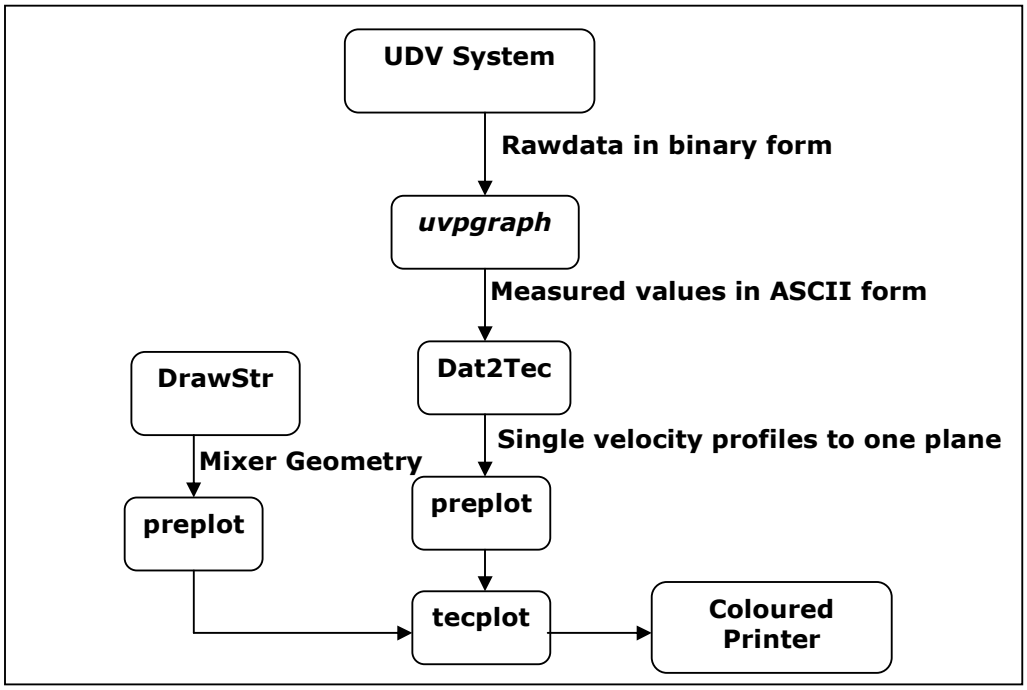

Figure 5.9 Evaluation process of the UDV data

5.2.4. Lightsheet Experiments

A test set-up has been built to record flow images of the investigated impellers by means of light sheet technique. The mixing tank was covered with black paper. Light coming from a 1000 watt light source was sent through a 4 mm rectangular hole which was made on the black paper covering the left side of the tank. The centerline of the hole was exactly the center of the tank in the direction of the mixer shaft in between two baffles. The previously added aluminum particles become shiny along the center of the mixing tank when the light source was activated. So, the flow field on the left side of the tank generated by the mixers could be visualized as long as the laboratory medium is kept dark. The Reynolds numbers studied were 118114 and 81254. The

aluminum particles used in the experiment was of type Standard Aluminium Powder, Lack OT Ch., Eckart Werke D-90763 Fürth, Germany. The diameter of aluminum particles were 80 μm. Small spoonful aluminium particles were enough to obtain a satisfactory visualization. For the aluminium particles to have a uniform distribution in water, a small amount of liquid soap was required to be added to it.

After turning on the light and starting up the mixer, the flow in the tank was recorded by the Sony Digital Video Camera Recorder, DCR-VX1000E. To obtain a satisfactory result in the flow visualization, main parameter to be adjusted in the camera settings was the shutter speed. The shutter time can be arranged from 1/3 to 1/10000. With higher shutter time the amount of light the camera lets in itself is higher and with a higher light the flow could be visualized more clearly. Adjusting a high shutter time is a must in the lightsheet experiments, since the medium is dark except the light sheet sent into the tank. In the experiment the recordings were done with the shutter times 1/3, 1/6, 1/12 and 1/25 s.

In the experiments working long time with the same water was a disadvantage. The aluminum particles got dissolved in water and disabled the visualization of the flow field. It is better to change the water in the tank before each recording. Another disadvantage was using more than one spoonful of particles. This also prevented a clear visualization of the flow field. Both of these disadvantages had been experienced in the lightsheet experiments of the combination 2 (submergence of the top hydrofoil impeller = 1.5 d) case.

5.3. Square Tank Experiments

Conductivity and aeration measurements were performed with different types of mixers in the square tank which is a geometry extensively used in waste water treatment. The drive motor used was of the firm MATTKE Antriebstechnik with a

maximum torque capacity of 32 Nm. The dimensions of the square Plexiglas mixing tank were 900x900 mm. The details of the tank configuration are given in Table 5.4.

Table 5.6 Dimensions of the rectangular stirred tank

l	Tank length	900 mm
w	Tank width	900 mm
H	Water height	450 mm
d	Mixer diameter	200 mm
Z	Mixer clearances	20 mm
W	Diameter of the conical mixer shaft	20 mm (upper part) 10 mm (lower part)

5.3.1. Mixers

In the experiments Generation 6 Hyperboloid, Generation 5 Hyperboloid (low rib) and Generation 5 Hyperboloid (high rib) mixers were used.
The properties of the mixers are given in Table 5.9. The photos of the mixers are shown in Figures 5.10-11-12.

Table 5.7 Dimensions of the impellers used in the experiment

Nr.	Mixer type	d	Number of transport ribs
1	Generation 6 Hyperboloid	200 mm	8
2	Generation 5 Hyperboloid (low rib)	200 mm	8
3	Generation 5 Hyperboloid (high rib, corrugated bottom)	200 mm	8

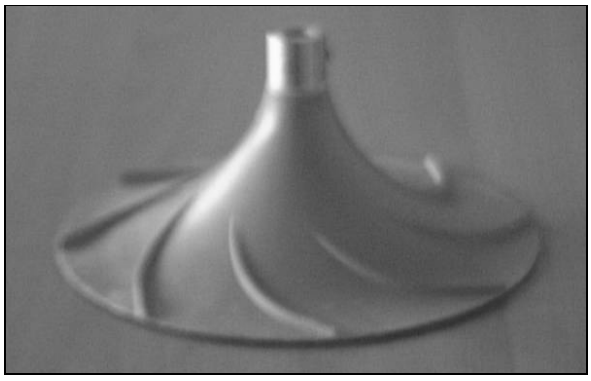

Figure 5.10 Generation 5 Hyperboloid (low rib)

Figure 5.11 Generation 5 Hyperboloid (high rib)

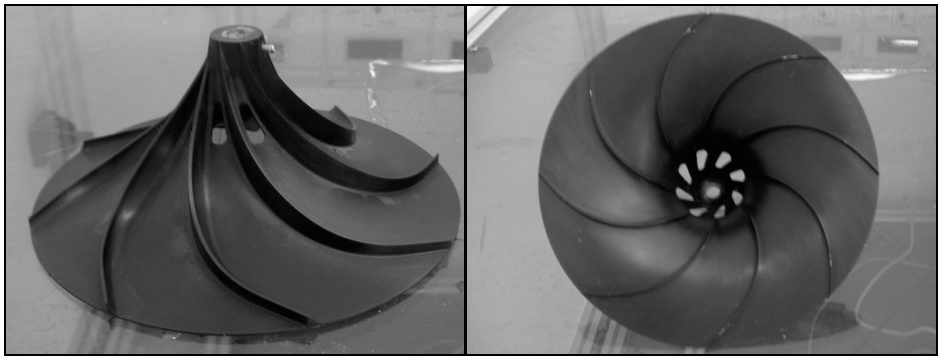

Figure 5.12 Generation 6 Hyperboloid (front and bottom view)

5.3.2. Determination of the macromixing time

The same experimental procedure explained in part 5.1 with the required scale-up was employed in the experiment.

365 ml (0.1 % of the tank volume) of sodium chloride (NaCl) was added to the free surface of the liquid near the mixer shaft. The prepared NaCl solution was 10 % by weight.

The conductivity recording was always started at the same time with the addition of the salt solution and until three or four minutes after the injection depending on the stirrer studied, so that the new steady state was reached.

The conductivity electrode was located inside the vessel, so that the conductivity cell was approximately at the midpoint of the liquid height and in the middle between the shaft and the vessel wall.

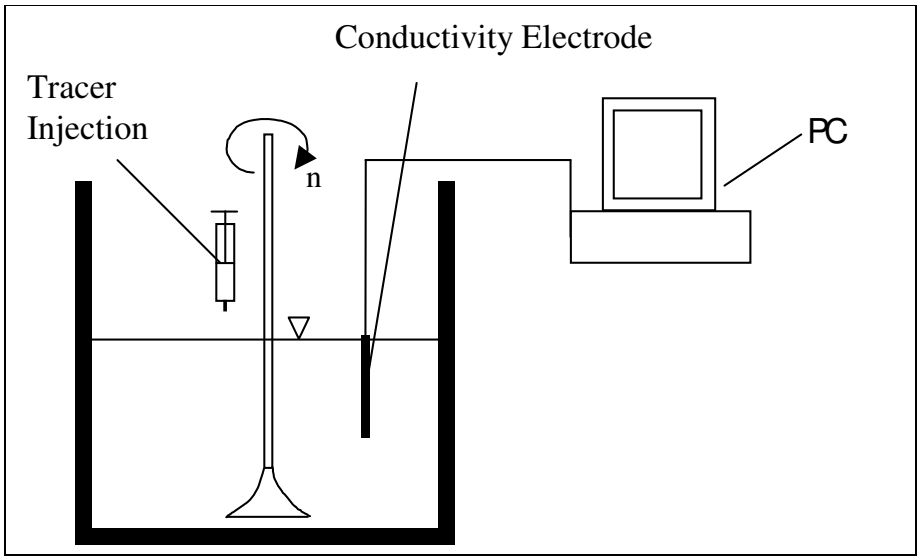

Figure 5.13 Mixing time setup for the rectangular tank

At each measurement the beginning and the end concentrations were recorded for 16 seconds and the mixing period was recorded for 246 seconds. The recording was done for every 10 milliseconds.

The same calibration curve was used for this experiment.

Table 5.8 Newton numbers of the impellers

Mixer type	Newton Number
Generation 6 Hyperboloid	0.55
Generation 5 Hyperboloid (low rib)	0.20
Generation 5 Hyperboloid (high rib)	0.36

These power figures were then interpolated to obtain the mixing time at the same power consumption.

5.3.3. Aeration Experiments

Aeration experiments were performed for Generation 5 low rib and Generation 6 hyperboloid impellers which are equipped with additional blades under them for enhancing the rate of oxygen transfer. The mixer-aerators were examined at different flow numbers for different air flow rates and mixer speeds.

The same mixing tank explained in part 5.3 was used in the aeration experiments.

There was an aeration ring under the mixer where the air was pumped to the system. The velocity and air flow rate were adjusted with the buttons on the panel which was at the right side of the tank.

Generation 5 low rib mixer which had blades under it is given in Figure 5.14. These blades were used for aeration purposes; to make the air bubbles smaller and consequently to increase the interfacial area between air and solution. The mixer clearance was 32 mm, which was 20 mm in the conductivity experiments, to account for the aeration ring.

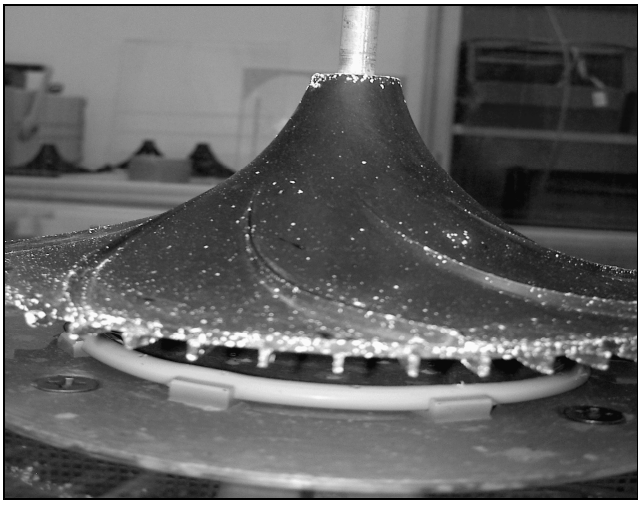

Figure 5.14 Front view of the mixer aerator

Oxygen-meter and Oxygen Sensor

The oxygen-meter and the oxygen sensor, model Cond 340i, of the Firm WTW (Germany) were used to determine the oxygen concentration in the tank. The

oxygen sensor was always placed at the front left corner of the tank. In order to determine the oxygen transfer coefficient, the oxygen entry to the system with respect to time is obtained in the form of a concentration curve with the help of the data collected by the oxygen electrodes. The procedure followed for the measurement of the oxygen transfer in clean water was the one "Absorption measurements following the lowering of the DO concentration using sodium sulphite" explained in the advisory leaflet ATV M 209 (1996). Detailed description of the procedure is given in Appendix E.

CHAPTER VI

RESULTS AND DISCUSSION

6.1. Cylindrical Tank Results

6.1.1. Power Consumption

Newton number and mixing time are two important parameters for evaluating the efficiency of impellers. Newton (power) number, Ne, is a dimensionless parameter which measures the power requirements of an impeller. Correlations for Ne as a function of Reynolds Number are available in literature. A good impeller is the one that has a small mixing time as well as a small power number.

Power characteristics of the impellers were investigated in the fully developed turbulent region at $\mathrm{Re}>40000$. The measured torque versus rotational speed data were converted to dimensionless Reynolds and Newton number data. The power consumption characteristics of the investigated impellers and impeller combinations are given in Figure 6.1. Newton numbers of the impellers turned out to be constant at $\mathrm{Re}>130000$ consequently at this range Newton Numbers were averaged to obtain the turbulent Newton numbers of the impellers. The highest Newton number, 0.60, was that of the Hydrofoil 1+Hyperboloid impeller combination's with the top impeller (hydrofoil 1) submergence of 1.5 d. Hydrofoil 1 impeller had the lowest Newton number, which was 0.15.

Two different hydrofoil impellers were investigated, the Newton number of hydrofoil 1 impeller (0.15) were found to be lower than the new design hydrofoil 2 impeller (0.32).

Schäfer (2001) worked with a profile 417 A hydrofoil impeller which has nearly the same geometry with the hydrofoil 1 impeller investigated in this study. He found the Newton number as 0.145 for a d/D ratio of 0.375 while the d/D ratio in this study is 0.333 and the found Newton Number is 0.15. He stated that this value was lower by a factor of 10-30 compared to other standard impellers' Newton numbers. Fentiman et al. (1998) also worked with a hydrofoil impeller and found the Newton number as 0.22.

The Newton number of the hyperboloid impeller (0.39) was found to be higher than that of the two hydrofoil impellers. It will be seen that the Newton numbers of the radial flow producing impellers are higher than that of the axial flow producing impellers in each case when the published literature is examined. Higher Newton number of the radial flow producing hyperboloid impeller than that of the axial flow producing hydrofoil impellers' can be due to this difference.

The Newton numbers of the two impeller combinations were found to be higher than the single impeller combinations as expected. Among the two impeller combinations the Hydrofoil 1+Hyperboloid impeller combination with the top impeller (hydrofoil 1) submergence of 1.5 d has a Newton Number of 0.60 while the combination with the top impeller (hydrofoil 1) submergence of d has a Newton Number of 0.55. Nere et al. (2003) have stated that the impeller off-bottom clearance plays an important role in the overall flow pattern generated by an impeller and also affects the power consumption. Rao et al. (1988) have investigated the Newton Numbers of axial-downflow pitched blade turbines and have found that as the impeller off-bottom clearance decreases the Newton Number increases; at $Z = D/3$ Ne=1.29, at $Z = D/4$ Ne=1.35 and at $Z = D/6$ Ne=1.61. The difference between the Newton numbers of the two mixer combinations might be due to the decrease in the axial flow producing

upper mixer off-bottom clearance as in the case for Rao et al. (1988). The raw data of the power consumption measurements in cylindrical tank are given in Appendix A.

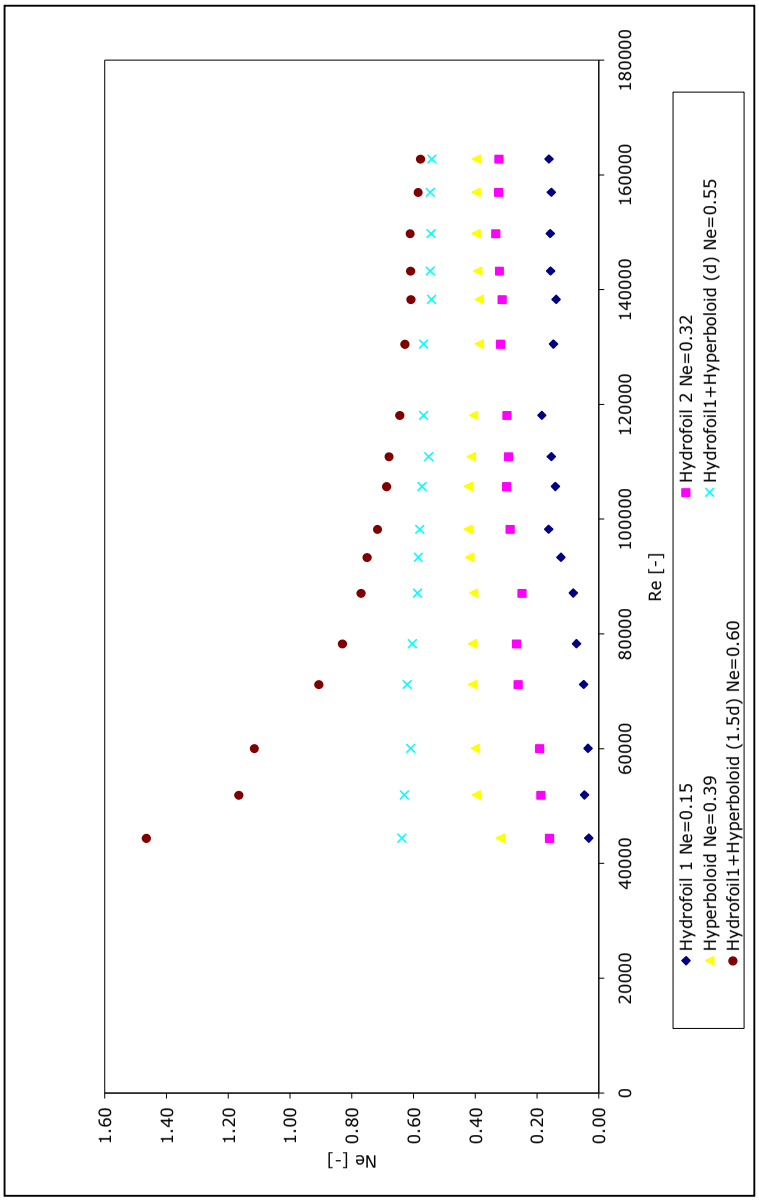

Figure 6.1 Power characterisitics of the investigated impellers

6.1.2. Macromixing Measurements

Because of the availability of the literature data the reliability of the macromixing measurements was first checked with the results of the 6-blade Rushton turbine experiments. Results of the macromixing experiments performed with the 6-blade Rushton turbine impeller checked with the data reported by Zlokarnik (1998). The results are depicted in Figure 6.2 along with the literature values.

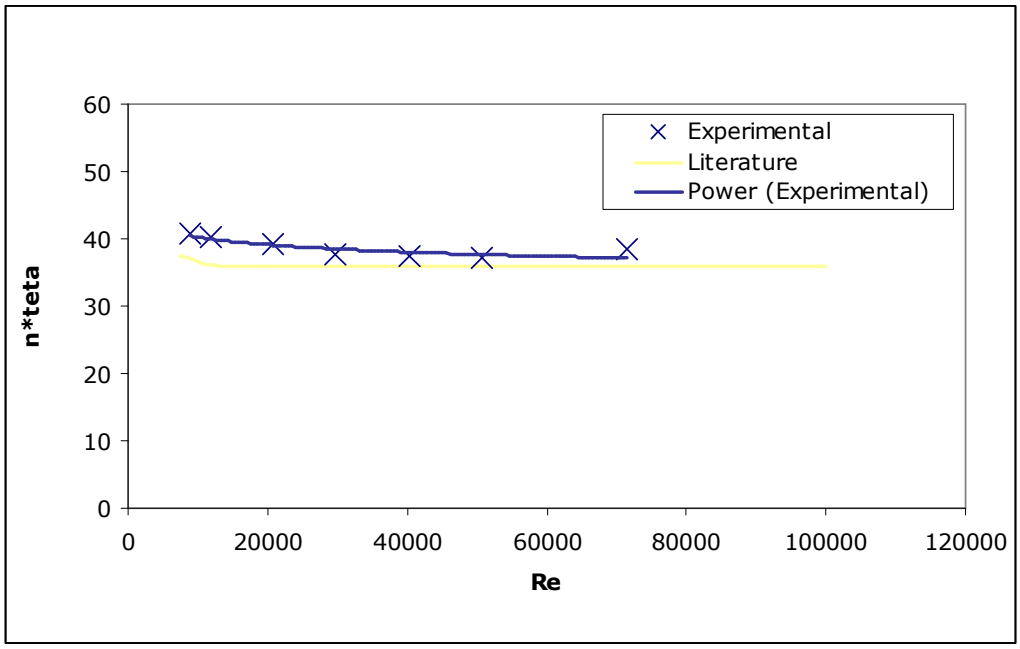

Figure 6.2 Mixing time characteristics for the 6 blade Rushton turbine

In Figure 6.2, y axis represents the dimensionless mixing time number, $n\theta$. Both results levels off approximately at 35 in the fully turbulent region. Despite the slight differences between the results, the employed mixing time measurement method was considered accurate enough to be used in the following stages of this study.

In Figure 6.3 the dimensionless macromixing time versus Reynolds number graph for the investigated impellers are shown. The dimensionless mixing time numbers have been obtained for a dimensionless mixing grade of M=0.95. Dimensionless times remain almost constant for each impeller type as opposed to the dimensional time. Therefore it should be the number of turns, not time itself, which affects the degree of mixing. Since Figure 6.3 is in terms of dimensionless numbers, it is universally applicable for the respective tank and impeller geometries. The dimensionless mixing time numbers of the impellers are given in Table 6.1. Rushton turbine has the lowest (38.70) and the hyperboloid impeller has the highest (177.92) dimensionless mixing time.

In Figure 6.4, variation of macromixing time with the rotational speed is given. As expected dimensional mixing time decreases sharply with increasing rotational impeller speed followed by a nearly constant mixing times at high rotational speeds. This behavior was exhibited by all impellers and impeller combinations although their quantitative responses were considerably different as given in Table 6.2.

As also stated earlier the most efficient impeller is the one with lowest Newton Number as well as the lowest dimensionless mixing time. The comparison between the impellers was done by determining their mixing times on the basis of equal power consumption. The power consumption of one of the mixers, i.e. hydrofoil 1, was selected as basis. Then the mixing time and the rotational speed values of the other mixers corresponding to the same power consumption were found by interpolation. At the same specific power consumption hydrofoil 1 impeller had the shortest mixing time, 7.81, whereas the hyperboloid impeller had the highest mixing time, 19.20.

In their review Nere et al. (2003) have mentioned about Rutherford et al.'s study, which was focused on the effect of blade thickness; Rutherford et al. have investigated the effect of the blade (w_{blade}) thickness on the flow and power numbers. They found that the flow number, power number, fluctuating velocity, and average velocity were higher for thinner impellers. Hence they observed lower mixing times for thinner impellers. With comparison on an equal power consumption basis, the mixing time was found to lower by 13% for the thinner impeller compared to the thicker radial flow impeller (Nere et al., 2003). Hydrofoil 1 impeller is better in mixing efficiency compared to hydrofoil 2 impeller, this might be due to the blade thickness of hydrofoil 2 impeller which is about three times larger than that of the the hydrofoil 1 impeller.

Hydrofoil 1 impeller proved to be the best in macromixing efficiency among the investigated impellers, this is due to the higher discharge flow produced by the hydrofoil 1 impeller compared to other impellers at equal power consumption; the study of Fentiman et al. (1998) regarding the characteristics of a hydrofoil impeller has been given in part 4.1.1. Distelhoff et al.'s study, as explained in part 4.1.1, also indicates that axial flow impellers have shorter mixing times compared to the radial ones at equal power consumption.

Hydrofoil mixers provide strong axial top to bottom flow all over the mixing tank, however hyperboloid mixers provide a radial flow especially in the tank bottom and a slower mixing occurs in the upper part of the mixing tank. The high mixing time value of hyperboloid mixer can be attributed to this, since in the experiments the salt solution is added from the surface of the mixing tank. Because of that the hyperboloid impeller is effective in the lower part of the tank; the upper part of the mixing tank might have not been mobilized as much as the lower part of the tank.

In selecting impeller type another important criteria is the physical nature of the material to be agitated or mixed. Appropriate configuration should be used depending on the solution viscosity, density, and multi-phase characteristics, i.e. if the solution to be treated is a suspension, emulsion or gas-liquid mixture. The

hyperboloid impellers were developed for suspension and dispersion purposes. Because of their design as close clearance impellers, they do not have good macromixing properties compared to standard impellers. The flow a hyperboloid produce goes radially over the tank bottom reach the tank wall and return back to the mixer top axially. This prevents the settling of heavy particles in the tank bottom, makes them get mobilized and also provides a good dispersion in aeration.

Considering the aforementioned characteristics of the hyperboloid mixer, a mixer combination of it, especially with an impeller having a high pumping capacity, is a reasonable choice for waste water treatment facilities since the bottom circulation produced by the hyperboloid mixer would be distributed along the whole tank and a complete top to bottom circulation will be achieved. Two different combinations of hyperboloid impeller with hydrofoil 1 impeller were used for this purpose in this study.

When the two hydrofoil 1 and hyperboloid impeller combinations are compared the one having the upper mixer off-surface clearance of d, in which the upper mixer is closer to the water surface, proved to be more efficient. This is an expected result; in the literature various studies indicate that the mixing time increases with a decrease in the off-bottom clearance of the axial flow impeller. Rao et al.'s (1988) study , which was explained in Part 6.1.1, have shown that for the axial flow producing downflow pitched blade turbine the value of the mixing time was found to increase with a decrease in the impeller clearance.

The raw data of the macromixing measurements in cylindrical tank are given in Appendix B.

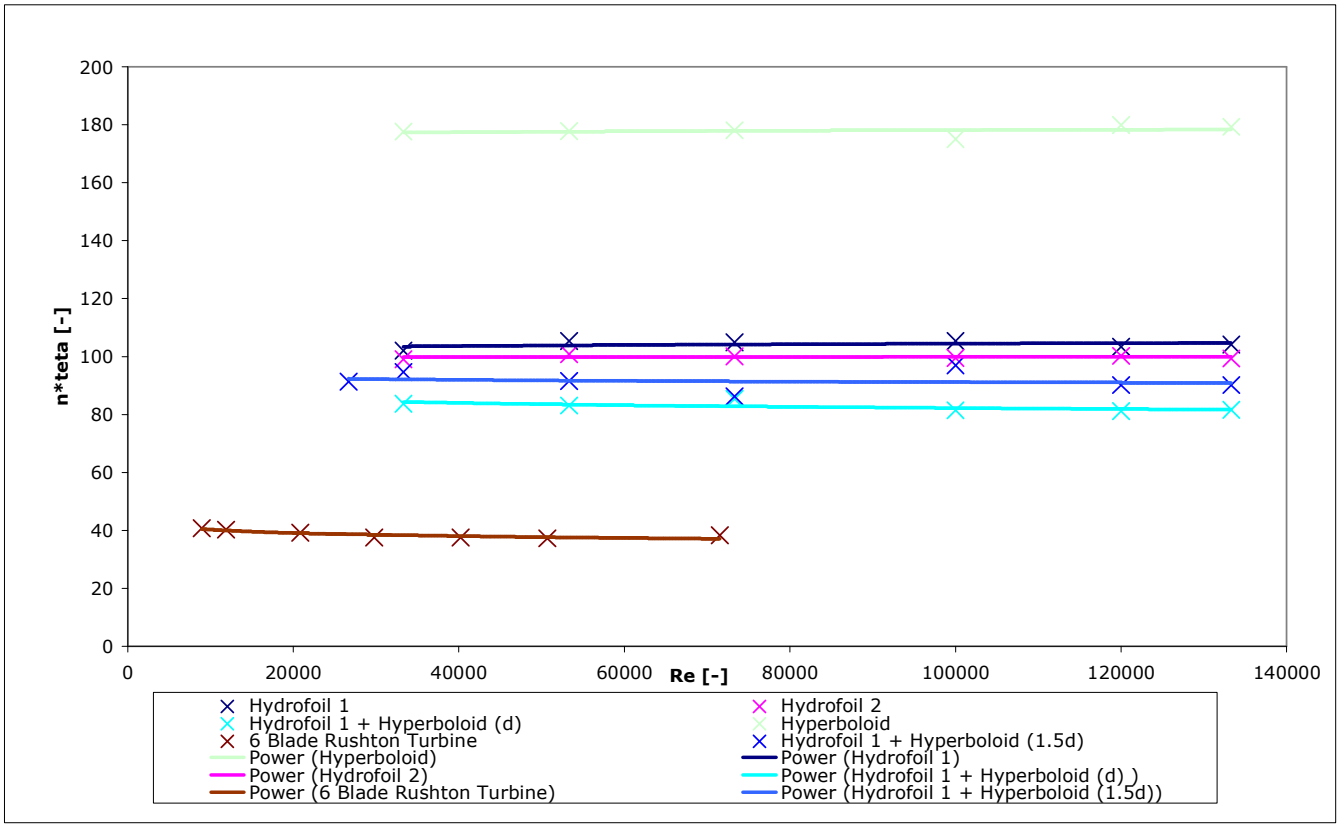

Figure 6.3 Variation of dimensionless mixing time with Reynolds number in cylindrical vessel

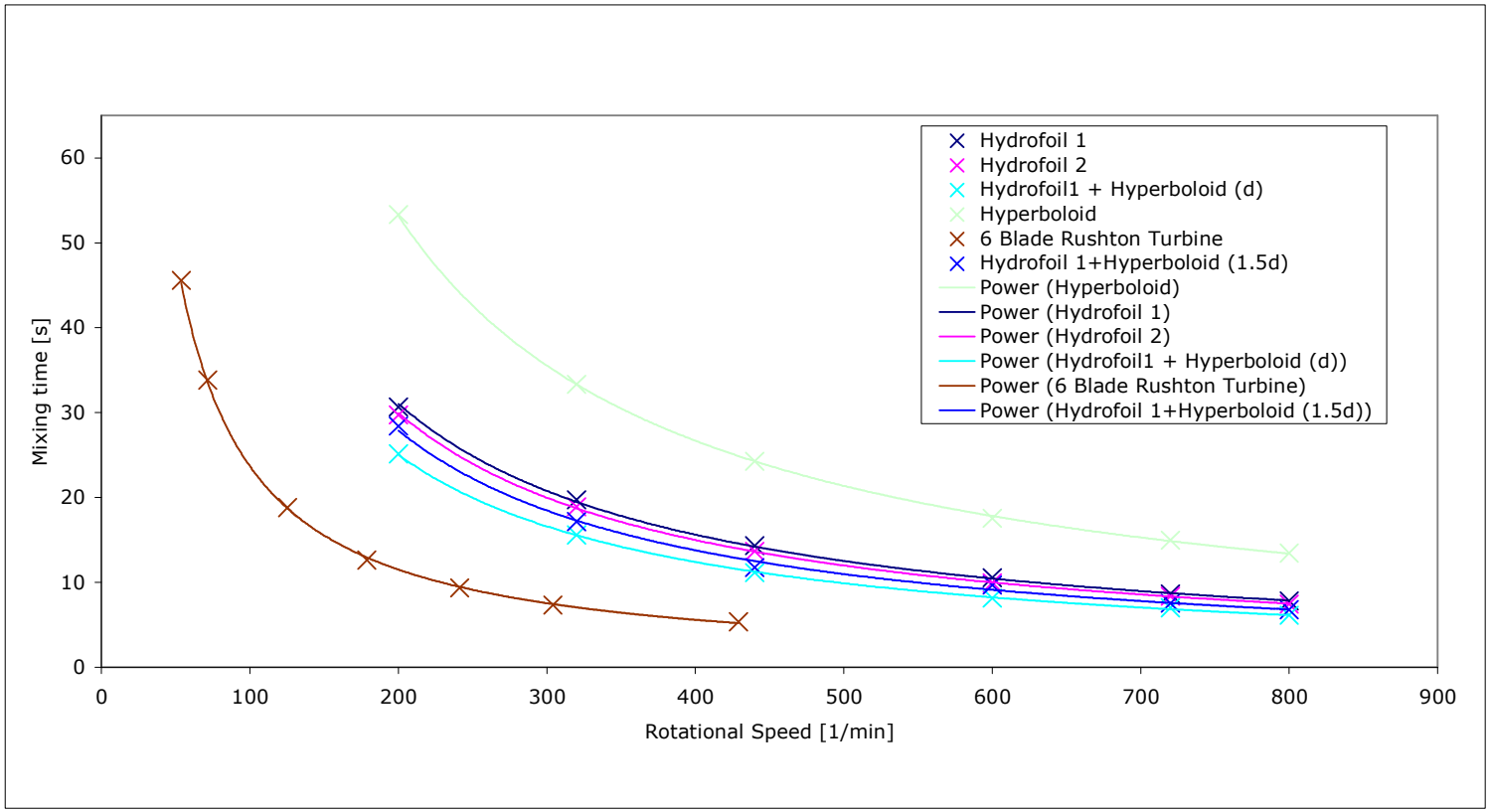

Figure 6.4 Variation of mixing time with rotational speed in cylindrical vessel

Table 6.1 Dimensionless mixing time numbers of the investigated impellers

Impeller Type	$n\theta$
Rushton Turbine	38.70
Hydrofoil 1 Impeller	104.2
Hydrofoil 2 Impeller	99.84
Hyperboloid Impeller	177.92
Hydrofoil 1 + Hyberboloid Combination (1.5d)*	91.61
Hydrofoil 1 + Hyberboloid Combination (d)	82.47
(*)Submergence of the top impeller (hydrofoil 1)	

Table 6.2 Mixing times at the same power consumption for the investigated impellers

	P/V [W/m^3]	$n \cdot \theta$ [-]	n [1/s]	θ [s]
Hydrofoil 1 Impeller	163	103.9	13.3	7.81
Hydrofoil 2 Impeller	163	100.59	10.5	9.58
Hyperboloid Impeller	163	178.6	9.3	19.20
Hydrofoil 1 & Hyperboloid Combination (d)*	163	83.08	8.3	10.01
Hydrofoil 1& Hyperboloid Combination (1.5d)*	163	86.33	7.31	11.81
* Submergence of the top impeller (hydrofoil 1)				

6.1.2.1. Comparison of the Mixing Time Results with Correlations

In the literature it is possible to find empirical correlations for the estimation of the mixing time. Ruszkowski (1994) obtained the following empirical correlation for the mixing time by working with 6 different types of pitched blade turbine, a disc turbine and a propeller:

$$\theta = 5.3\left(\frac{1}{n}\right)\left(\frac{1}{Ne^{1/3}}\right)\left(\frac{D}{d}\right)^{2} \tag{6.1}$$

In the Ruszkowski correlation, power number was used to account for the effect of impeller type. Such correlations are useful to have an approximate idea about the mixing times before an experimental study. In Figure 6.5 the Ruszkowski correlation given in Equation 6.1 was used to determine the mixing time of the two hydrofoil impellers. There is considerable underestimation of mixing times. This may be due to the usage of large quantity of pitched blade turbine data and a radial flow producing disk turbine data, the mixing time of which is quite short, in determining the correlation. The mixing times get closer to each other as the Reynolds number increases for both experimental results and estimations.

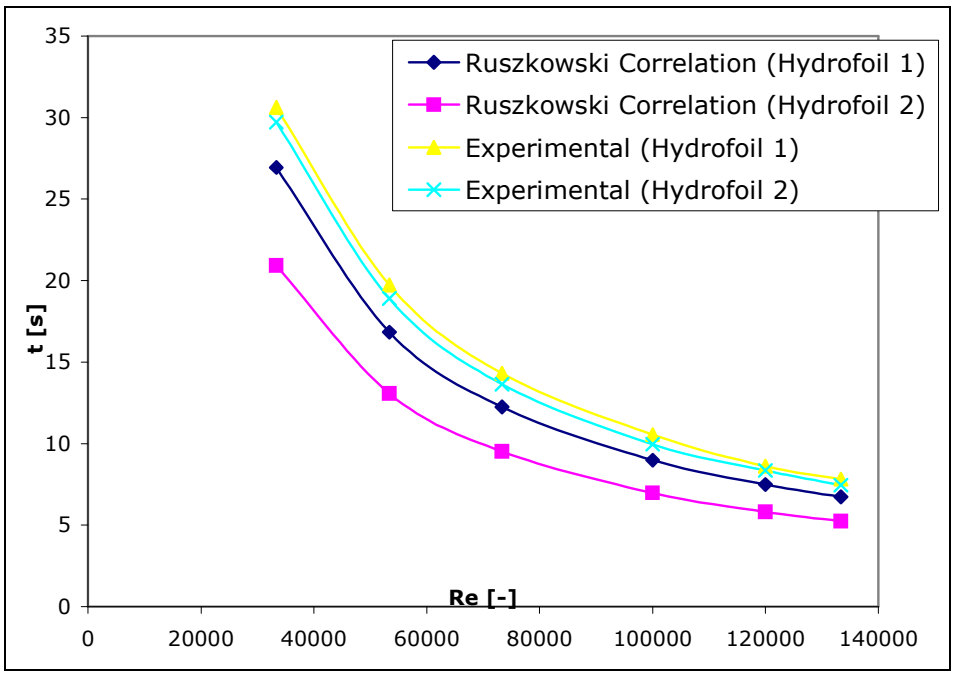

Figure 6.5 Comparison of the experimental results with the Ruszkowski correlation estimations

Ruszkowski had rearranged Equation 6.2 to show the dependency of mixing time on impeller diameter, given constant scale and constant power input:

$$\Theta = 5.91 D^{2/3} \left(\frac{\rho V}{P} \right)^{1/3} \left(\frac{D}{d} \right)^{1/3} \tag{6.2}$$

The comparison with the correlation given in Equation 6.2 was done and the results are shown in Figures 6.6 and 6.7.

Further correlations for the estimation of macromixing time, e.g. Mersmann (1994) and Corssin (1968), have been summarized in Nere et al.'s (2003) overview.

As explained in part 3.1.1. Schäfer (2001) has also studied the macromixing efficiency of a hydrofoil impeller which has also the profile form 417 A with d/D ratio of 0.375. He stated that an estimation of macromixing efficiency through Ruszkowski's correlation wasn't possible then on for hydrofoil impellers since the estimation of mixing time was about 25% higher than his experimental results. When Figure 6.6 is examined, it will be seen that the hydrofoil 1 impeller results are in good agreement with Equation 6.2. Hence Ruszkowski correlation is still helpful for the mixing time estimation of the hydrofoil 1 (profile 417 A) impeller with stirred tank configuration used in this study as opposed to Schäfer's (2001) statements.

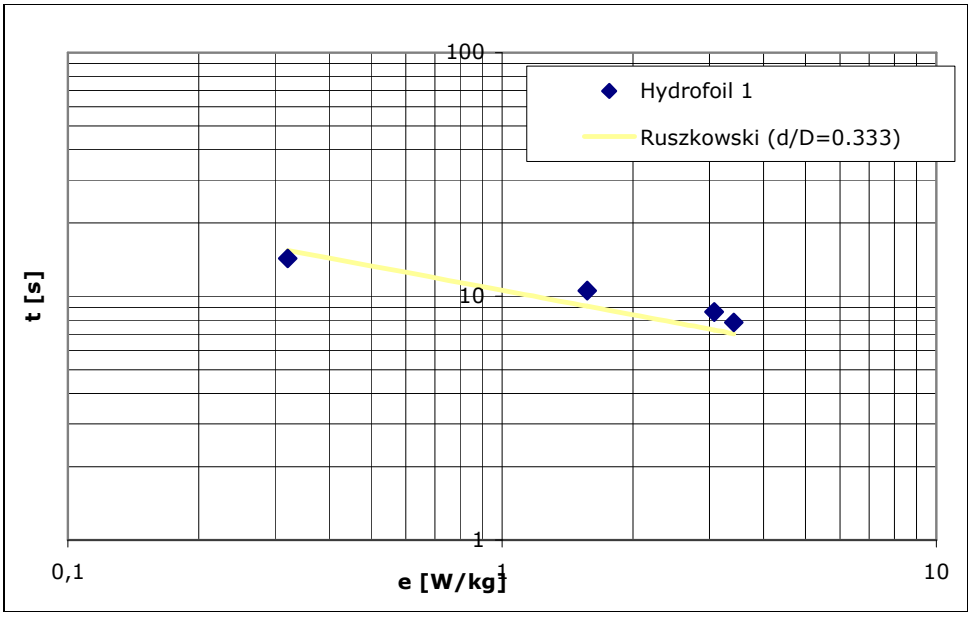

Figure 6.6 Estimation of the mixing efficiency of the hydrofoil 1 impeller

As it is seen in Figure 6.7, there is an underestimation of the Ruszkowski correlation for the hydrofoil 2 impeller. The previously tabulated mixing time results have already shown that hydrofoil 2 impeller was less efficient compared to hydrofoil 1 impeller. In this respect this is an expected result.

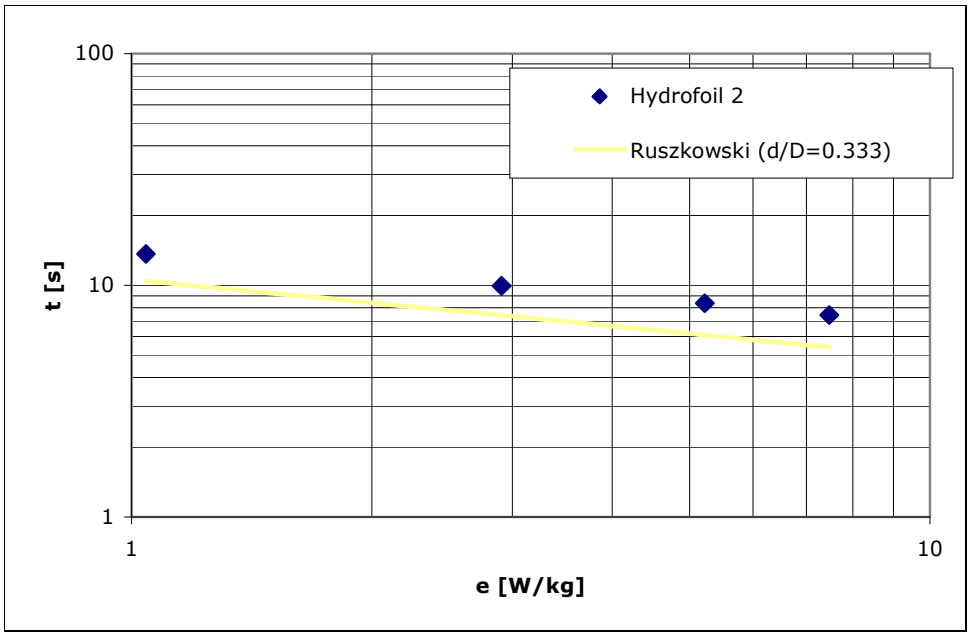

Figure 6.7 Estimation of the mixing efficiency of the hydrofoil 2 impeller

In the recent studies it was shown that the minor dimensions such as the mixer hub, blade thickness have been found to have an influence on the flow, power and mixing characteristics, and in some cases modification of these dimensions may prove relatively more beneficial as compared to major dimensions such as the blade length and blade width. Especially the length of the impeller hub has been shown to have a considerable effect on the power number (Nere et al., 2003).

If the length of the hub and the blade thickness of the hydrofoil 2 impeller were lowered, a higher discharge flow at lower power consumption could be achieved compared to the hydrofoil 1 mixer, which proved to be the most efficient among the impellers investigated.

6.1.3. Ultrasound Doppler Measurements

In this section UDV results are presented. Both radial and axial components of the flows in the selected region of the tanks are measured. In the experiments the impeller tip velocity was 2 m/s corresponding to a Reynolds number of 63600. Axial and radial flow measurements were performed according to the procedure explained in Part 5.2.3. The set value for the maximum velocity was 722 mm/s, consequently the maximum depth was 91 mm for all experiments. The axial measurements were performed as explained in part 5.2.3; the probe was fixed to a certain height from the tank bottom in the direction of the mixer shaft and in the middle of two baffles. At the set axial heights the measurements were taken with 1 cm spacing in between the mixer shaft and the tank wall. For the axial measurements of hydrofoil 1 and hydrofoil 2 impellers the probe was placed at height of 14 cm ($0.47D$) from the tank bottom. Axial measurements of combination 1 and 2 were done at two locations; the probe was placed at 14 and 24 cms from the tank bottom. All of the radial measurements were performed from 5 to 30 cm from the tank bottom in the direction of the mixer shaft and in between two baffles. Unsatisfactory results were obtained for radial measurements due to refractive effects at the curved surface of the mixing vessel. In the radial flow measurements the measuring technique was completely non-intrusive however in axial measurements the probe was fixed inside the mixing tank.

The velocities are non-dimensionalised with the impeller tip speed $U_{tip} = \pi Dn$; the colours in the contour representation show the relative velocities. The axial velocities in the direction from tank bottom to the water surface are displayed as

blue and those from the tank surface to tank bottom are displayed as red. The radial and axial turbulence intensity ($Tu = \frac{\sqrt{\overline{u_i'^2}}}{\overline{U_i}}$) distributions in the agitated vessel were also determined. The only mixer geometry that can be displayed in the DrawSTR is the hydrofoil 1 impeller, because of this reason the hydrofoil 2, hyperboloid and the hydrofoil 1+hyperboloid combinations can not be displayed in Figures 6.12 to 6.23. In Figures 6.12 to 6.15 hydrofoil 1 impeller geometry was used to display the hydrofoil 2 impeller geometry.

6.1.3.1. Results of Hydrofoil 1 Impeller

Axial Measurements

The axial flow produced by the hydrofoil 1 impeller is given in Figure 6.8. The fluid is sucked by the impeller axially and it is pumped downwards. It goes along the tank bottom, reaches the tank wall, goes up the tank wall and returns to the impeller again. The red region near the impeller blades shows the downward pumping in the axial direction. In the impeller region the values of the axially downwards velocities reaches to 0.125 x U_{tip}, i.e., 25 cm/s, at a height of 1/3 D from the tank bottom. Near the tank wall axial upward velocities, reaches to 0,025 x U_{tip}, i.e. 50 cm/s at a height of 1/3 D from the tank bottom. The axially downwards velocity is very large in the vicinity of the impeller and is rapidly decreased in accordance with the distance from the impeller approaching a uniform distribution in between the tank wall and the impeller and the axially upwards velocity becomes large in the vicinity of the tank wall.

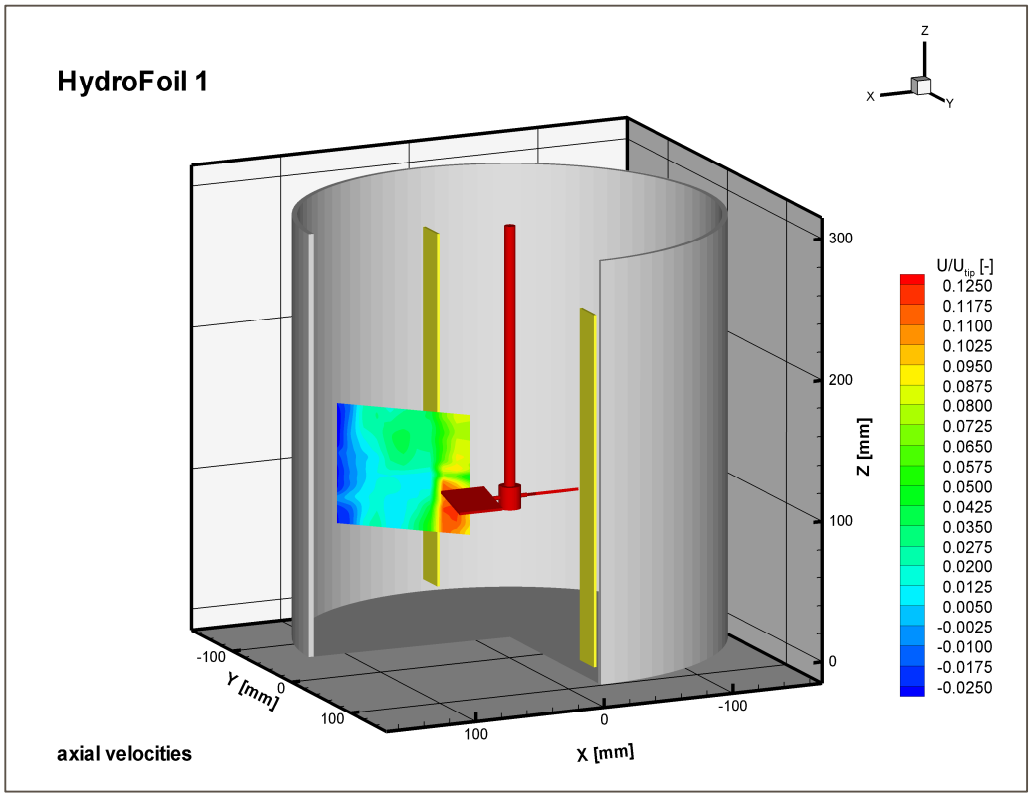

Figure 6.8 Axial dimensionless velocities of hydrofoil 1 impeller

The turbulence intensity, for axial measurements of hydrofoil 1 impeller is given in Figure 6.9. The axial turbulent intensity is very large in the vicinity of the impeller and is rapidly decreased in accordance with the distance from the impeller approaching a uniform distribution just the same way as time-mean velocity distribution; maximum observed turbulence intensity was 0.15 in the vicinity of the impeller. The turbulence intensities decrease as it is approached from the impeller region to the tank wall. This due to the strong downflow pumping capacity of the hydrofoil 1 impeller whose strength is lowered gradually towards the tank wall.

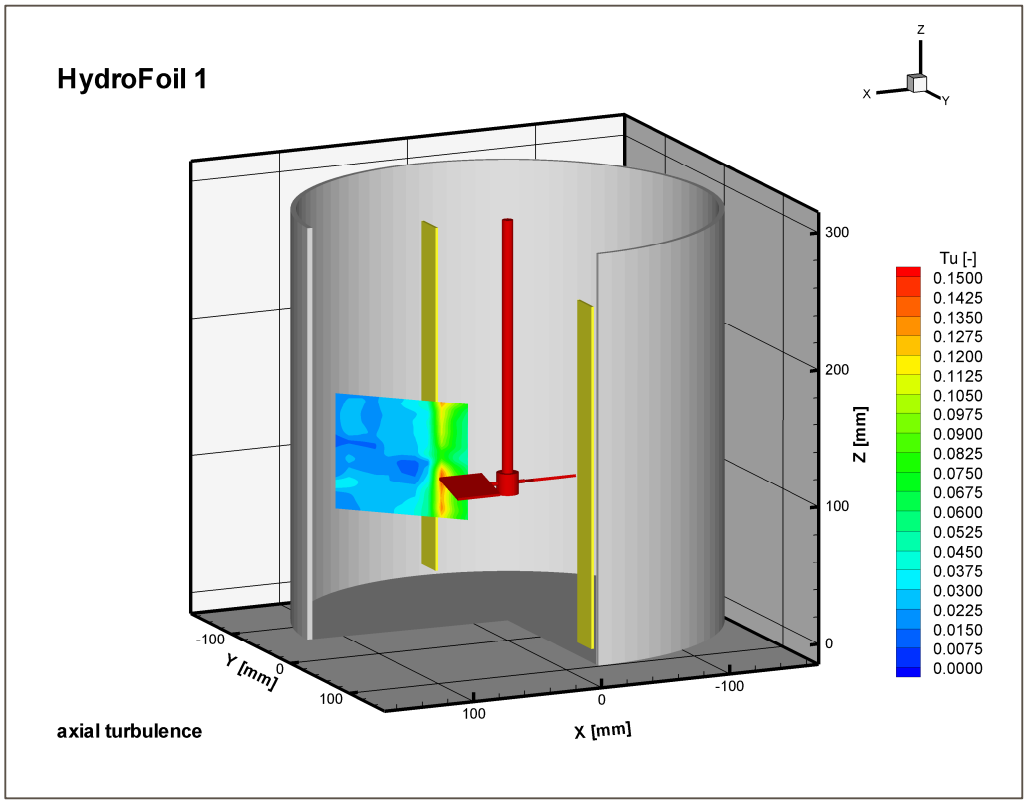

Figure 6.9 Axial turbulence of hydrofoil 1 impeller

Kresta and Wood (1992) have stated that the turbulence intensity close to the impeller blades is of the order of 100 %, and drops rapidly to the order of 10 % or less in the bulk of the tank. In this study the turbulence intensities observed in axial measurements also verify this statement.

Radial Measurements

Hydrofoil 1 is an axial flow producing impeller consequently it was not expected to observe any radial flow in the mixing tank. Presence of a large green region, i.e. low radial component in Figure 6.10, indicates that the flow was mainly in the axial direction. Radial flow is observed only in the near impeller region and in between the tank wall and the mixer shaft. The hydrofoil 1 impeller sucks the fluid and pumps it downwards, during this pumping the fluid inbetween the mixer shaft and the tank wall is also sucked radially to the near-impeller region. This is the reason of the partly formed radial flow in the mixing tank. The radial flow formed between the tank wall and the impeller has a velocity about 0.02 x U_{tip}, i.e., 40 cm/s, at a height of about $1/3D$ from the tank bottom mostly close to the tank wall.

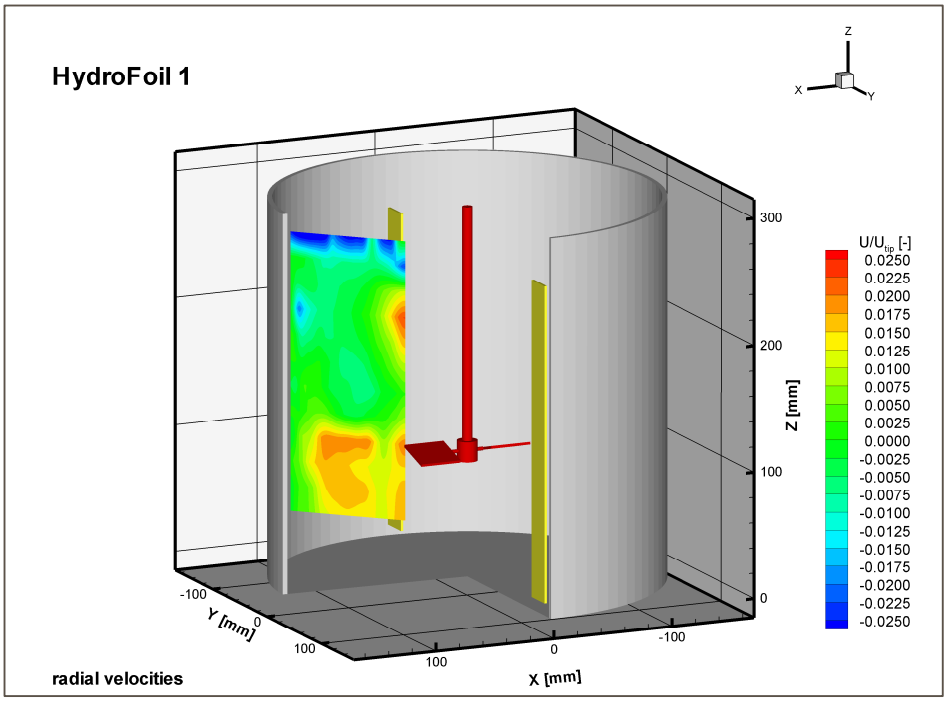

Figure 6.10 Radial dimensionless velocities of hydrofoil 1 impeller

Since the velocity of the radial flow is smaller compared to the axial flow in the tank, the turbulence intensity of it is nearly zero in the investigated region as it will be seen in Figure 6.11. The highest turbulence intensity observed was 0.025 at about the midheight of the tank. Axial turbulence intensities are six times as large as the radial turbulence intensities in the near impeller region, so the discharge flow is in a state of non-isotropic turbulence. In a remote part from the impeller, turbulence intensities have an almost equal value, so the turbulence seems to be almost isotropic.

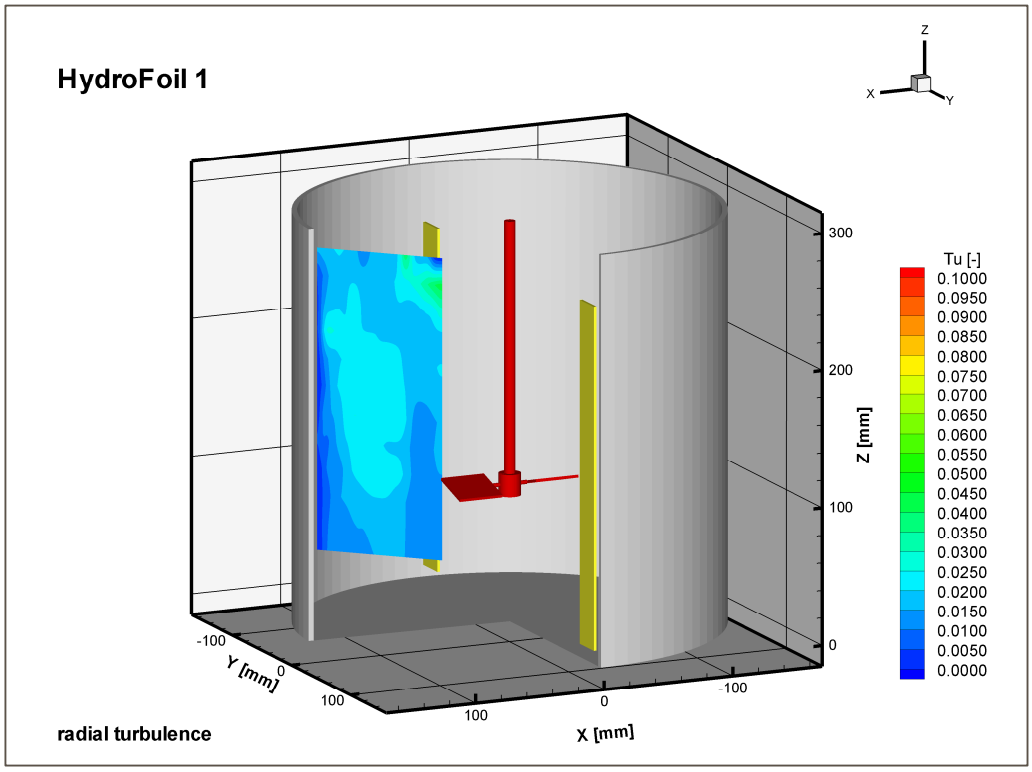

Figure 6.11 Radial turbulence of hydrofoil 1 impeller

6.1.3.2. Results of Hydrofoil 2 Impeller

Axial Measurements

The hydrofoil 2 impeller is also an axial flow impeller, the flow field of which is similar to that of hydrofoil 1's, however the flow produced by it but is not as strong as that of hydrofoil 1 impeller's as can also be understood from mixing time experiment results given in Part 6.1.1. When the UDV results of hydrofoil 1 and 2 impellers are compared, the similarity in the generated flow will also be observed as well as the lower velocities occurred in the hydrofoil 2 case. Highest velocities are observed in the vicinity of the impeller as in the case of hydrofoil 1 impeller. In the impeller region, where the fluid is sucked and pumped axially downwards, higher velocities are observed; at the red coloured small region in the vicinity of the impeller velocities reach up to 0.110 x U_{tip}, i.e., 22 cm/s. The mixing time results also demonstrate the higher efficiency of hydrofoil 1 impeller compared to hydrofoil 2.

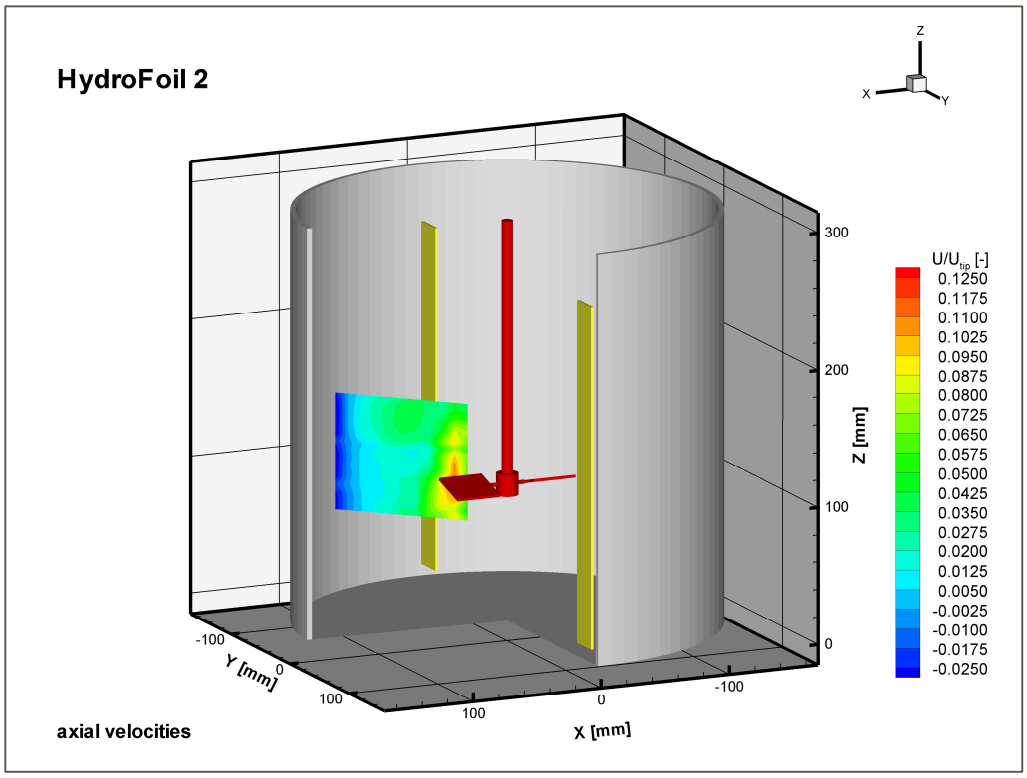

Figure 6.12 Axial dimensionless velocities of hydrofoil 2 impeller

The turbulence intensity for axial measurements of hydrofoil 2 impeller is given in Figure 6.13. Near the impeller region where the fluid is sucked by the impeller, higher turbulence intensity was observed; in the axial direction of near impeller region turbulent intensities of about 0.08 were observed while in the remaining part of the tank they were close to zero.

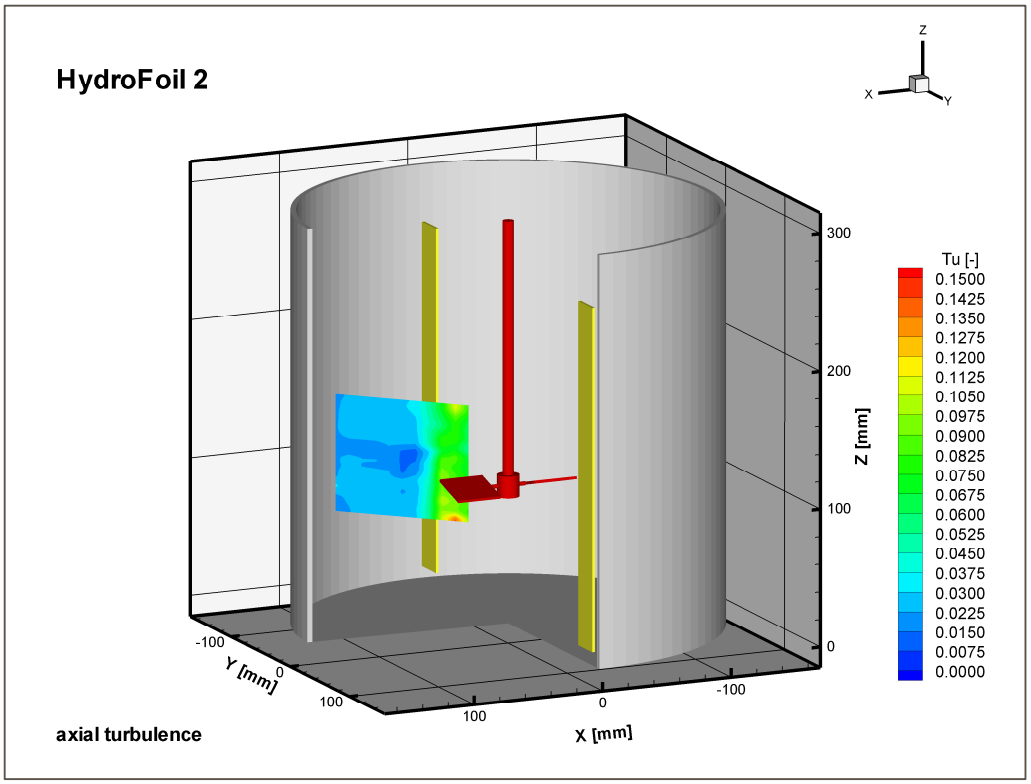

Figure 6.13 Axial turbulence of hydrofoil 2 impeller

Radial Measurements

There is also a large green region in the radial measurements of hydrofoil 2 impeller which demonstrates that the radial velocities in the given region are zero. A red region exists at the mid-height between the tank wall and the impeller. It can be said that at the mid-height the fluid is directed radially to the impeller through the suction. This radial flow formation can be seen in the lightsheet photo of hydrofoil 2 in the following section. The radial flow formed between the tank wall and the impeller has a velocity about 0.02 x U_{tip}, i.e., 40

cm/s, at a height of about $1/3D$ from the tank bottom in the middle of the mixer shaft and the tank wall.

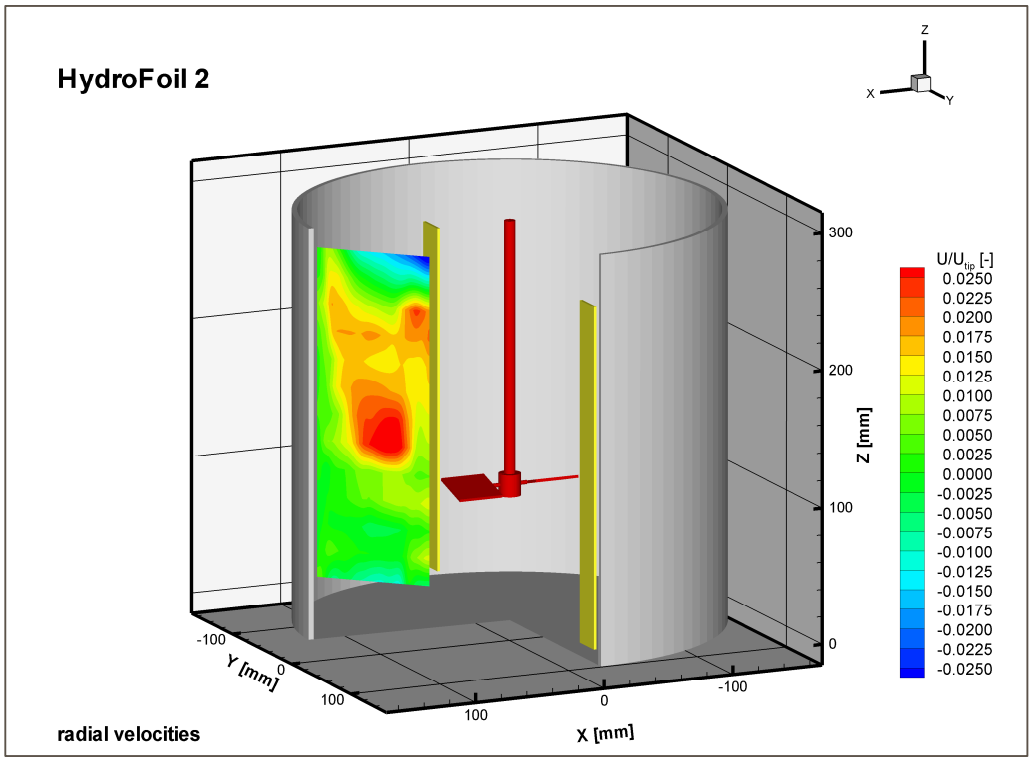

Figure 6.14 Radial dimensionless velocities of hydrofoil 2 impeller

The turbulence intensity for radial measurements of hydrofoil 2 impeller is given in Figure 6.15. Radial turbulence intensities obtained are nearly zero in the investigated region. Highest turbulence intensities are observed slightly above the mid-height of the tank with a value of 0.02. Axial turbulence intensities are four times as large as the radial turbulence intensities at the impeller height, so the discharge flow is in a state of non-isotropic turbulence. In a remote part from

the impeller, turbulence intensities have an almost equal value, so the turbulence seems to be almost isotropic as in the case of hydrofoil 1 impeller.

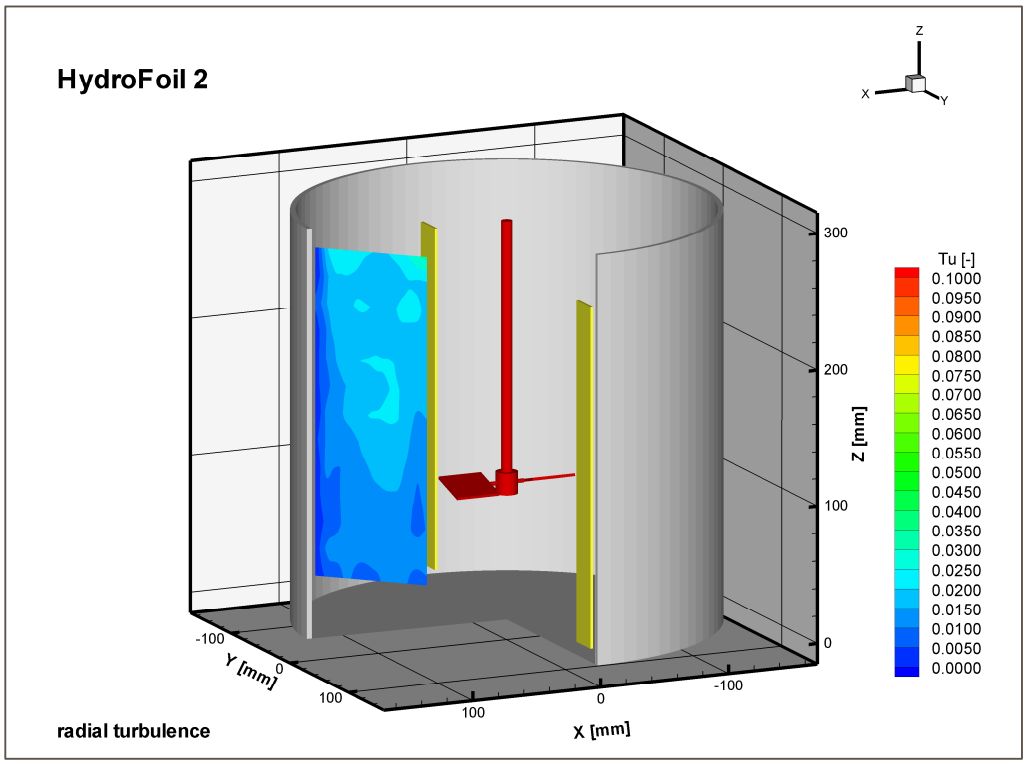

Figure 6.15 Radial turbulence of hydrofoil 2 impeller

6.1.3.4. Results of Combination 1 (submergence of the top hydrofoil impeller = d)

Axial Measurements

The so called mixer "combination 1" (submergence of the top hydrofoil impeller = (d) and the off-bottom clearance of hyperboloid mixer = ($d/10$)) was also examined by the UDV method. The results are given in Figure 6.16. The probe was placed at two positions, 14 cm and 24 cm from the tank bottom, since the probe could be placed at only these two positions because of the position of the upper mixer. In between heights 5 cm and 14 cms, a partly red region was displayed near the mixer shaft where the fluid is pumped axially downwards along the hyperboloid mixer body. In this region higher axial velocities are observed at higher measuring points from the tank bottom because of the effect of the upper hydrofoil 1 impeller. At the highest point maximum velocities reach up to 0.125 x U_{tip}, i.e., 25 cm/s. As it is approached from the mixer shaft to the tank wall, first the value of the axially downwards velocities decrease gradually, and as it is approached to the tank wall the direction of the axially downwards velocities change; they go axially upwards and increase gradually, which is displayed as dark blue in Figure 6.16. The maximum value of the axial velocities that go up along the tank wall are 0.025 x U_{tip}, i.e., 5 cm/s, which is smaller compared to the axially downwards velocities near the mixer shaft. At the upper measuring location; between 24 cm and 15 cms from the tank bottom and in between the upper impeller tip and the tank wall, the value of the axially downwards velocities are smaller. The value of the axially upwards velocities near the tank wall are same as the measurements at 9 cm – 14 cms from the tank bottom.

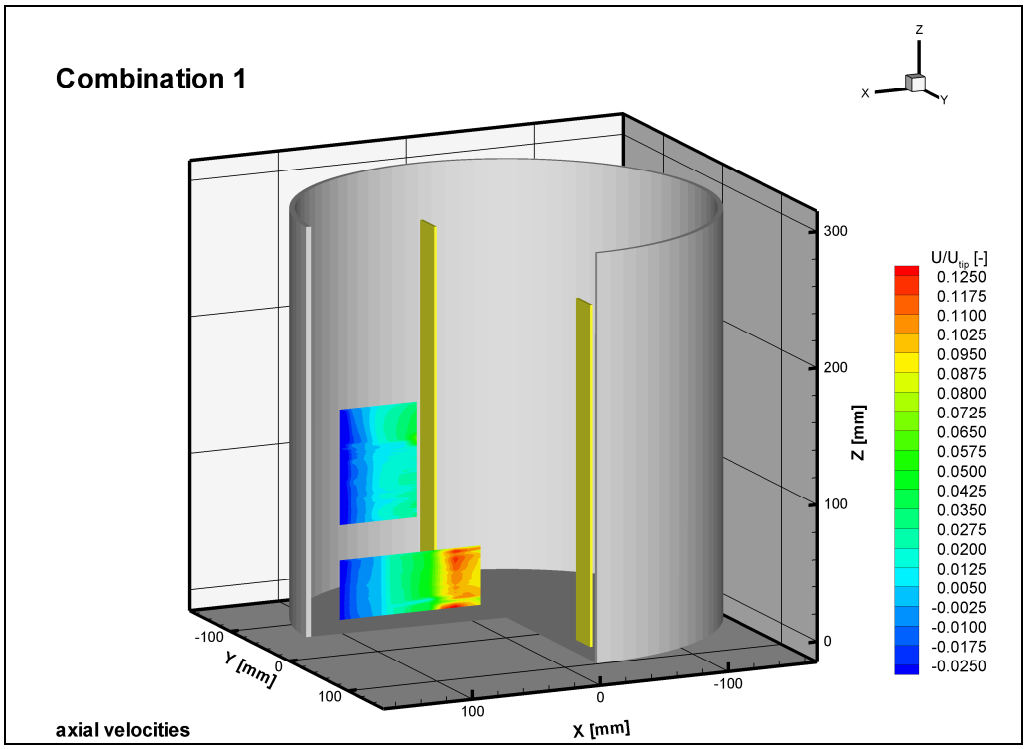

Figure 6.16 Axial dimensionless velocities of hydrofoil 1 and hyperboloid combination (d)

Axial turbulence of combination 1 is given in Figure 6.17. In the investigated regions the turbulence intensities are quite close to zero. In the lower measuring region near the mixer shaft where the highest axial velocities are observed, the turbulence intensities are about 0.0975 and the highest turbulence intensity observed was 0.1125.

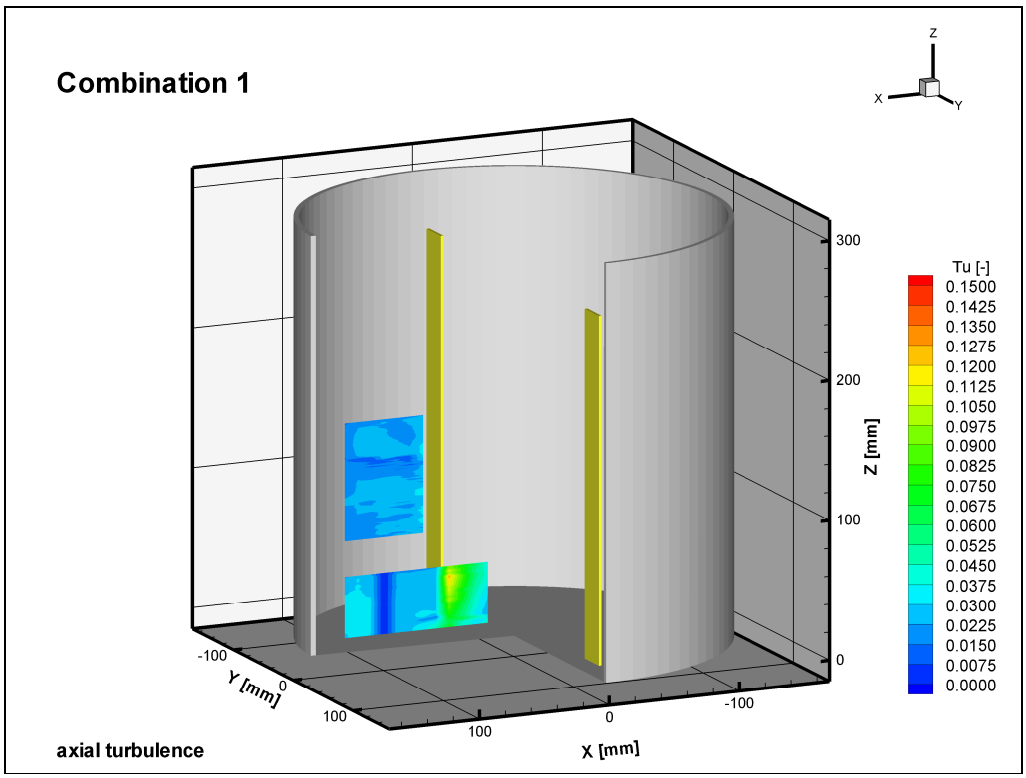

Figure 6.17 Axial turbulence of hydrofoil 1 and hyperboloid combination (d)

Radial Measurements

Radial dimesionless velocities are given in Figure 6.18. As most of the measuring region is displayed as green, radial velocities obtained are mainly close to zero. At about 12 cms from the tank bottom, in between the mixer shaft and the tank wall, higher radial velocities are observed which was displayed as red-yellow in Figure 6.18. This is due to the radial flow produced by the hyperboloid impeller which gets stronger in this region. This can also be visualized in the lightsheet photos given in the following part.

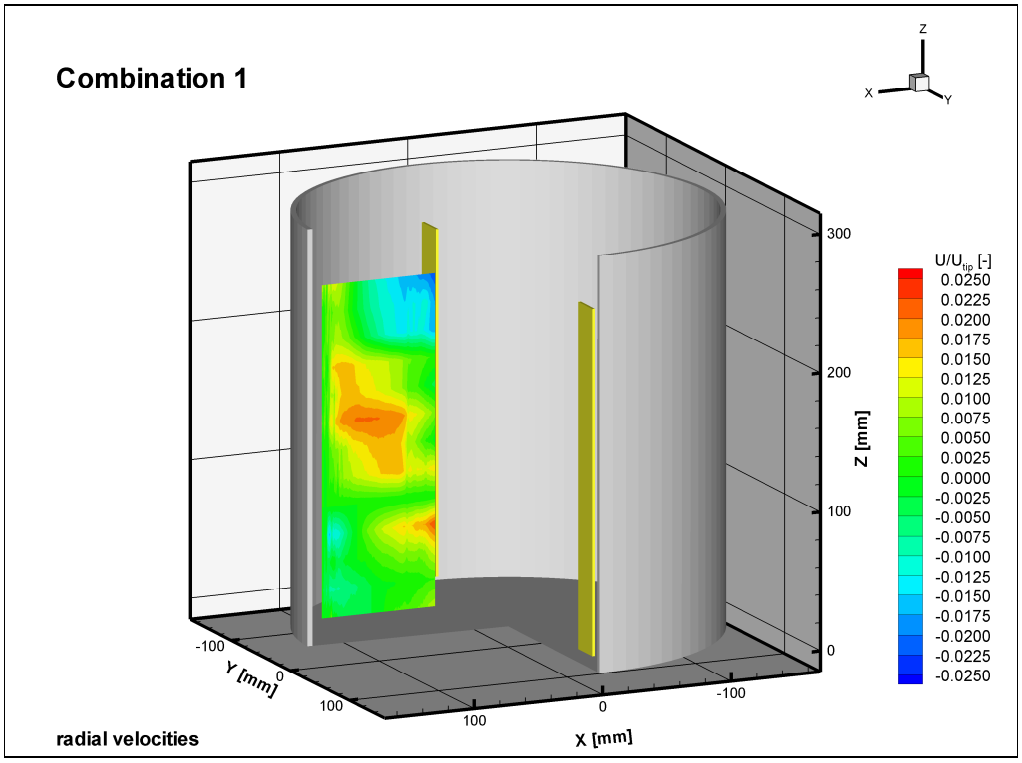

Figure 6.18 Radial dimensionless velocities of hydrofoil 1 and hyperboloid combination (d)

Near the tank wall the turbulence intensities are zero. Their values get increased towards the impeller region. Their distributions are similar to the time mean velocity distribution in Figure 6.18. Highest turbulence intensity observed is 0.03 near the upper impeller region at a height of $2/3D$ from the tank bottom. The S/N ratio was quite low in radial measurements due to the refraction of ultrasonic beam in the cylindirical tank wall, so insufficient results were obtained for radial measurements.

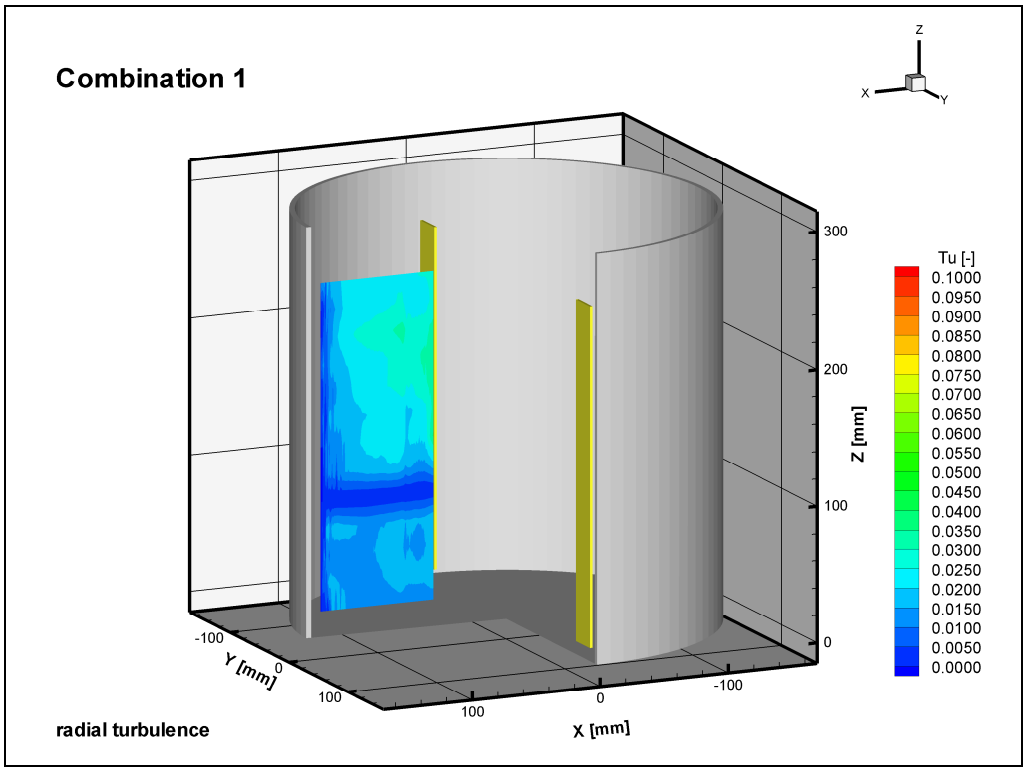

Figure 6.19 Radial turbulence of hydrofoil 1 and hyperboloid combination (d)

The radial measurements were not that much helpful for understanding the stirred tank hydrodynamics. The obtained velocities of radial measurements were close to zero. There is of course a strong axial flow in the tank; however the main reason for obtaining most velocities as zero should be due to the experimental errors, i.e., the refraction of the ultrasonic beam in the cylindrical tank wall. For example the dark blue region which has zero value between the tank wall and the mixer shaft at a height about 8 cm from the tank bottom indicates that no signals from that region could be obtained.

6.1.3.5. Results of Combination 2 (submergence of the top hydrofoil impeller = 1.5d)

The so called mixer "combination 2" (submergence of the top hydrofoil impeller $=1.5d$ and the off-bottom clearance of hyperboloid mixer = $d/10$) was also examined by the UDV method. The results can be seen in Figure 6.20. The probe was placed at two positions, 14 cm and 24 cm from the tank bottom. In between heights 5 cm and 14 cms, a partly red region was displayed near the mixer shaft where the fluid is pumped axially downwards along the hyperboloid mixer body, as in the case of mixer combination 1. In this region higher axial velocities are observed at higher measuring points from the tank bottom because of the effect of the upper hydrofoil 1 impeller. Since the position of the hydrofoil 1 impeller in mixer combination 2 is closer to the measuring location compared to its position in mixer combination 1, the red region showing the downward axial velocities is intenser. Maximum velocity observed was 0.125 x U_{tip}, i.e., 25 cm/s. As it is approached from the mixer shaft to the tank wall, first the value of the axially downwards velocities decrease gradually, and as it is approached to the tank wall the direction of the axially downwards velocities change; they go axially upwards and increase gradually, which is displayed as dark blue in Figure 6.20. The change to axially downwards velocities from axially upwards velocities, from the mixer towards the tank wall) occurs more gradual in mixer combination 2 compared to mixer combination 1. The value of the axially upwards velocities in the vicinity of the tank wall at 9 cm – 14 cms from the tank bottom are the same as the upwards velocities in the vicinity of the tank wall at 24 cm – 15 cms from the tank bottom. However the highest axially downward velocities at 24 cm – 15 cms in the vicinity of the tank wall extends radially towards the impeller for a larger region compared to velocities at 9 cm – 14 cms from the tank bottom, the change is more gradual in the lower part of the tank.

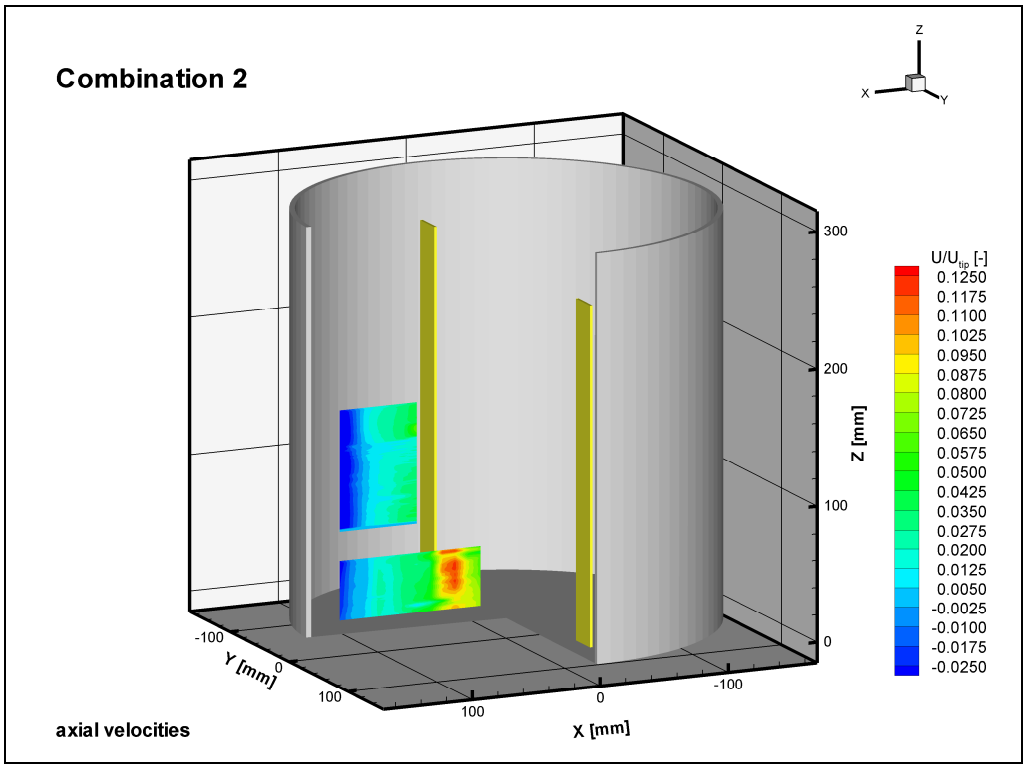

Figure 6.20 Axial dimensionless velocities of hydrofoil 1 and hyperboloid combination (1.5d)

Axial turbulence of combination 2 is given in Figure 6.17. In the investigated regions the turbulence intensities are quite close to zero. In the lower measuring region near the mixer shaft where the highest axial velocities are observed, the turbulence intensities are about 0.0065 and the highest turbulence intensity observed was 0.095. The turbulence intensities of mixer combination 1 are higher compared to mixer combination 2 in this region.

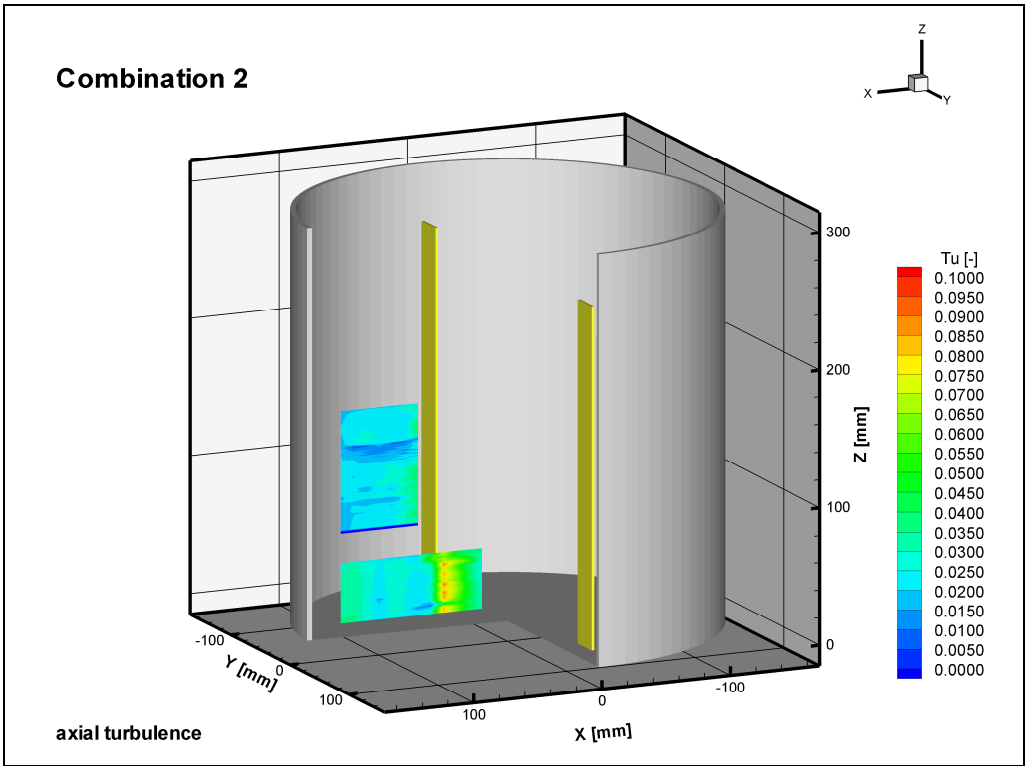

Figure 6.21 Axial turbulence of hydrofoil 1 and hyperboloid combination 2 (1.5d)

Radial Measurements

Radial dimesionless velocities are given in Figure 6.22. As most of the measured region is displayed as green, radial velocities obtained are mainly close to zero. At the midheight of the tank, in between the mixer shaft and the tank wall, higher radial velocities are observed which was displayed as red in Figure 6.22. A radial flow is formed in this region at the upper mixer height, where the part of the fluid (leaving the hyperboloid impeller, going radially over the tank bottom, going up the tank wall) returning back to the hyperboloid impeller body, is sucked by the hydrofoil 1 impeller together with the fluid in the upper-half part

of the tank. This can also be visualized in the lightsheet photos given in the following part.

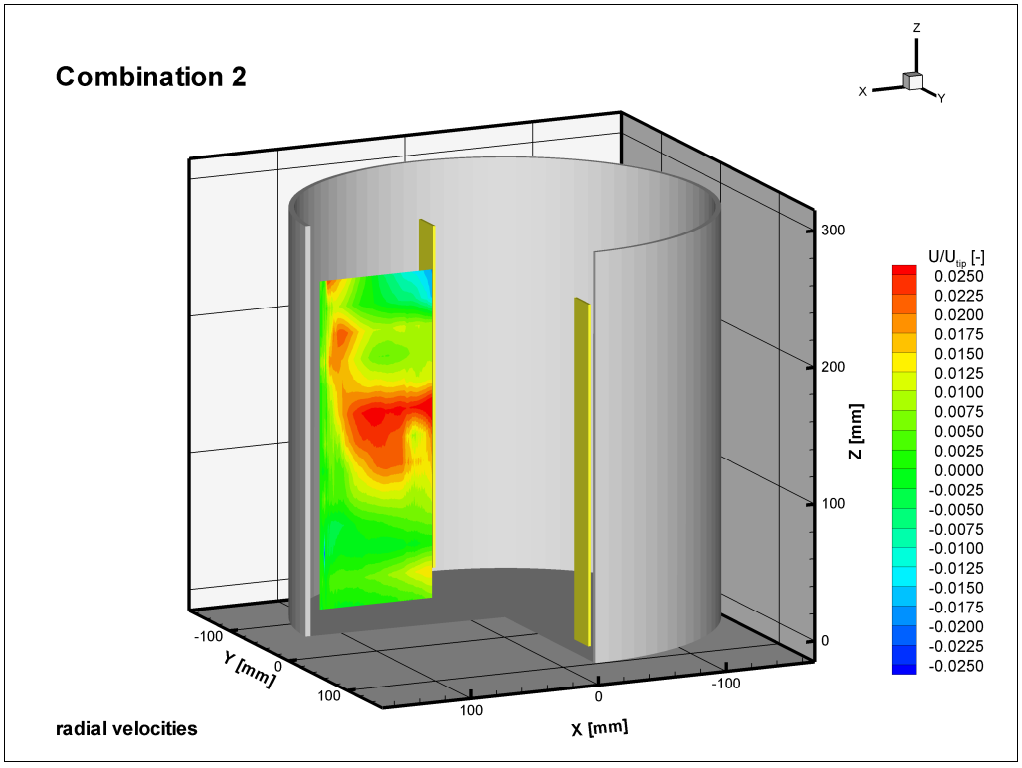

Figure 6.22 Radial dimensionless velocities of hydrofoil 1 and hyperboloid combination (1.5d)

Near the tank wall the turbulence intensities are zero. Their values get increased as it is approached to the impeller region. Their distributions are similar to the time mean velocity distribution in Figure 6.21. Highest turbulence intensity observed is 0.035 near the impeller region at the midheight of the tank. As it has been stated, the S/N ratio was quite low in radial measurements due to the refraction of ultrasonic beam in the cylindirical tank wall. It is recommended to the place the probe to a hole which has been made on the tank wall up to certain

deepness or to place the vessel in a square Plexiglas tank filled with water, which was used by Armenante et al. (1997), in order to minimize the refractive effects at the curved surface of the mixing vessel.

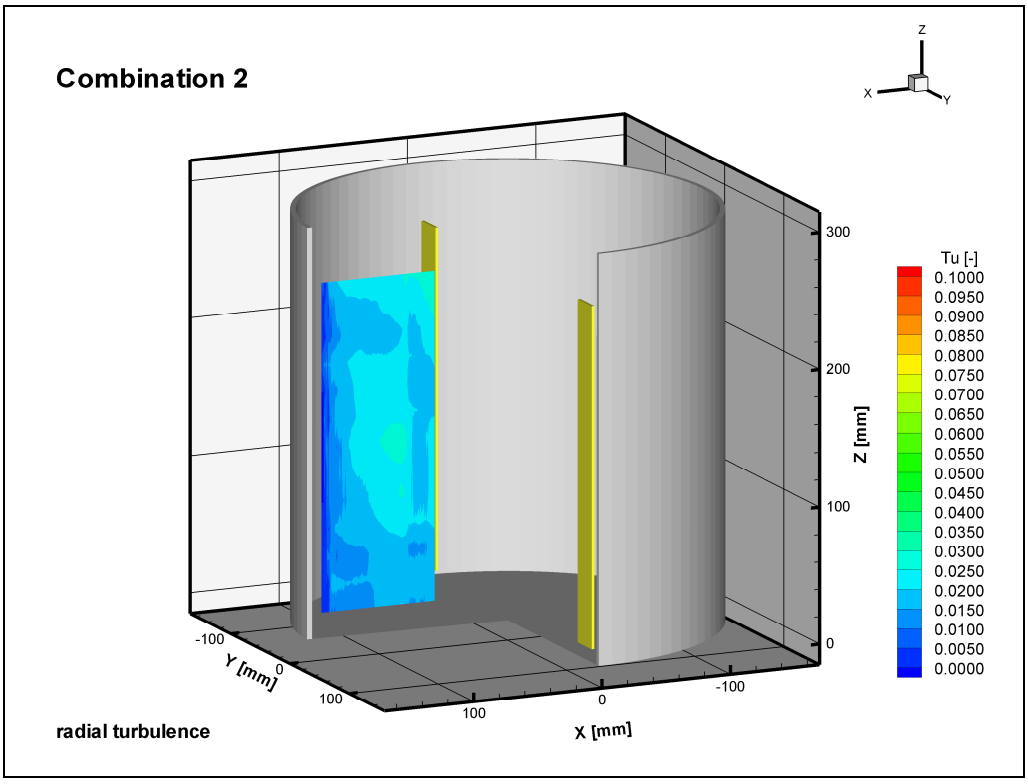

Figure 6.23 Radial turbulence of hydrofoil 1 and hyperboloid combination (1.5d)

6.1.4. Flow Visualization (Lightsheet) Experiments

Lightsheet experiments were performed for hydrofoil 1, hydrofoil 2, hyperboloid impellers and the two impeller combinations. The extracted pictures of the video records are given below. The pictures allow one to observe general flow characteristics of the impellers qualitatively. It should be noted that quantitative analysis of these results are not possible as opposed to the UDV experiments at which velocities and turbulence intensities were determined.

Armenante et al. (1997) have worked with a downward pumping, six-blade, 45º pitched-blade turbine with a D/d ratio of 3 in an unbaffled tank at two Reynolds numbers; 71000 and 111000. They have found that the dimensionless velocity and turbulent kinetic energy profiles were nearly identical at two different agitation speeds indicating that the impeller speed plays a minor role in the direction and magnitude of the dimensionless velocities and turbulent kinetic energies at any point (including the region near the impeller). In this study the UDV and lightsheet experiments were performed in the turbulent regime at different Reynolds numbers, as stated in the work of Armenante et al. (1997) the flow field at different Reynolds number do not differ from each other.

The axial flow produced by the hydrofoil 1 impeller can be seen in Figure 6.24. The fluid is sucked by the impeller and pumped down axially, goes along the tank bottom, goes up the tank wall and returns to the impeller again. The upper part, above the impeller region, is also in motion since the flow going up the tank wall, returning back to impeller also carries the unmoving fluid in the upper part of the tank to the impeller region so that a movement occurs in all over the tank and no dead zones exist. This can be visualized in the lightsheet movie given in Appendix F. This complete movement in the overall tank and of course the power consumption characteristics of the hydrofoil 1 impeller makes it the most efficient impeller in macromixing time experiments among other investigated impeller configurations.

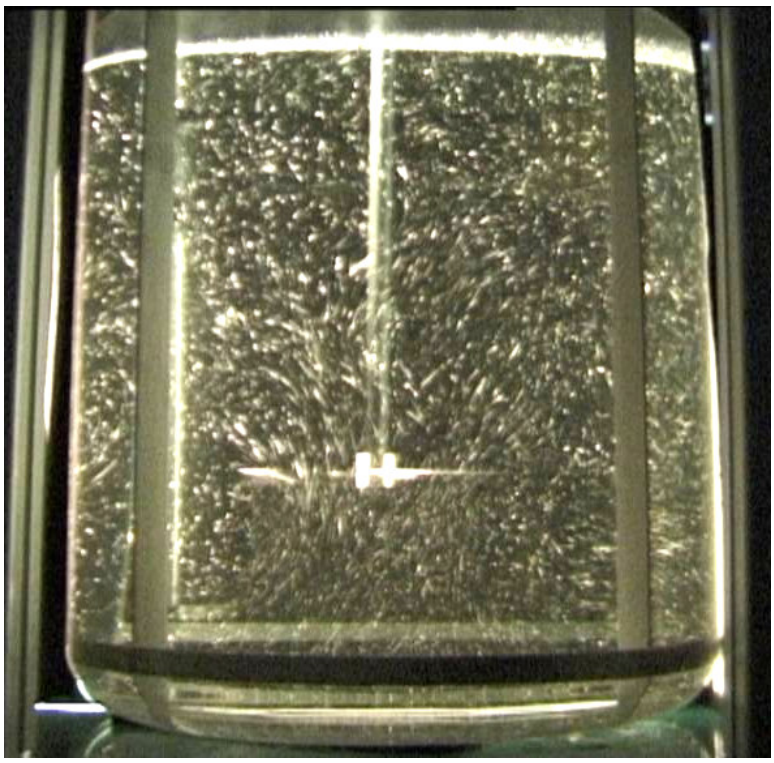

Figure 6.24 Lightsheet photo of the hydrofoil 1 impeller

Hydrofoil 2 impeller provides a similar flow field to that of hydrofoil 1 as can be seen in Figure 6.25. A complete movement in the whole tank without any dead zones was observed. The complete movement in the overall tank is the advantage of the hydrofoil 2 impeller however when its power consumption and macromixing characteristics are considered hydrofoil 1 impeller is more efficient compared to hydrofoil 2 impeller.

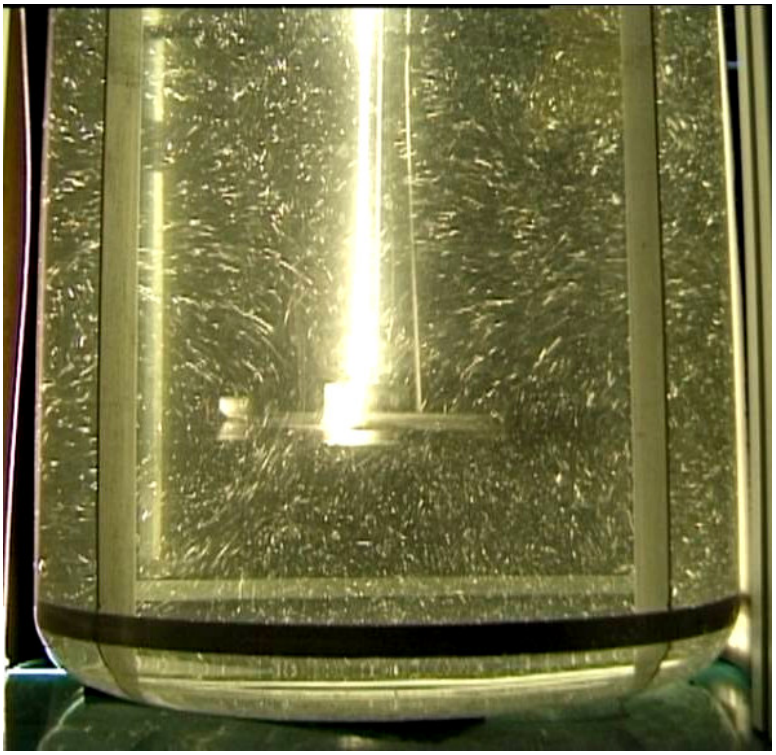

Figure 6.25 Lightsheet photo of the hydrofoil 2 impeller

Hyperboloid impeller provides a radial flow originated from the mixer-body over the tank bottom, going up the wall and returning to the centre of the mixed cell. But this circulation pattern is mainly confined to the regions closer to the tank bottom. This can be seen in Figure 6.26. There is a movement in all over the tank however the movements in the fluid higher than a D/2 clearence is slower compared to the lower part of the tank, which was not the case in hydrofoil 1 and 2 impellers. This is the main reason why the hyperboloid impeller had the highest mixing time at equal power consumption in macromixing measurements, especially when the injection point of the tracer solution is considered. These types of mixers are especially used for the mixing of suspensions, i.e. for preventing the sedimentation of the particles in suspensions.

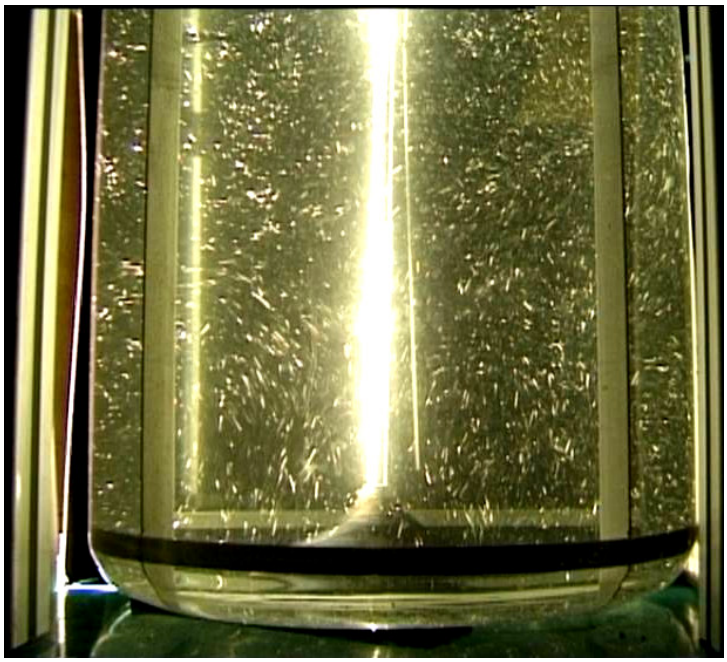

Figure 6.26 Lightsheet photo of the hyperboloid impeller (1)

The lightsheet photo of the "combination 1" (submergence of the top hydrofoil impeller = (d) and the off-bottom clearance of hyperboloid mixer = ($d/10$)) is given in Figure 6.27. A complete movement in the whole tank without any dead zones was observed. In the lower part of the tank radial flow produced by hyperboloid impeller was observed. In the upper part of the tank axial flow produced by hydrofoil 1 impeller dominates. The fluid which is pumped axially downwards is mixed radially with the radial flow produced by the hyperboloid impeller at slightly above the midheight of the tank consequently a considerable mixing degree is achieved in the contents of the whole tank. The red zone in Figure 6.18 in radial UDV measurements also indicates this radial flow.

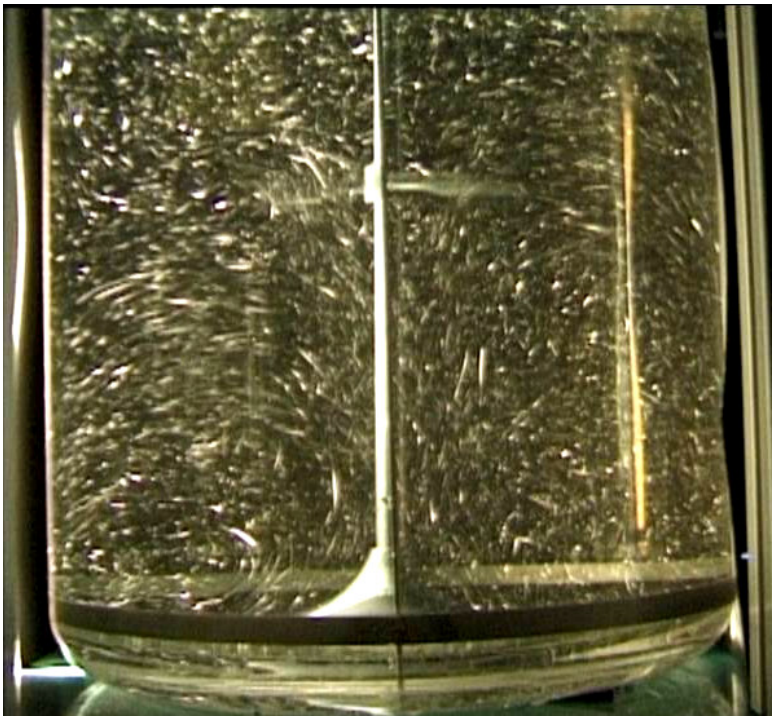

Figure 6.27 Lightsheet photo of mixer combination (d)

The lightsheet photo of the "combination 2" (submergence of the top hydrofoil impeller = ($1.5d$) and the off-bottom clearance of hyperboloid mixer = ($d/10$)) is given in Figure 6.28. A complete movement in the whole tank without any dead zones was also observed. Hydrofoil 1 impeller which is located at the midheight of the tank produces an axial flow which also disturbs the radial flow produced by hyperboloid impeller. The radial flow formed by the hyperboloid impeller reaches the tank wall and formes a circular flow there and than this flow is disturbed by the axial pumping of the hydrofoil 1 impeller. In lower half part of the tank a considerable mixing degree is achieved. The fluid in the upper half part of the tank is sucked by the hydrofoil impeller and a radial flow occurs during this pumping at the midheight of the tank. The mixing in the upper part of the tank is slower compared to that of the "combination1". The red zone in Figure 6.18 in radial UDV measurements also indicates this radial flow.

Figure 6.28 Lightsheet photo of mixer combination (1.5d)

Before examining the turbulent characteristics of a stirred tank, it is important to understand some of the unusual characteristics of this highly complex flow field. On the largest scales of length and time, overall circulation patterns can be observed. These are important for the determination of dead zones and macromixing characteristics. If the flow generated by an axial impeller is observed over a shorter time scale, however, it becomes apparent that the circulation pattern varies with time. While one pattern may dominate, others appear and disappear with varying frequency and stability. (Kresta and Wood, 1992) The above given lightsheet photos might be suffering from Kresta and Wood stated (1992) "time variation of the circulation patterns". Therefore it is

recommended that the lightsheet movie CD given in Appendix G is seen, so that the appearing and disappearing patterns with change of time are best visualized.

6.2. Square Tank Experiments

6.2.1. Macromixing Measurements in the Square Tank

Macromixing time measurements were carried out at four different impeller speeds that were in the turbulent regime. Three impeller types were employed in the 900 mm square tank measurements. These are Generation 5 low and high rib impellers and Generation 6 hyperboloid impeller photos of which are given in Figure 5.10, 5.11 and 5.12. The ribs of Generation 5 high rib impeller are higher than that of Generation 5 low rib's. Generation 6 had the highest transport ribs extending from mixer tip to mixer hub and additional holes on the mixer hub. It has also a profiled bottom which also affects its efficiency. In Figure 6.29 variation of mixing time with rotational speed is shown. The mixing time values of square tank experiments are generally about 10 times higher the cylindrical tank mixing time values experiments. The water volume in the square tank is about 18 times the water volume in the cylindrical tank. Generation 5 low rib impeller is used both in the cylindrical tank and square tank experiments. The improvements in the mixer geometry of the hyperboloid impellers resulted in considerable differences in the mixing times.

For the measured mixing times the dimensionless mixing time $n\theta$ was obtained and in Figure 6.30 the $n\theta$ versus Reynolds number graph is shown. The highest mixing time value obtained was Generation 5 low rib hyperboloid's impeller, while the smallest one was Generation 6's.

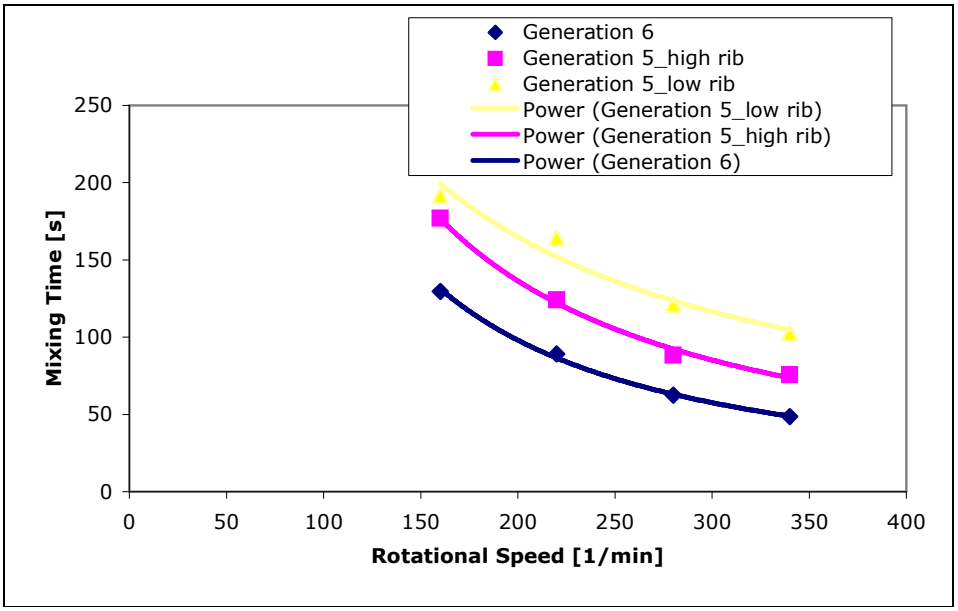

Figure 6.29 The dependency of the macromixing time on rotational speed in square tank

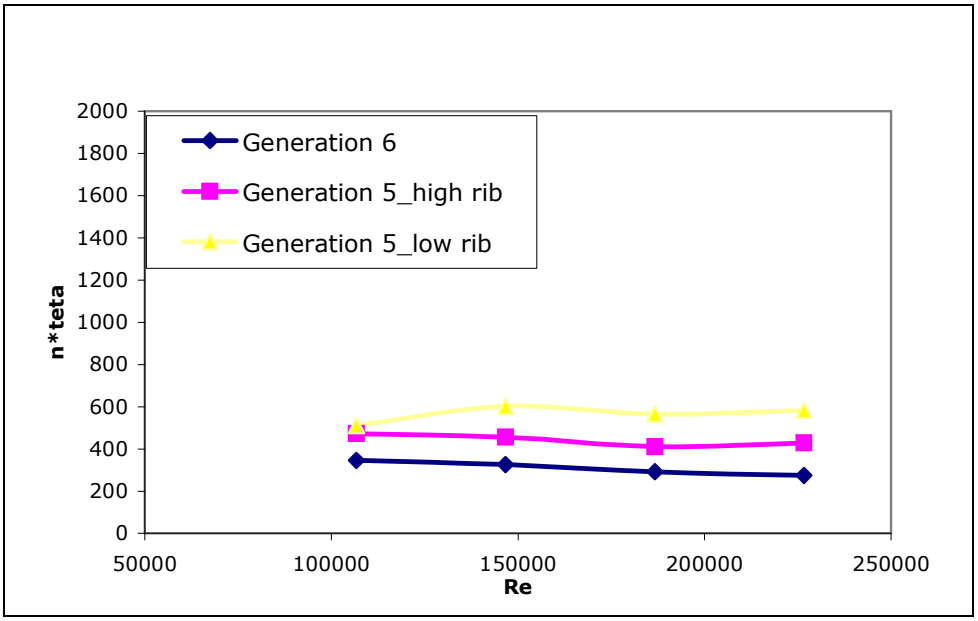

Figure 6.30 Macromixing time characteristics in square tank

As seen in Figure 6.30, the dimensionless macromixing time was nearly constant along the measured data range except the first data of Genenaration 5 low rib impeller. Obtaining such a value may be due to an experimental error. The last three data given in Figure 6.30 were averaged to get an approximate nθ value. The $n\theta$ values were found as 297.8, 431.9 and 583.6 for the Generation 6, Generation 5 high rib and Generation 5 low rib hyperboloid impellers, respectively. The $n\theta$ value of Generation 5 low rib impeller in cylindrical tank experiments was 177.92 which 0.31 times that of the square tank experiments. When the 0.33 scaling between lengths of two mixing tanks are considered, this ratio between the two dimensionless mixing times value is reasonable. The experimental data for Figures 6.29 and 6.30 can be found in Appendix C.

To find the most efficient mixer, that is the mixer having the shortest mixing time at the same power consumption; first the specific power consumption of one of the mixers, i.e., generation 5 low rib, was selected as basis, then the mixing time and the rotational speed values of the other mixers were found by interpolating them for their value corresponding to this specific power consumption. At the same specific power consumption the generation 6 impeller has the shortest mixing time as shown in Table 6.3. Therefore by improvements in the impeller geometry a better mixing efficiency can be obtained. For hyperboloid impellers, it was observed that higher the rib of a hyperboloid mixer, better the mixing efficiency of it. Additional holes on the mixer hub also increase the efficiency of a hyperboloid mixer.

Table 6.3 Mixing time and specific power data for the investigated impellers

	P/V [W/m3]	$n \cdot \theta$ [-]	n [1/s]	θ [s]
Generation 5 Low Rib	88.44	582.88	5.67	102.8
Generation 5 High Rib	88.44	412.41	4.67	88.66
Generation 6	88.44	315.33	3.97	80.51

6.2.2. Results of Aeration Experiments

Nagata (1975) states that bubble in agitated vessels consist of two groups. One is a group of newly formed; having rather large diameter and the other is small bubbles group. Small bubbles are also called as "dead bubbles" due to their long residence times in the solution so that solute in these small bubbles is already absorbed. By the hyperboloid mixer-aerator systems for which the experiments were carried out, the aim is to obtain the optimum size and retention time for the air bubbles.

For the evaluation of the efficiency of the aeration systems the overall mass transfer coefficient, $k_L a$ is used. $k_L a$ depends essentially on the specific interface area A/V and the retention time of the fluid particles at the interface. By means of hyperboloid mixer-aerator system, increasing the specific interface area and decreasing the retention time of the fluid particles at the interface were aimed. An increase in the oxygen transfer area can be achieved by mechanical division of the gas into small bubbles by the blades under the hyperboloid mixers. The retention time was decreased by a high turbulence degree of the fluid particles at the interface and at the same time by a good distribution of them over the entire basin. By the hyperboloid mixer form, which provides predominantly radial flow, the gas bubbles are distributed at appropriate number of revolutions to the edge of the basin and the turbulence is introduced.

Aeration characteristics of the Generation 5 low rib and Generation 6 hyperboloid impellers, which have blades under them, were examined in the rectangular mixing tank. Figure 6.31 and Figure 6.32 show the variation of overall mass transfer coefficients with change of gas flow rates and rotational speeds. When Figures 6.31 and 6.32 are examined, it will be seen that at the same rotational speed the $k_L a$ values have an increasing trend with the increasing flow number that is with increasing air flow rate however the differences are not that much considerable. The impact of the rotational speed on the $k_L a$, however, is more

pronounced than the air flow rate for both impellers. When the $k_L a$ values data in Appendix F is examined, it will be seen that Generation 6 impeller has higher $k_L a$ values compared to Generation 5 low rib at the same conditions. The reason for this is the improved geometry of the Generation 6 compared to Generation 5 low rib impeller. However they should further be compared on equal power consumption basis.

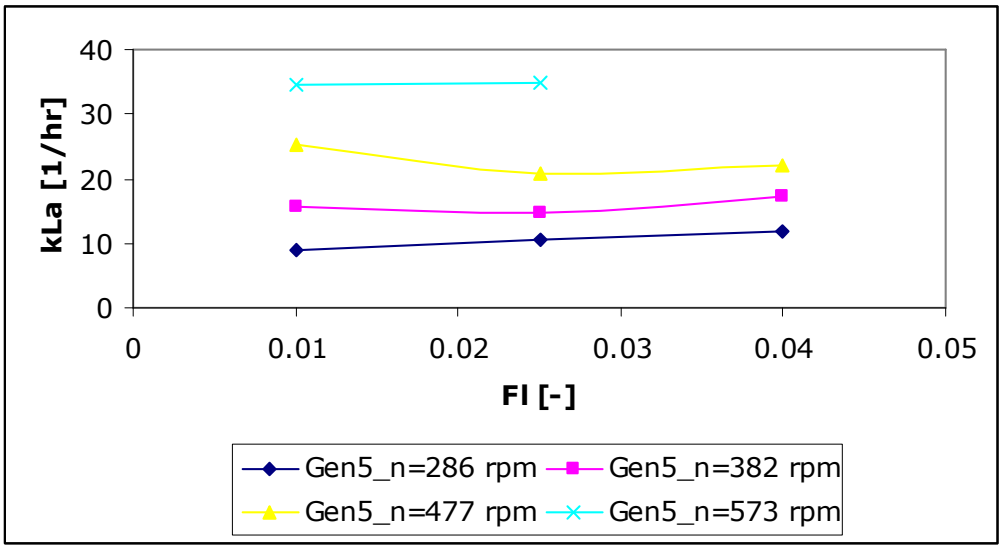

Figure 6.31 Variation of $k_L a$ with change of gas flow rate for Generation 5 impeller

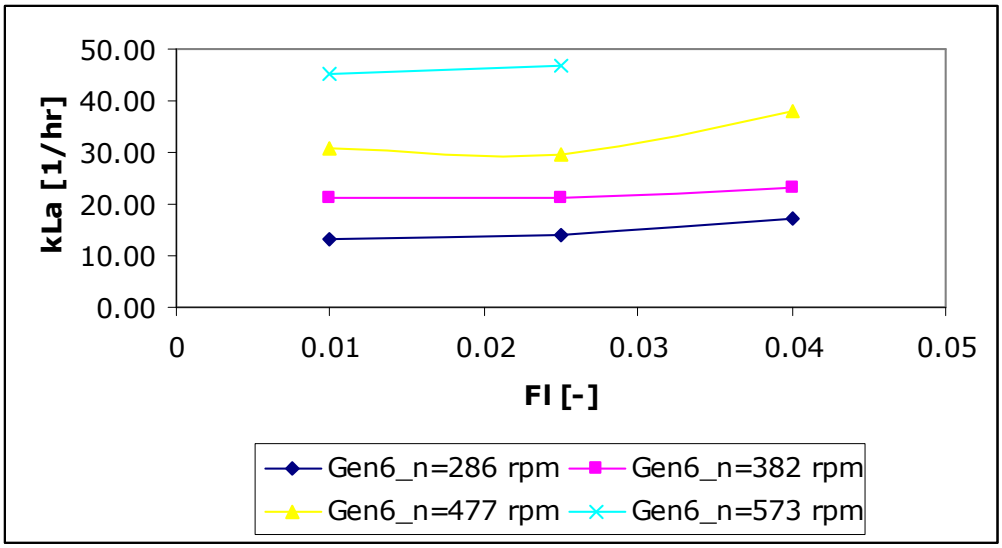

Figure 6.32 Variation of $k_L a$ with change of gas flow rate for Generation 6 impeller

At different rotational speeds and air flow rates, the specific oxygen capacity of water in the tank was investigated. The results are shown in Figures 6.33 and 6.34. Fl is the dimensionless flow number, $Fl = \frac{Q_A}{n * d^3}$, where Q_A is the air flow rate [m^3/s] with an oxygen concentration of 0.299 kg/m^3, n is the rotational speed [s^{-1}] and d is the diameter of the mixer [m], OA [%] is the oxygen utilization efficiency which is equal to $OA = \frac{100 * OC}{(Q_A * 2.99)}$. Here OC is the oxygen concentration in the mixing tank. By increasing the rotational speed the oxygen transfer efficiency also increases at Fl =0.01. As the flow number increases the differences in the efficiencies at different rotational speeds decrease for both impellers. At Fl =0.04 both impellers exhibit nearly the same performance. It can be said that when the air flow rate is small the air transferred to the system is dominated by the mixing efficiency of impeller. When the air flow rate is large,

the effect of the impellers mixing efficiency is minimized. To achieve an optimum working condition at a treatment plant, the cost of the power consumption of the pressurized air should be considered together with power consumption of the mixer. When Figures 6.33 and 6.34 are compared, it will be seen that Generation 6 impeller exhibit higher OA values at the same conditions. This behaviour can be seen in Figures 6.35, 6.36 and 6.37 in a more detailed form. In these figures the transferred oxygen amounts are also compared at different rotational speeds for the same flow numbers, and in each case Generation 6 impeller exhibited higher OC values.

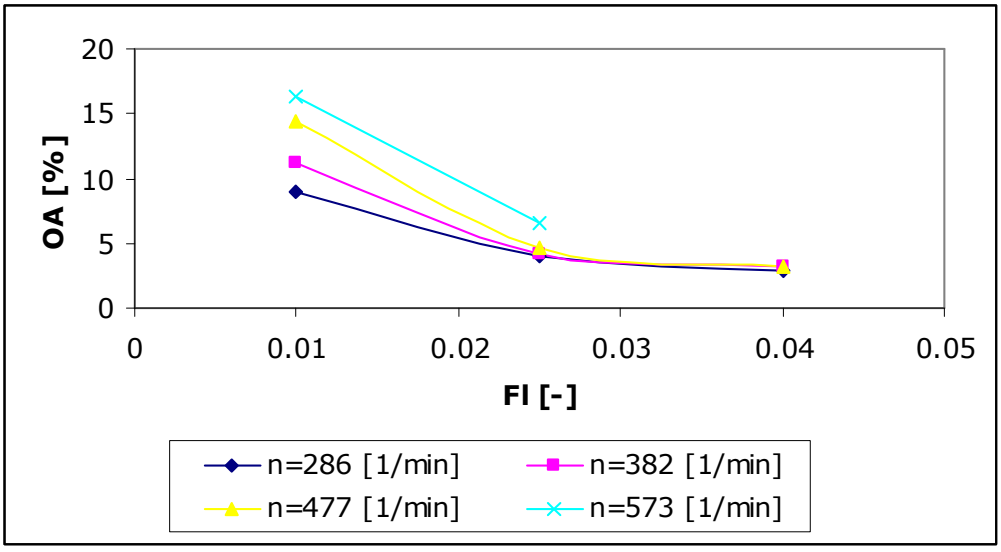

Figure 6.33 Variation of OA [%] with Fl [-] at different rotational speeds for Generation 5

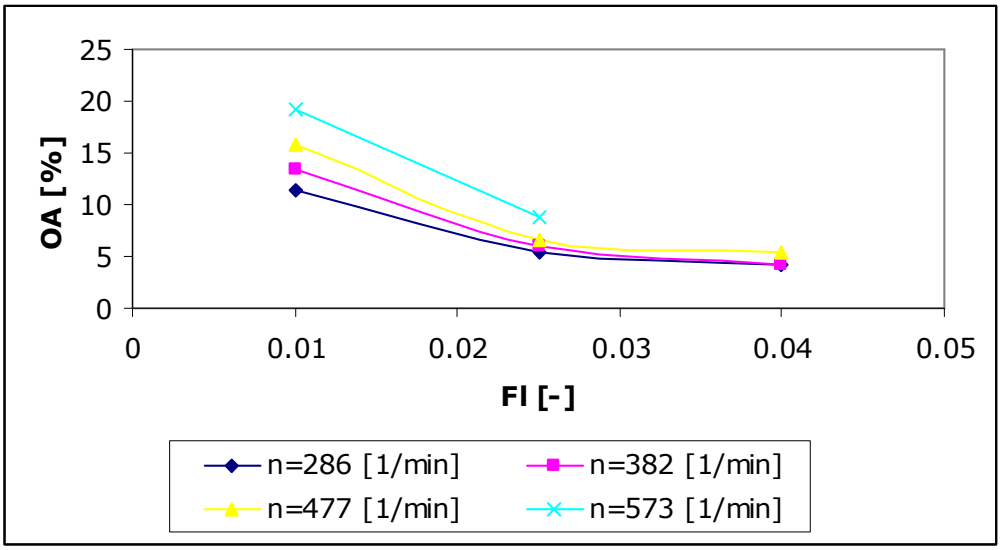

Figure 6.34 Variation of OA [%] with Fl [-] at different rotational speeds for Generation 6

In Figure 6.35 the amount of oxygen transferred to the system at different flow rates at Fl =0.01 is compared for Generation 5 and Generation 6 impellers.

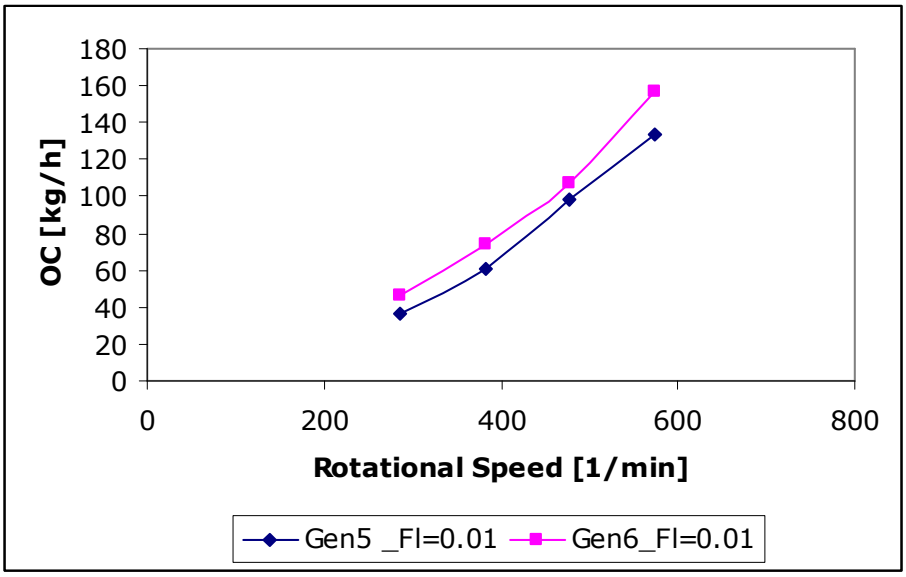

Figure 6.35 Amount of oxygen transferred to the system at Fl=0.01 for Generation 5 and Generation 6

Generation 6 impeller exhibited a better performance about 20% than Generation 5 impeller. This is due to improved design of Generation 6 impeller. Higher transport ribs extending from mixer tip to mixer hub and additional holes on the mixer hub provide Generation 6 impeller a better performance. As can be seen in Figures 6.36 and 6.37, the Generation 6 provides a better performance compared to Generation 6 also at Fl =0.025 and Fl =0.04. These results should also be compared on equal power consumption basis in order to decide about the efficiencies of the mixer aerator systems.

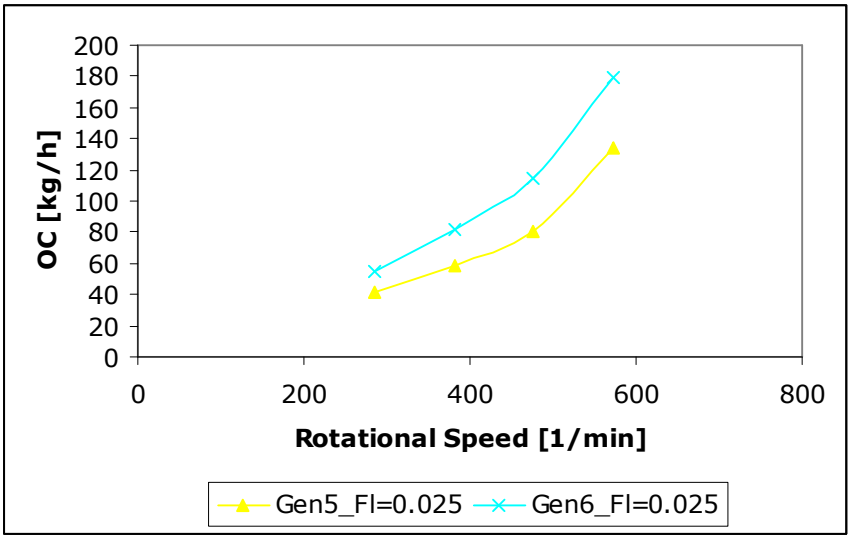

Figure 6.36 Amount of oxygen transferred to the system at Fl=0.025 for Generation 5 and Generation 6

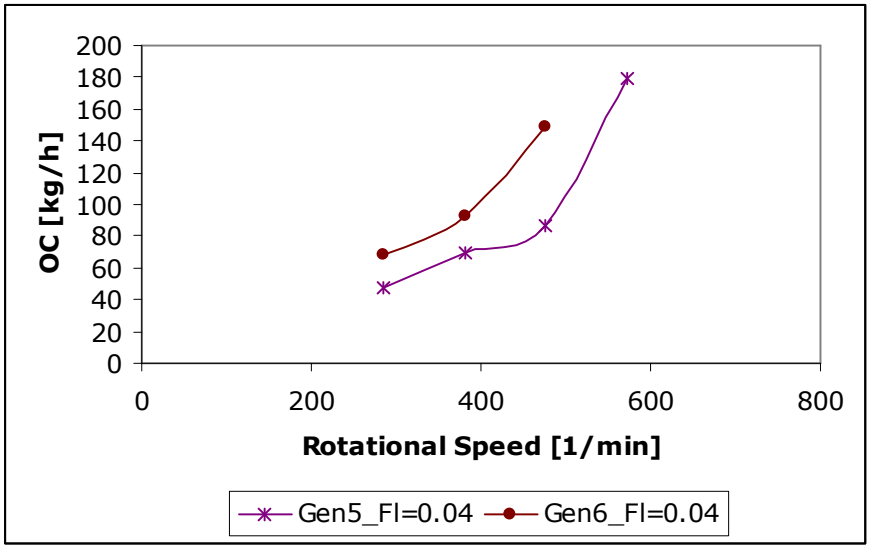

Figure 6.37 Amount of oxygen transferred to the system at Fl=0.04 for Generation 5 and Generation 6

Nagata (1975) have stated the major factors in order to apply shear forces effectively on to the bubbles as follows:

- Gas inlet pipe should be set close to the impeller blades
- Gas should be blown from many holes bored in a ring sparger than from a single nozzle.
- The loop diameter of discharge hole arrangement is chosen to be 80% of the impeller diameter

As a remark, it should be added that the investigated hyperboloid mixer-aerator configurations conforms to the factors stated above.

CHAPTER VII

CONCLUSIONS

Macromixing and power consumption measurements were performed in the 300 mm diameter cylindrical tank and experimental data have been analyzed on the basis of equal power consumption. From two new design hydrofoil impellers, the so called hydrofoil 1 impeller had a shorter mixing time than the hydrofoil 2 impeller at equal power consumption; this is mainly due to smaller blade thickness and hub length of the hydrofoil 1 impeller as well as its improved blade angle. These two impellers have considerably low Newton numbers compared to that of the standard impellers'. Their mixing times were also comparable to that of the standard impellers'. For all the impellers and impeller combinations investigated, the $n\theta$ value, the product of mixing time and impeller rotational speed, was constant. It changed depending on the impeller type. The flow fields produced by the impellers where also investigated quantitatively by UDV. In axial UDV measurements the turbulence intensity close to the impeller blades is about 10 times of the bulk of the tank. Unsatisfactory results were obtained for radial measurements due to refractive effects at the curved surface of the mixing vessel. Flow visualization experiments performed in the cylindrical tank also provided qualitative information about the flow field. From both UDV and lightsheet observations, it can be concluded that both hydrofoil impellers were found to have a strong pumping capacity, providing a top to bottom circulation in the stirred tank. This study indicates that impeller design greatly affects the mixing time; minor dimensions such as impeller hub, blade width and thickness play an important role in the mixing efficiency. In this respect the new design hydrofoil type impellers can also be improved with changes in their minor parameters and a higher discharge flow may be obtained at lower power consumption.

Macromixing measurements were also performed in a 900x900 mm square tank for three different generations of hyperboloid impellers. These were Generation 5 low rib, Generation 5 high rib and Generation 6 impellers. Generation 5 low rib and Generation 5 high rib impellers were of the same geometry, the only difference was that Generation 5-high rib had a higher rib height. Generation 6 has a similar geometry to Generation 5 high rib however its transport ribs reaches to the upper part of the impeller, the ribs get higher as they go up and at the upper part there are holes in between them. It has also a corrugated bottom. For all the three types of hyperboloid impellers, $n\theta$, the product of mixing time and impeller rotational speed, was constant. These three different designs of hyperboloid impellers were compared for their mixing time on the basis of equal power consumption. The mixing times at equal power consumption were found as $\theta_{Gen6} < \theta_{Gen5highrib} < \theta_{Gen5lowrib}$. From this result, it can again be concluded that improving the minor dimensions of an impeller can lead to an increase in its mixing efficiency.

Aeration characteristics of Generation 5 low rib and Generation 6 impellers, which have blades under them for aeration purposes, were investigated. When the air flow rate sent to the mixer-aerator system is small, the amount of dispersed oxygen in the system is dominated by the mixing efficiency of impeller. When the air flow rate is large, the affect of the impellers mixing efficiency is minimized. To achieve an optimum working condition at a treatment plant, the cost of the power consumption of the pressurized air should be considered together with power consumption of the mixer. Generation 6 impeller exhibit higher oxygen transfer efficiencies at the same rotational speeds and air flow rates compared to Generation 5 low rib impeller. This is due to the improved design of the Generation 6 impeller. However, these mixer-aerators should be compared on the basis of equal power consumption so that the mixer with the higher efficiency can be done.

CHAPTER VIII

RECOMMENDATIONS

Different techniques can be used for the determination of the mixing time to have mixing grade lower than 10%. Multiple probes can be helpful for the determination of the slow mixing zones.

Further mixing efficiency tests should be carried out with hydrofoil type of impellers by making changes in their minor dimensions. Lowering the d/D ratio may also provide a better mixing efficiency. The use of empirical equations of Ruszkowski is still helpful for the estimation of the mixing times of the hydrofoil impellers.

UDV measurements are not helpful when the probe is directly mounted on the cylindrical tank with the ultrasonic gel as the coupling medium. It is recommended that the probe be placed on a hole made in the tank wall up to a certain depth so that the refractions of the ultrasonic beams can be kept at minimum. The cylindrical vessel can be also placed in a square Plexiglas tank filled with water and the probe can be placed on the outer side of the square tank.

In the lightsheet experiments it is recommended to change the water in the tank before each recording since the aluminum particles got dissolved in water and disabled the visualization of the flow field.

Power consumption tests of the hyperboloid mixer-aerator systems should be performed so that a comparison of the efficiencies on the basis of equal power consumption can further be done.

REFERENCES

1. Alves, S.S., Vasconcelos, J.M.T., Orvalho, S.P., "Mass transfer to clean bubbles at low turbulent energy dissipation" Chemical Engineering Science, article in press. (2005)

2. Armenante, M. P., Luo, C., Chou, C., Fort, I., Medek, J., "Velocity profiles in a closed vessel: comparison between experimental LDV data and numerical CFD predictions" Chemical Engineering Science, Vol.52 (20), pp. 3483-3492. (1997)

3. ATV-Arbeitsblatt M 209, Regelwerk Abwasser-Abfall, Messung der Sauerstoffzufuhr von Belüftungseinrichtungen in Belebungsanlagen, in Reinwasser und in belebtem Schlamm, Abwassertechnische Reinigung e.V. (1996)

4. Batchelor, G. K., The Theory of Homogenous Turbulence, Univ. Press., Cambridge. (1953)

5. Bishof, F., "Untersuchung der Blasenbildung und des Stoffaustausches unter dem Einfluss oberflächenaktiver Substanzen und gelöster Gase", Dissertation, Universität Erlangen-Nürnberg. (1994)

6. Bouillard, J., Alban., B., Jacques, P., Xuereb, C., "Liquid velocity flow measurements in stirred tanks by ultra-sound Doppler Velocimetry", Chemical Engineering Science, Vol.56, pp. 747-754. (2001)

7. Brito, D., Nataf., H., Cardin, P., Aubert, J., Masson, J., "Ultrasonic Doppler velocimetry in liquid gallium", Experiments in Fluids, Vol.31, No.6, pp 653-663. (2001)

8. Brodkey, R.S., "Mixing, Theory and Practice", Academic Press New York-London. (1966)

9. Calderbank, P.H., Moo-Young, M.B., "The continuous phase heat and mass transfer of dispersions", Chemical Engineering Science, Vol.16, pp. 39-54. (1961)

10. Corrsin, S., Vol.12, pp. 403, AIChE Journal. (1968)

11. Costes, J., Couderc, J. P., "Study by laser Doppler anemometry of the turbulent flow induced by a Rushton turbine in a stirred tank: influence of the size of the units (Parts I&II)", Chemical Engineering Science, Vol.43 (10), pp. 2754-2772. (1988)

12. Chisti, Y., Jauregui-Haza, U.J., "Oxygen transfer and mixing in mechanically agitated airlift bioreactors", Biochemical Engineering Journal, Vol.10, pp 143-153. (2001)

13. Ciofalo, M., Brucato, A., Grisafi, F., Torraca, N., "Turbulent flow in closed and free-surface unbaffled tank stirred by radial impellers", Chemical Engineering Science, Vol.51 (14), pp. 3557-3573. (1988)

14. Danckwerts, P.V., "Significance of liquid-film coefficients in gas absorption", Industrial and Engineering Chemistry 43, pp.1460–1467. (1951)

15. Fentiman, N. J., Hill, N.S., Lee, K.C., Paul G.R., Yianneskis, M.A., "Novel Profiled Blade Impeller for Homogenization of Miscible Liquids in Stirred Vessels", Trans. Inst. Chem. Eng., 76A, 835. (1998)

16. Frey, T., Entwicklung verbesserter Auslegungsrichtlininen für Begasungssysteme und Valideirung in der Praxis, Masters thesis, Universität Erlangen-Nürnberg. (1999)

17. Gao, Z., Niu, G., Shi. L., Smith, J. M., "Mixing in Stirred Tanks with Multiple Hydrofoil Impellers", 11th European Conference on Mixing, Bamberg. (2003)

18. Hiby, J. W., "Definition und Messung der Mischgüte in flüssigen Gemischen", Chem.-Ing.-Tech., Vol. 51, pp. 704-709. (1979)

19. Hinze, J.O., Turbulence McGraw-Hill. (1959)

20. Higbie, R., "The rate of absorption of a pure gas into a still liquid during a short time of exposure", Transactions of the American Institute of Chemical Engineers 31, 365–389. (1935)

21. Höfken, M., Bischof, F. und Durst, F., "Untersuchungen von Rühr- und Mischvorgängen mit Hilfe der Ultraschall-Doppler-Anemometrie", Erlangen. (1995)

22. Höfken, M. : Moderne experimentelle Methoden für die Untersuchung von Strömungen in Rührbehältern und für Rührwerksoptimierung, Dissertation, Erlangen. (1994)

23. Höfken, M., Steidl, W., Huber P., "About the Design of Mixing Systems for Anaerobic and Anoxic Basins for Large Wastewater Treatment Plants", MIXIN XIX, North American Mixing Forum. (2003)

24. Kawase, Y., Halard, B., Moo-Young, M., "Theoretical prediction of volumetric mass transfer coefficients in bubble columns for Newtonian and non-Newtonian fluids", Chemical Engineering Science, Vol. 42, pp. 1609–1617. (1987)

25. Khang, S. J., Levenspiel, O., "New Scale-up and Design Method for Stirrer Agitated Batch Mixing Vessels", Chemical Engineering Science, Vol. 31, pp. 569-577. (1976)

26. Kolmogoroff, A.N., C.R. (Doklady) Acad. Sci. U.S.S.R, Vol.30, pp. 301. (1941)

27. Kresta, M.S., Wood, P.E., "The flow field produced by a pitched blade turbine: Characterization of the turbulence and estimation of the dissipation rate", Chemical Engineering Science, Vol. 42 (10), pp. 1761–1774. (1993)

28. Lamont, J.C., Scott, D.S., "An eddy cell model of mass transfer into surface of a turbulent liquid", American Institute of Chemical Engineers Journal 16, 513–519. (1970)

29. Levenspiel, O., Chemical Reaction Engineering, John Wiley&Sons: New York. (1991)

30. Mann, R., Dickin., F.J., Wang, M., Dyakowski, T., Williams, R.B., Edwards, R.B., Forrest, P. J., Holden, P.J., "Application of Electrical Resistance Tomography to Interrogate Mixing Processes at Plant Scale", Chemical Engineering Science, Vol. 52, pp 2087-2097. (1997)

31. Motarjemi, M., Jameson, G.J., „Mass Transfer from very small bubbles-the optimum bubble size for aeration", Chem. Eng. Sci., Vol. 33, pp 1415-1423. (1978)

32. Mersmann, A., Geisler, R. : Strömungsmechanische Grundlagen des Rührens, Hochschulkurs Rühr- und Mischtechnik, München. (1994)

33. Met-Flow SA, "UVP Method", www.met-flow.com, 2005, last access date May 2006.

34. Nagata, S., Mixing – Principles and Applications, Kodansha Ltd., Tokyo. (1975)

35. Nath, B., Löber, W., Baetz, W., Holzapfel, W., "Laser Light Sheet Imaging of Gas Flow with Laser Diodes", Vol. 3 (1), pp. 102-199. (1999)

36. Nere, N. K., Patwarhan, A.W. and Joshi, J. B., "Liquid Phase Mixing in Stirred Vessels: Turbulent Flow Regime", Ind. Eng. Chem.. Res., Vol. 42, pp. 2661-2698. (2003)

37. Nowak, M., "Wall shear stress measurement in a turbulent pipe flow using ultrasound Doppler velocimetry", Experiments in Fluids, Vol. 33, pp. 249-255. (2002)

38. Operational Manual Ultrasonic Velocity Profile Monitor, Ser. No 10202. (1991)

39. Ozaki, Y., Tatsuya, K., Takeda, Y., Hishida, K., Masanobu, M., High Time Resolution Ultrasonic Velocity Profiler, Experimental Thermal and Fluid Science, Vol. 26, pp. 253-258. (2001)

40. Pasveer, A., "Oxygenation of Water with Air Bubbles", Sewage and Industrial Waste, Vol.27, pp.1130-1146. (1955)

41. Prasher, B.D., Wills, G.B., Mass transfer in an agitated vessel, Industrial and Engineering Chemistry Process Design and Development, Vol. 12, pp. 351 354. (1973)

42. Prochazka, J.; Landau, J., "Homogenization of Miscible Liquids in the Turbulent Region", Collect. Czech. Chem. Commun., Vol. 26, pp. 2961. (1961)

43. Ranade, V.V., Joshi, J.B., "Flow generated by a disc turbine: Part I. Experimental", Trans. Instn. Chem. Engng, Vol. 68(A), 19-33. (1990a)

44. R. Rao, K. S. M. S.; Joshi, J.B., "Liquid Phase Mixing in Mechanically Agitated Vessels", Chem. Eng. Commun., Vol. 74, pp.1. (1988)

45. Rewatkar, V.B., Joshi J.B., Effect of Impeller Design on Liquid Phase Mixing in Mechanically Agitated Reactors, Chem. Eng. Commun., Vol. 91, pp. 322. (1991)

46. Rielly, C.D.; Britter, "R.E. Mixing Times for Passive Tracers in Stirred Tanks", Proc. 5th Eur. Conf. Mixing, pp. 365. (1985)

47. Ruszkowski, S. A., "Rational Method for Measuring Blending Performance and Comparison of Different Impeller Types", Proc. Eighth Eur. Conf. Mixing, pp. 283. (1994)

48. Sano, Y., Usui, H., "Interrelations Among Mixing Time, Power. Number and Discharge Flow Rate Number", J. Chem. Eng. Japan, Vol. 18, pp.47. (1985)

49. Sasakura, T., Kato, Y., Yamamuro, S.; Ohi, N., "Mixing Process in a Stirred Vessel", Int. Chem. Eng., Vol. 20, pp. 251. (1980)

50. Schäfer, M., Höfken, M., Durst, F., "Detailed LDV-Measurements for Visualization of the Flow Field within a Stirred Tank Reactor Equipped with a Rushton-Turbine", Trans IChemE, Vol. 75 (A), pp. 729-736. (1997)

51. Schäfer, M., Characterisierung, "Ausslegung und Verbeseserung des Makro- und Mikromischens in gerührten Behältern", PhD Thesis at University Erlangen, 2001

52. Schäfer, M., Karasözen, B., Uludag, Y., Yapici, K., Ugur, Ö., "Numerical Methods for Optimizing Stirrer Configurations", METU IAM preprints. (2004)

53. Schubert, H., "Mechanische Verfahrenstechnik, Deutscher Verlag für Grundstoffindustrie", Leipzig. (1990)

54. Scientific Update LLP, "Mixing and the Selectivity of the Chemical Reactions", www.scientificupdate.co.uk/pdfs/generic_pdfs/mixing.pdf, 2003, last access date May 2006.

55. Sellens, R.W., Deljouraveshi R., Wang, G., Olesen, M.J., Bardon, M.F., "An Optical Spray Pattern Analyzer", ILASS Americas '97, Ottawa, Canada. (1997)

56. Shiue, SJ, Wong, CW., "Studies on homogenization Efficiency of Various Agitators in Liquid Blending", Canadian Journal of Chemical Engineering, Vol. 62, pp 602-609. (1984)

57. Signal Processing SA, "Background of Ultrasonic Doppler Velocimetry", www.signal-processing.com, 2006, last access date June 2006

58. Steidl, W., "Experimentelle Untersuchung zur Auslegung von Hyperboloidrührern in einem universellen Versuchsstand zue Simulationverschiedener Behältergeometrien", Diplomarbeit am Lehrstuhl für Strömungsmechanik, Erlangen. (1995)

59. Steidl, W., DatToTec 1.3 - Installation and User Manual. (1995)

60. Steidl, W., DrawSTR 1.2 - Installation and User Manual. (1995)

61. Strauss K., Stromungsmechanik, VCH, Weinheim. (1991)

62. Taishi, T., Kikura, H., and Aritomi. M., "Effect of the mesurment volume in turbulent pipe flow measurement by the ultrasonic velocity profile method (mean velocity profile and Reynolds stress measurement)", Experiments in Fluids, Vol.32, pp. 188-196. (2002)

63. Tatterson, Gary B., Fluid and Gas Dispersion in Agitated Tanks. (1991)

64. Taylor, G. I., Proc. Roy. Soc. London A, 151, pp. 421. (1935)

65. Tenekkes, H., Lumley, J.L., A First Course in Turbulence, MIT Press: Cambridge, England. (1972)

66. Uhl, V. W., Gray, J. B., Brodkey, R.S., Mixing – Theory and Practice – Volume 1, New York. (1966)

67. Wu, H., Patterson, G.K., "Laser-Doppler measurements of turbulent-flow parameter in a stirred mixer", Chemical Engineering Science, Vol. 44 (10), pp. 2207-2221. (1989)

68. Yamanaka, G., H. Kikura, T. Sawada, T. Tanahashi & Y. Takeda, "Velocity Profile Measurement on an Oscillatory Pipe Flow of Magnetic Fluid by UVP Method", Proceedings of the 9th Symposium on Electromagnetics and Dynamics, Vol.Sapporo, pp.467-470, Proceedings. (1997)

69. Zlokarnik, M. Stirring: Theory and Practice, Wiley-VCH: Weinheim, Germany. (2001)

APPENDIX A

POWER CONSUMPTION DATA FOR CYLINDRICAL TANK MEASUREMENTS

Table A.1 Experimental Power Consumption Data of Hydrofoil 1 Impeller

Hydrofoil 1 Impeller								
f [Hz]	**n [1/s]**	**T without [Nm]**	**T with [Nm]**	**T diff. [Nm]**	**P [w]**	**Re**	**Ne**	
13.7	4.441	0.149	0.150	0.001	0.028	44415	0.03	
16	5.192	0.162	0.164	0.002	0.065	51915	0.05	
18.5	6.007	0.176	0.178	0.002	0.075	60068	0.03	
21.9	7.116	0.190	0.194	0.004	0.179	71155	0.05	
24.1	7.833	0.195	0.202	0.007	0.345	78329	0.07	
26.8	8.713	0.203	0.213	0.010	0.547	87134	0.08	
28.7	9.333	0.209	0.226	0.017	0.997	93330	0.12	
30.2	9.822	0.210	0.235	0.025	1.543	98221	0.16	
32.5	10.572	0.214	0.239	0.025	1.661	105722	0.14	
34.1	11.094	0.217	0.247	0.030	2.091	110939	0.15	
36.3	11.811	0.220	0.261	0.041	3.043	118114	0.18	**Average**
40.1	13.051	0.227	0.267	0.040	3.280	130505	0.15	0.15
42.5	13.833	0.230	0.272	0.042	3.650	138332	0.14	0.15
44	14.322	0.224	0.275	0.051	4.589	143223	0.16	0.15
46	14.975	0.221	0.277	0.056	5.269	149745	0.16	0.15
48.2	15.692	0.220	0.280	0.060	5.916	156919	0.15	0.15
50	16.279	0.218	0.286	0.068	6.955	162789	0.16	0.15

Table A.2 Experimental Power Consumption Data of Hydrofoil 2 Impeller

Hydrofoil 2 Impeller								
f [Hz]	**n [1/s]**	**T without [Nm]**	**T with [Nm]**	**T diff. [Nm]**	**P [w]**	**Re**	**Ne**	
13.7	4.441	0.14	0.145	0.005	0.140	44415	0.16	
16	5.192	0.151	0.159	0.008	0.261	51915	0.19	
18.5	6.007	0.162	0.173	0.011	0.415	60068	0.19	
21.9	7.116	0.174	0.195	0.021	0.939	71155	0.26	
24.1	7.833	0.18	0.206	0.026	1.280	78329	0.27	
26.8	8.713	0.19	0.22	0.03	1.642	87134	0.25	
30.2	9.822	0.195	0.239	0.044	2.715	98221	0.29	
32.5	10.572	0.2	0.253	0.053	3.521	105722	0.30	
34.1	11.094	0.202	0.259	0.057	3.973	110939	0.29	
36.3	11.811	0.207	0.273	0.066	4.898	118114	0.30	**Average**
40.1	13.051	0.212	0.298	0.086	7.052	130505	0.32	0.32
42.5	13.833	0.215	0.31	0.095	8.257	138332	0.31	0.32
44	14.322	0.213	0.318	0.105	9.449	143223	0.32	0.32
46	14.975	0.214	0.333	0.119	11.196	149745	0.33	0.32
48.2	15.692	0.215	0.342	0.127	12.522	156919	0.32	0.32
50	16.279	0.217	0.353	0.136	13.911	162789	0.32	0.32

Table A.3 Experimental Power Consumption Data of Hyperboloid Impeller

Hyperboloid Impeller								
f [Hz]	**n [1/s]**	**T without [Nm]**	**T with [Nm]**	**T diff. [Nm]**	**P [w]**	**Re**	**Ne**	
13.7	4.441	0.140	0.150	0.010	0.279	44415	0.32	
16	5.192	0.148	0.165	0.017	0.555	51915	0.40	
18.5	6.007	0.159	0.182	0.023	0.868	60068	0.40	
21.9	7.116	0.171	0.204	0.033	1.475	71155	0.41	
24.1	7.833	0.178	0.218	0.040	1.969	78329	0.41	
26.8	8.713	0.185	0.234	0.049	2.683	87134	0.41	
28.7	9.333	0.188	0.246	0.058	3.401	93330	0.42	
30.2	9.822	0.189	0.254	0.065	4.011	98221	0.42	
32.5	10.572	0.193	0.268	0.075	4.982	105722	0.42	
34.1	11.094	0.196	0.277	0.081	5.646	110939	0.41	
36.3	11.811	0.201	0.291	0.090	6.679	118114	0.41	**Average**
40.1	13.051	0.207	0.312	0.105	8.610	130505	0.39	0.39
42.5	13.833	0.211	0.329	0.118	10.256	138332	0.39	0.39
44	14.322	0.213	0.341	0.128	11.519	143223	0.39	0.39
46	14.975	0.214	0.356	0.142	13.360	149745	0.40	0.39
48.2	15.692	0.217	0.373	0.156	15.381	156919	0.40	0.39
50	16.279	0.219	0.386	0.167	17.081	162789	0.40	0.39

Table A.4 Experimental Power Consumption Data of Hydrofoil 1 and Hyperboloid Impeller Combination (d)

Hydrofoil 1 (d)* + Hyperboloid Combination								
f [Hz]	**n [1/s]**	**T without [Nm]**	**T with [Nm]**	**T diff. [Nm]**	**P [w]**	**Re**	**Ne**	
13.7	0.149	0.149	0.169	0.020	0.558	44415	0.64	
16	0.159	0.159	0.186	0.027	0.881	51915	0.63	
18.5	0.169	0.169	0.204	0.035	1.321	60068	0.61	
21.9	0.181	0.181	0.231	0.050	2.235	71155	0.62	
24.1	0.189	0.189	0.248	0.059	2.904	78329	0.60	
26.8	0.197	0.197	0.268	0.071	3.887	87134	0.59	
28.7	0.202	0.202	0.283	0.081	4.750	93330	0.58	
30.2	0.204	0.204	0.293	0.089	5.493	98221	0.58	
32.5	0.209	0.209	0.311	0.102	6.776	105722	0.57	
34.1	0.212	0.212	0.320	0.108	7.528	110939	0.55	
36.3	0.216	0.216	0.342	0.126	9.351	118114	0.57	**Average**
40.1	0.218	0.218	0.372	0.154	12.628	130505	0.57	0.55
42.5	0.222	0.222	0.387	0.165	14.341	138332	0.54	0.55
44	0.224	0.224	0.402	0.178	16.018	143223	0.55	0.55
46	0.226	0.226	0.420	0.194	18.253	149745	0.54	0.55
48.2	0.228	0.228	0.442	0.214	21.099	156919	0.55	0.55
50	0.228	0.228	0.456	0.228	23.321	162789	0.54	0.55

Table A.5 Experimental Power Consumption Data of Hydrofoil 1 and Hyperboloid Impeller Combination (1.5d)

Hydrofoil 1 (1.5d)* + Hyperboloid Combination								
f [Hz]	**n [1/s]**	**T without [Nm]**	**T with [Nm]**	**T diff. [Nm]**	**P [w]**	**Re**	**Ne**	
13.7	4.441	0.135	0.181	0.046	0.039	44415	1.47	
16	5.192	0.145	0.195	0.05	0.046	51915	1.17	
18.5	6.007	0.156	0.22	0.064	0.063	60068	1.11	
21.9	7.116	0.169	0.242	0.073	0.078	71155	0.91	
24.1	7.833	0.177	0.258	0.081	0.090	78329	0.83	
26.8	8.713	0.183	0.276	0.093	0.107	87134	0.77	
28.7	9.333	0.187	0.291	0.104	0.122	93330	0.75	
30.2	9.822	0.19	0.3	0.11	0.131	98221	0.72	
32.5	10.572	0.195	0.317	0.122	0.149	105722	0.69	
34.1	11.094	0.197	0.33	0.133	0.165	110939	0.68	
36.3	11.811	0.203	0.346	0.143	0.182	118114	0.64	**Average**
40.1	13.051	0.206	0.376	0.17	0.220	130505	0.63	0.60
42.5	13.833	0.21	0.395	0.185	0.244	138332	0.61	0.60
44	14.322	0.211	0.41	0.199	0.264	143223	0.61	0.60
46	14.975	0.212	0.43	0.218	0.290	149745	0.61	0.60
48.2	15.692	0.213	0.442	0.229	0.306	156919	0.58	0.60
50	16.279	0.223	0.466	0.243	0.340	162789	0.58	0.60

* Submergence of the top impeller (hydrofoil 1)

APPENDIX B

MACROMIXING TIME DATA FOR CYLINDRICAL TANK MEASUREMENTS

Table B.1 Experimental Macromixing Time Data of 6 Blade Rushton Turbine

6 Blade Rushton Turbine					
n [1/min]	**n [1/s]**	**Mixing time**	**Re**	**n*Mixing Time**	**Average Value**
54	0.89	45.54	8940	40.71	38.70
72	1.19	33.83	11920	40.33	38.70
125	2.09	18.78	20860	39.18	38.70
179	2.98	12.62	29800	37.59	38.70
241	4.02	9.33	40230	37.52	38.70
304	5.07	7.34	50660	37.20	38.70
429	7.15	5.36	71520	38.34	38.70

Table B.2 Experimental Macromixing Time Data of Hydrofoil 1 Impeller

Hydrofoil 1 Impeller					
n [1/min]	**n [1/s]**	**Mixing time**	**Re**	**n*Mixing Time**	**Average Value**
200	3.33	30.62	33333	102.07	104.2
320	5.33	19.74	53333	105.28	104.2
440	7.33	14.31	73333	104.93	104.2
600	10.00	10.54	100000	105.40	104.2
720	12.00	8.62	120000	103.39	104.2
800	13.33	7.81	133333	104.15	104.2

Table B.3 Experimental Macromixing Time Data of Hydrofoil 2 Impeller

Hydrofoil 2 Impeller					
n [1/min]	**n [1/s]**	**Mixing time**	**Re**	**n*Mixing Time**	**Avarage Value**
200	3.33	29.72	33333	99.08	99.84
320	5.33	18.90	53333	100.81	99.84
440	7.33	13.65	73333	100.09	99.84
600	10.00	9.95	100000	99.50	99.84
720	12.00	8.35	120000	100.22	99.84
800	13.33	7.45	133333	99.35	99.84

Table B.4 Experimental Macromixing Time Data of Hyperboloid Impeller

Hyperboloid Impeller					
n [1/min]	**n [1/s]**	**Mixing time**	**Re**	**n*Mixing Time**	**Avarage Value**
200	3.33	53.29	33333	177.63	177.92
320	5.33	33.33	53333	177.76	177.92
440	7.33	24.27	73333	178.00	177.92
600	10.00	17.51	100000	175.07	177.92
720	12.00	14.99	120000	179.84	177.92
800	13.33	13.44	133333	179.19	177.92

Table B.5 Experimental Macromixing Time Data of Hydrofoil 1 and Hyperboloid Impeller Combinations (d)

Hydrofoil 1 (d) + Hyperboloid Impellers					
n [1/min]	**n [1/s]**	**Mixing time**	**Re**	**n*Mixing Time**	**Average Value**
200	3.33	25.10	33333	83.68	82.47
320	5.33	15.59	53333	83.13	82.47
440	7.33	11.12	73333	81.55	82.47
600	10.00	8.12	100000	81.20	82.47
720	12.00	6.97	120000	83.64	82.47
800	13.33	6.12	133333	81.60	82.47

Table B.6 Experimental Macromixing Time Data of Hydrofoil 1 and Hyperboloid Impeller Combinations (1.5d)

Hydrofoil 1 (1.5 d) + Hyperboloid Impellers					
n [1/min]	**n [1/s]**	**Mixing time**	**Re**	**n*Mixing Time**	**Avarage Value**
200	3.33	28.39	33333	94.64	91.61
320	5.33	17.16	53333	91.51	91.61
440	7.33	11.77	73333	86.28	91.61
600	10.00	9.69	100000	96.92	91.61
720	12.00	7.52	120000	90.21	91.61
800	13.33	6.76	133333	90.10	91.61

APPENDIX C

MACROMIXING TIME DATA FOR SQUARE TANK MEASUREMENTS

Table C.1 Experimental Macromixing Time Data of Generation 5 Hyperboloid (Low Rib) Mixer

Generation 5 Hyperboloid Mixer (Low Rib)					
n [1/min]	**n [1/s]**	**Mixing time**	**Re**	**n*Mixing Time**	
160	2.67	191.69	106667	511.17	**Average Value**
220	3.67	164.35	146667	602.62	583.6
280	4.67	121.24	186667	565.78	583.6
340	5.67	102.78	226667	582.41	583.6

Table C.2 Experimental Macromixing Time Data of Generation 5 Hyperboloid (High Rib) Mixer

Generation 5 Hyperboloid Mixer (High Rib)					
n [1/min]	**n [1/s]**	**Mixing time**	**Re**	**n*Mixing Time**	
160	2.67	177.09	106667	472.25	**Average Value**
220	3.67	124.19	146667	455.38	431.9
280	4.67	88.28	186667	411.95	431.9
340	5.67	75.61	226667	428.48	431.9

Table C.3 Experimental Macromixing Time Data of Generation 6 Hyperboloid Mixer

Generation 6 Hyperboloid Mixer					
n [1/min]	**n [1/s]**	**Mixing time**	**Re**	**n*Mixing Time**	
160	2.67	129.50	106667	345.35	**Average Value**
220	3.67	89.08	146667	326.61	297.8
280	4.67	62.49	186667	291.62	297.8
340	5.67	48.59	226667	275.32	297.8

APPENDIX D

AERATION DATA FOR SQUARE TANK MEASUREMENTS

Table D.1 Experimental Aeration Data of Generation 5 (Low Rib) Hyperboloid Mixer

Fl [-]	**0.01**							
n [U/min]	286		382		477		573	
Q_A [Nm^3/h]	1.37		1.83		2.29		2.75	
Cond. [µS/cm]	705	861	1020	1181	1340	1500	1655	1812
T(H2O) [°C]	13.6	13.7	13.9	14.1	14.3	14.5	14.7	14.9
kLa [1/h]	9.24	8.92	15.79	16	26.57	26.43	37.3	37.7
OC [kg/h]	36.4	35.2	62.11	62.63	102.86	102.14	144	144
kLa corr.* [1/h]	9.35	8.9	15.54	15.52	25.41	24.91	34.65	34.51
OC corr. [kg/h]	36.82	35.13	61.12	60.76	98.37	96.26	133.77	131.8
	8.9		15.54		25.41		34.65	
	35.13		61.12		98.37		133.77	
OA Efficiency [%]	8.56		11.15		14.37		16.27	

* Correction curve: 0.0087*x-7.2917

Table D.1 continued

Fl [-]	**0.025**							
n [U/min]	286		382		477		573	
Q_A [Nm^3/h]	3.43		4.58		5.72		6.88	
Cond. [µS/cm]	1013	1166	1320	1472	1626	1782	1940	2100
T(H2O) [°C]	13.5	13.7	13.9	14.1	14.2	14.3	14.5	14.6
kLa [1/h]	10.68	10.32	15.42	15.74	22.71	22.57	38.6	40.1
OC [kg/h]	42.4	40.8	60.53	61.58	88.57	87.86	149	155
kLa corr. [1/h]	10.52	10.03	14.77	14.87	21.16	20.72	34.9	35.7
OC corr. [g/h]	41.75	39.64	57.99	58.18	82.5	80.64	134.72	137.98
	10.52		14.77		20.72		34.9	
	41.75		57.99		80.64		134.72	
OA Efficiency [%]	4.07		4.23		4.71		6.55	
Fl [-]	**0.04**							
n [rev/min]	286		382		477			
Q_A [Nm^3/h]	5.49		7.33		9.16			
Cond. [µS/cm]	701	858	1014	1173	1333	1490		
T(H2O) [°C]	13.2	13.3	13.5	13.6	13.7	13.9		
kLa [1/h]	11.84	11.36	17.68	18.42	25.14	23.43		
OC [kg/h]	47.2	45.2	70	72.63	98.57	92.14		
kLa corr. [1/h]	11.98	11.34	17.41	17.88	24.06	22.1		
OC corr. [kg/h]	47.76	45.12	68.93	70.52	94.33	86.92		
	11.98		17.41		22.1			
	47.76		68.93		86.92			
OA Efficiency [%]	2.91		3.14		3.17			

Table D.2 Experimental Aeration Data of Generation 6 Hyperboloid Mixer

Fl [-]	**0.01**							
n [rev/min]	286		382		477		573	
Q_A [Nm^3/h]	1.37		1.83		2.29		2.75	
Cond. [µS/cm]	915	1070	1226	1383	1542	1697	1854	2010
T(H2O) [°C]	18.4	18.5	18.6	18.7	18.8	18.9	19	19.1
kLa [1/h]	13.3	13.55	21.8	22.2	32.82	33	49.63	50.13
OC [kg/h]	47	47.5	76	77.33	114.55	114.55	172.5	173.75
kLa corr. [1/h]	13.21	13.28	21.06	21.15	30.81	30.53	45.24	45.01
OC corr. [kg/h]	46.69	46.54	73.44	73.67	107.53	105.99	157.25	156.04
	13.31		21.15		30.81		45.24	
	46.69		73.67		107.53		157.25	
OA Efficiency [%]	11.37		13.44		15.71		19.12	
Fl [-]	**0.025**							
n [rev/min]	286		382		477		573	
Q_A [Nm^3/h]	3.43		4.58		5.72		6.88	
Cond. [µS/cm]	1004	1161	1316	1470	1625	1779	1939	2090
T(H2O) [°C]	13.8	14	14.2	14.3	14.5	14.6	14.8	15
kLa [1/h]	14.15	13.75	22.07	22.27	32.18	32.36	53.13	52.75
OC [kg/h]	55.5	53.5	86	86.67	124.55	124.55	203.75	201.25
kLa corr. [1/h]	13.95	13.36	21.15	21.04	29.98	29.71	48.04	47
OC corr. [kg/h]	54.7	52	82.42	81.9	116.02	114.35	184.24	179.33
	13.95		21.04		29.71		47	
	54.7		81.9		114.35		179.33	
OA Efficiency [%]	5.33		5.98		6.68		8.72	

Table D.2 continued

Q [-]	**0.04**					
n [rev/min]	286		382		477	
Q_A [Nm^3/h]	5.49		7.33		9.16	
Cond. [µS/cm]	860	1016	1172	1330	1484	1641
T(H2O) [°C]	13.3	13.4	13.6	13.8	14	14.1
kLa [1/h]	17.35	16.95	24.07	29.2	40.73	41
OC [kg/h]	69	67	95.33	114.67	159.09	160
kLa corr. [1/h]	17.32	16.69	23.37	27.95	38.44	38.14
OC corr. [kg/h]	68.87	65.96	92.56	109.76	150.15	148.82
	17.32		23.37		38.14	
	68.87		92.56		148.82	
OA Efficiency [%]	4.19		4.22		5.43	

APPENDIX E

ANALYSIS OF TORQUE AND ROTATIONAL SPEED DATA

Torque was measured as $T = 0.04$ Nm for hydrofoil 1 impeller at a rotational speed of 783 RPM. Following calculations were done to obtain Ne and Re from these data:

$$\omega = 2\pi(\frac{783}{60})(rps) \tag{E.1}$$

$$\omega = 82.00 rps$$

$$P = T\omega \tag{E.2}$$

$$P = 0.04 * 82.00$$

$$P = 3.28 \text{ Watt}$$

$$Ne = \frac{P}{\rho * d^5 * n^3} \tag{E.3}$$

$$Ne = \frac{3.28 Watt}{(1000)\left(\frac{kg}{m^3}\right) * (0.1)^5 (m^5) * \left(\frac{783}{60}\right)^3 (rps)^3}$$

$$Ne = 0.15$$

$$\mathrm{Re} = \frac{d^2 * n}{\upsilon(T)} \tag{E.4}$$

$$\mathrm{Re} = \frac{(0.1)^2 (m^2) * (783/60)(rps)}{10^{-6} (m^2/s)}$$

$$\mathrm{Re} = 130505$$

APPENDIX F

DISSOLVED OXYGEN MEASUREMENT PROCEDURE

The dissolved oxygen that exists in water is removed before the aeration measurements by combining it chemically with sodium sulphite according to the reaction given in Equation F.1.

$$Na_2SO_3 + \frac{1}{2}O_2 \rightarrow Na_2SO_4 \qquad \text{(F.1)}$$

The amount of sodium sulphite required for one experiment depends on the dissolved oxygen amount in water and on the requirement for a suitable lag time for admixture. The volume of the tank used in the experiment was 0.365 m^3 and the DO concentration of the tank at 10.8 °C was C=11.08 mg/L. The oxygen transfer capacity, (the highest OC value ever measured, i.e. the saturation value of the oxygen solubility) at this temperature was $OC_{10.8}$=97.36 g/h = 0.097 kg/h. With a lag time of 15 sec the following is calculated:

Na_2SO_3 for DO bonding: $0.365 * 0.01108 * 8 = 0.032kg = 32g$ (F.2)

Na_2SO_3 for lag time: $0.097 * (15/3600) * 8 = 0.00323kg = 3.23g$. (F.3)

So, the total sodium sulphite requirement for one test end in a total of 35.23 g and to be on the safe side 45 g of sodium sulphite was used for one test measurement. The amount of water required to dissolve the 45 g of sodium sulphite was taken from the mixing tank so that exactly the same amount of water is preserved.

The oxidation of sodium sulphite accelerates in the presence of cobalt salt since it catalyses the reaction. Therefore before beginning the experiment a certain amount of $CoCl_2.6H_2O$ was added to ensure a minimum concentration of cobalt ions in water. 0.2 g of cobalt salt was added before beginning the experiment.

The mixer and the air flow rate were adjusted to required value by the switches on the right side of the mixing tank.

The process of oxygen saturation is determined with the DO-sensor which was placed always at the same place, to the left corner of the tank. The signals coming from the sensor were sent to the measurement amplifier and then to the interphase card in the PC. The measured signals were visualized in the screen with the help of a measured data processing program and the ASCII data, where the concentration value per second, were recorded at the same time.

The aeration is started and the oxygen transfer (absorption) curve is drawn with the data obtained by the measurements of the oxygen transfer electrodes.

The $k_L a$ is determined from the slope of the absorption curve through the program OCA which uses the exponential regression method to obtain the best fit line to the data.

The increased salt content in water affects the measured values on the basis that the increasing bubble polarity decreases the normal coalescence. The water in the tank requires to be changed when a salt content of 2000 mg/L is reached since this can lead up to a deviation of 10 %. This value can be controlled with a conductivity measurement probe.

As the oxygen in air dissolve in water, the oxygen amount increases according to the saturation function:

$$\frac{dc(t)}{dt} = k_L a \cdot (c_S - c(t)) \qquad \text{(F.4)}$$

After integration:

$$c(t) = c_S - (c_S - c_0) \cdot e^{-k_L a \cdot t} \qquad \text{(F.5)}$$

where $k_L a$ = overall mass transfer coefficient, sec^{-1}

c_s = saturation concentration of gas in solution, mg/L

c_t = concentration of gas in solution, mg/L

The integrated form of this equation is:

$$\int_{c_0}^{c_t} \frac{dc}{c_S - c_t} = \int_0^t k_L a dt \qquad \text{(F.6)}$$

$$\ln(c_S - c_t)\Big|_{C_0}^{C_t} = -k_L a.t \qquad \text{(F.7)}$$

$$\ln(c_S - c_t) - \ln(c_S - c_0) = -k_L a t \qquad \text{(F.8)}$$

Since the equation is in linear form it can be plotted against experimental data taken when aeration is turned on. Recording the time (sec) versus DO concentration (mg/L) one can obtain $(c_S - c_t)$, and rearranging the equation $k_L a$ can be calculated directly from the data:

$$k_L a = \frac{\ln(c_S - c_1) - \ln(c_S - c_2)}{t_2 - t_1} \qquad \text{(F.9)}$$

Drawing the graph of the $\ln(c_S - c_t)$ versus time and using the slope of the linear fit to this data one can obtain the overall mass transfer coefficient (oxygen transfer coefficient), $k_L a$ in (h^{-1}).

After obtaining the $k_L a$, the oxygen transfer capacity in clean water, OC [kg/h] can be determined. OC is the oxygen supply, that is the mass [kg] of oxygen transferred by an aeration system in one hour in a tank of certain size filled with clean water at DO of C=0 mg/L, a water temperature of 20 °C and normal atmospheric pressure (1013 hPa). The following applies:

$$OC = \frac{V * k_L a_{20} * c_{S,20}}{1000} \qquad \text{(F.10)}$$

where

V= Tank volume; $c_{S,20}$=measured DO saturation concentration from the estimation of a clean water test; $k_L a_{20}$ is the oxygen transfer coefficient at clean water at 20 °C.

Different characteristic numbers provide a comparison between different system parameters regarding the oxygen transfer efficiency e.g. $OC_{A,h}$ [g/(m^3_N/m)] and OA_h [%/m] :

$$OC_{A,h} = \frac{OC}{Q_A * h_w} * 1000 \qquad \text{(F.11)}$$

$OC_{A,h}$ is the specific oxygen supply where Q_A is the absorbed air [m^3/s] with an oxygen concentration of 0.299 kg/m^3 and h_w is the water height [m]. OA_h is the specific oxygen utilization efficiency and defined as follows:

$$OA_h = \frac{100 * OC}{h_w * (Q_A * 0.299)} \qquad \text{(F.12)}$$

For the evaluation of the aeration experiment, the program of the firma Aquadata was used. The program conforms to the guidelines in ATV-M 209E and uses the algorithm given above. The program requests the tank volume, the temperature measured during the experiment and the air injection height (h_w) of the aerator and the volumetric air flow (Q_A) as well as the $c(t), t$ data pair. The program gives the OC_{20} value besides the $k_L a$ value. For the characterisation of the quality of the measurements, the residues were calculated by the program and shown graphically. The residues show the deviation of the each calculated value from the real measured value. A random distribution of the residues indicates a proper measurement while a waveform distribution of them means a wrong start of the experiment such as an incomplete mixing of the tank content or a late sulphide oxidation. By adjusting the starting time the calculation can be corrected (Frey, 1999).